Aus dem Institut für Tierschutz, Tierverhalten und Versuchstierkunde
des Fachbereichs Veterinärmedizin der
Freien Universität Berlin

Entwicklung und Evaluierung neuer niedrig-molekularer Sonden für die Charakterisierung von abdominalen Aortenaneurysmen mittels der Magnetresonanztomographie (MRT)

Inaugural-Dissertation
zur Erlangung des Grades eines
Doktors der Veterinärmedizin
an der
Freien Universität Berlin

vorgelegt von
Julia Brangsch
Tierärztin aus Berlin

Berlin 2021
Journal-Nr.: 4253

Aus dem Institut für Tierschutz, Tierverhalten und Versuchstierkunde
des Fachbereichs Veterinärmedizin der
Freien Universität Berlin

Entwicklung und Evaluierung neuer niedrig-molekularer Sonden für die Charakterisierung von abdominalen Aortenaneurysmen mittels der Magnetresonanztomographie (MRT)

Inaugural-Dissertation
zur Erlangung des Grades eines
Doktors der Veterinärmedizin
an der
Freien Universität Berlin

vorgelegt von
Julia Brangsch
Tierärztin
aus Berlin

Berlin 2021

Journal-Nr.: 4253

Gedruckt mit Genehmigung des Fachbereichs Veterinärmedizin
der Freien Universität Berlin

Dekan:	Univ.-Prof. Dr. Jürgen Zentek
Erster Gutachter:	Univ.-Prof. Dr. Christa Thöne-Reineke
Zweiter Gutachter:	Prof. Dr. Marcus R. Makowski
Dritter Gutachter:	Univ.-Prof. Dr. Robert Klopfleisch

Deskriptoren (nach CAB-Thesaurus):

mice, animal models, aorta, aneurysm, arteries, inflammation, interleukin 1, diagnostic techniques, magnetic resonance imaging

Tag der Promotion: 10.02.2021

Nothing in life is to be feared, it is only to be understood. Now is the time to understand more, so that we may fear less.

Marie Curie

Table of contents

List of abbreviations

AAA	abdominal aortic aneurysm
ACE	angiotensin-converting enzyme
Ang II	angiotensin-II
ApoE	apolipoprotein-E
AT1	angiotensin-II type 1 receptor
AT2	angiotensin-II type 2 receptor
CNR	contrast to noise ratio
CT	computed tomography
ECM	extracellular matrix
EvG	Elastica van Gieson
FDA	U.S Food and Drug Administration
^{18}F-FDG	^{18}F-Fluorodeoxyglucose
Gd	gadolinium
Gd-DTPA	gadolinium diethylenetriamine pentaacetic acid
HE	hematoxylin and eosin
ICP-MS	inductively-coupled mass spectrometry
IL	interleukin
IL-1R	interleukin 1 receptor
ILT	intraluminal thrombus
LA-ICP-MS	laser coupled mass spectrometry
LDL	low density lipoprotein
LOD	limit of detection
LOQ	limit of quantification
MMP	matrix metalloproteinase

MRA	magnetic resonance angiography
MRI	magnetic resonance imaging
NK cell	natural killer cell
PA	plasminogen activator
PPE	porcine pancreatic elastase
RF	radiofrequency
ROI	region of interest
SMC	smooth muscle cell
SNR	signal to noise ratio
SPIO	superparamagnetic iron oxide
T	Tesla
T1	longitudinal relaxation time
T2	transverse relaxation time
TE	echo time
T_H-cells	T helper cells
TI	inversion time
TIMP	tissue inhibitor of metalloproteinases
TNF	tumor necrosis factor
TOF	time of flight
TR	repetition time
USPIO	ultra-small superparamagnetic iron oxide
US	ultrasound

List of Figures

1 Introduction

1.1 Abdominal aortic aneurysms

Abdominal aortic aneurysms (AAAs) represent a cardiovascular disease with severe complications and represent the most common arterial aneurysms (1). An aneurysm is defined as a local permanent and irreversible dilatation of a vessel. Although aneurysms can occur in any region of the abdominal aorta, common practice restricts the definition of AAAs to aneurysms of the infrarenal aorta (2). The normal infrarenal aortic diameter depends on age, sex and body weight and represents 1.7 cm in elderly men > 50 years or 1.5 cm in women > 50 years (3). An infrarenal aorta greater than 30 mm in diameter is considered aneurysmal representing an increase in size of more than 50%. The disease is more common in males than in females with a prevalence of 3% in women older than 50 years and 10% in men older than 65 years (1). Due to the ageing population and improvement of diagnostic tools, the incidence of AAAs is increasing steadily, causing 175 000 deaths per year globally (4). With the enlargement of the aneurysm, the risk of rupture increases (5). Ruptured AAAs represent a life-threatening emergency with an overall mortality rate > 90%. More than 50% of the patients die before reaching the surgical room (6-8).

The exact causes of aneurysmal dilatation remain still unknown although AAAs can develop due to specific causes such as acute or chronic infections (brucellosis, salmonellosis, tuberculosis), connective tissue disorders (Takayasu disease, Marfan Syndrome) or trauma (2, 9, 10). The prevalence of aneurysms is strongly associated with several risk factors, including smoking, hypertension or hypercholesterolemia (6). Furthermore, relatives of patients with AAAs were reported to have a significantly increased risk for aneurysmal degeneration (11).

1.1.1 Pathophysiology

The pathophysiology of aneurysms involves two different key processes which are inseparably connected, degradation and inflammation (12). On the one hand, degradation of the extracellular matrix (ECM) proteins of the aortic wall contributes to the initiation and progression of AAAs (13) (Figure 1). Above all, elastin and collagen are involved in this process. Elastin is most abundant in the tunica media and provides an energy-independent elastic recoil in response to intraluminal pulse pressure (13). The fragmentation of elastin in the media results in progressive dilatation of the aorta (14). It was shown that a correlation between progressive medial elastin reduction, an increase in diameter and aortic rupture exists (15). The fragmentation of elastin is the decisive factor for the onset, progressive enlargement

and rupture of AAAs. Collagen also plays an important role in the development of AAAs. Two specific types of fibrillar collagen (type I and III) are present in the media and adventitia of the vessel wall and contribute to their tensile strength (14). The loss of collagen is also a relevant factor for the development and rupture of AAAs (14, 16). The reduced density of elastin and collagen in the aneurysmal aortic wall is a result of a defective synthesis and increased degradation by different specific enzymes (14). Various proteases produced by vascular wall cells, including medial smooth muscle cells (SMCs), adventitial fibroblasts and migrated inflammatory cells, are involved in this process. The highest elastolytic activity was reported for proteases of the family of matrix metalloproteinases (MMPs). Especially MMP-2 (gelatinase, A/72 kDa), produced by mesenchymal cells, and MMP-9 (gelatinase, B/92 kDa), expressed by macrophages and neutrophils, demonstrates a significant proteolytic activity against elastin (17). Both are activated by plasmin, which is generated by plasminogen activators u-PA (urokinase-type) and t-PA (tissue-type) (18). The activity of MMPs is regulated by unspecific endogenous inhibitors, such as α2-macroglobulin and specific tissue inhibitors of metalloproteinases (TIMPs) (19). During the onset and progression of aortic aneurysms, an imbalance between MMPs and their respective inhibitors occurs. This imbalance results in an overall increase of proteolytic activity (20). Elastase is another enzyme involved in the degradation of elastin. In several experimental models of AAA, it was shown that elastase infusion results in aortic dilatation (21, 22). Concerning collagen, Menashi *et al.* measured an increase in the amount of collagen in the central part of AAAs due to the progressive reactive synthesis of new collagen fibers and the degradation of medial non-collagenous material (23). During the early stages of aneurysm formation, collagen synthesis increases, suggesting the activation of a compensatory repair mechanism. Nevertheless, with the progression of the disease, collagen degradation exceeds its synthesis and increases the risk of AAA rupture (24). Several studies confirmed collagenase activity in the aneurysmal wall, which may play an important role in the progressive expansion and rupture of AAAs (25). The proteolysis of ECM proteins not only causes disruption of the aortic wall, it is also essential for the initial translocation of inflammatory cells from the vascular lumen into the aortic media and adventitia (12) (Figure 1).

This leads to the second key process of the AAA's pathophysiology, inflammation. The inflammatory response comprises the full range of cell types, including macrophages, T_H2-cells (T helper cells), mast cells, B cells, NK (natural killer) cells and polymorphic neutrophils (26). These cells percolate through all layers of the vessel wall and secrete various humoral factors (24). The recruitment of inflammatory cells is initiated by proinflammatory cytokines, chemokines and specific changes in ECM proteins (14, 27). In this context, Koch *et al.* showed an increased expression of cytokine interleukin-8 (IL-8), chemotactic for neutrophils,

lymphocytes and endothelial cells, as well as the monocyte chemoattractant protein-1 (MCP-1), a potent chemotactic cytokine for monocytes. Both are expressed by cells within the aortic wall such as macrophages and to lesser degree endothelial cells and smooth muscle cells (27). Additionally, the presence of elevated interleukin-1β (IL-1β), interleukin-6 (IL-6) and tumor necrosis factor-α (TNF-α) is associated with AAA disease (28). As a result of these inflammation processes, smooth muscle cell apoptosis and neovascularization occur in the medial wall (29, 30). The rarefaction of smooth muscle cells is caused by cytotoxic mediators such as cytokines, perforin and Fas death factor, expressed by macrophages and T-lymphocytes. This process leads to a thinning of the tunica media (31). Medial neovascularization was shown to be spatially correlated with the destruction of elastin, chronic inflammation and hypoxia due to the mural thrombus (32, 33). The density of endothelial cells was shown to be 15-fold higher in AAAs compared to normal aortas (33). Because of the absence of vasa vasorum in the healthy human infrarenal aorta (34), neoangiogenesis is likely to play a significant role in AAA development by providing a route for recruiting pro-inflammatory cells (8).

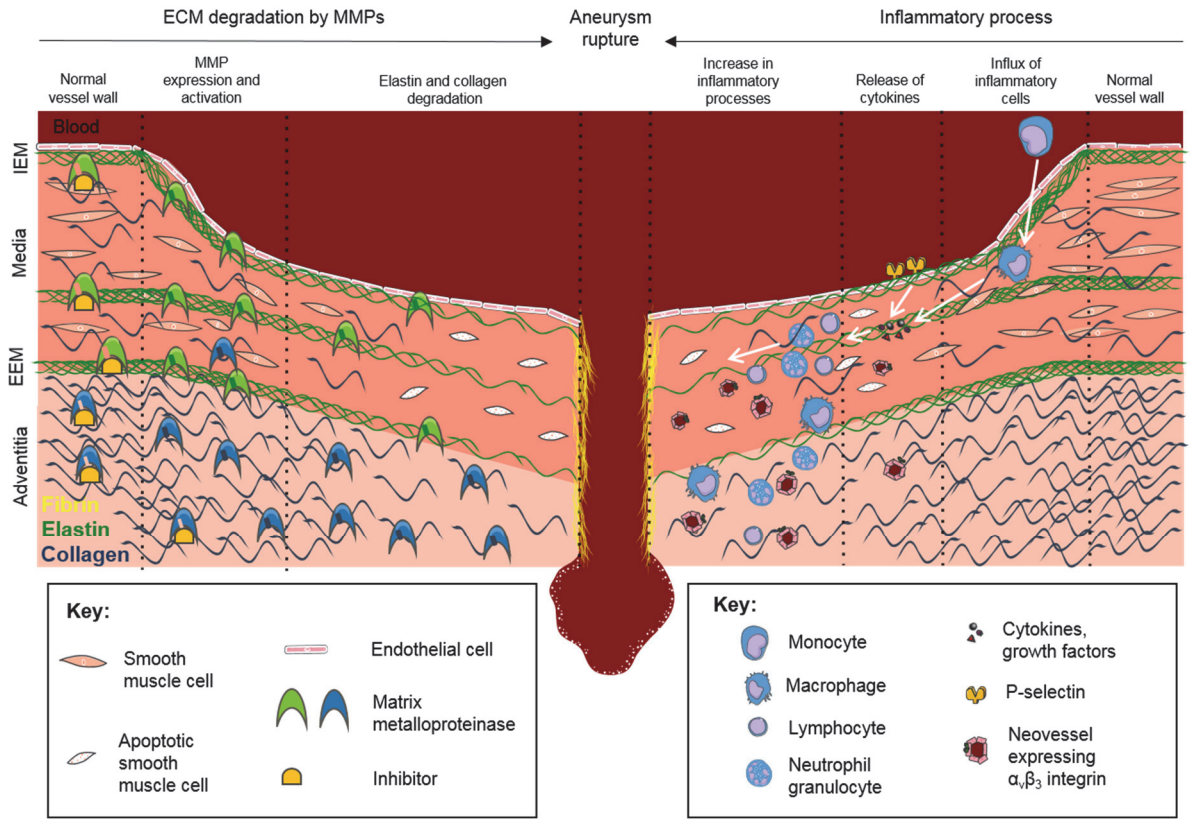

Figure 1: Development and progression of aortic aneurysms (From Brangsch J, Reimann C, Collettini F, Buchert R, Botnar RM, Makowski MR. Molecular Imaging of Abdominal Aortic Aneurysms. Trends in Molecular Medicine. 2017;23(2):150-64)

1.1.2 Clinical diagnosis

The majority of AAAs is asymptomatic until rupture although a few patients report abdominal or back pain previous to the rupture of the AAA. In the case of AAA rupture, patients present hypotension due to a hemodynamic shock as well as different abdominal signs, including a pulsatile abdominal mass and a distended abdomen (35).
The diagnosis of an asymptomatic AAA is often incidentally because of routine check-ups or examinations for other purposes. Abdominal palpation during routine physical examination reveals approximately 30% of asymptomatic AAAs as a pulsatile, expansile mass at or above the umbilicus (36). However, the sensitivity of physical examination is extremely dependent on abdominal girth as well as AAA diameter and can range from 53% to 100% (37).

Identification and assessment of AAAs are usually performed with different imaging techniques including ultrasound (US), computed tomography (CT) or magnetic resonance imaging (MRI). Each of these imaging techniques has its advantages and disadvantages but offers a high diagnostic sensitivity (8).
Because of its high sensitivity and specificity as well as its safety, availability and low costs, abdominal US is the method of choice for AAA screening and follow-ups. US is accurate within 0.3 cm in estimating aortic diameter and may also show thrombus or echogenic calcifications in or adjacent to the aortic wall (36, 38, 39). US imaging is however limited in patients who are obese or have overlying bowel gas. Furthermore, the presence of periaortic disease, iliac aneurysms or the proximal and distal extent of the aneurysm cannot reliably be assessed (39).
CT imaging provides a more accurate assessment of AAA size and morphology as well as clinical valuable information about the surrounding abdominal anatomy (35). Therefore, it is especially used for the diagnosis of suspected ruptured AAAs and in the preoperative work-up for the repair of AAAs. In contrast to US, there is no interobserver variation or limitation due to body size, obesity or bowel gas (39). The disadvantages of CT scanning include higher costs and exposure to radiation.
The gold standard of the AAA identification is MRI in combination with magnetic resonance angiography (MRA). Although high costs, reduced availability and potential motion artefacts, as well as contraindications like patient claustrophobia or metal implants limit the widespread use of MR imaging (39), the high resolution yields an even more accurate detection and anatomical assessment of AAAs without the need of a contrast medium or ionizing radiation (40).

1.1.3 Management

There are different management options for patients with asymptomatic AAAs including watch and wait using imaging, medical therapy and surgical treatment. The treatment of an intact aneurysm is essentially prophylactic to prevent fatal aortic rupture. The choice of treatment procedure is deduced from the estimated risk of rupture and surgery as well as the estimated patient's life expectancy (2). There is a broad consensus that the risk of aneurysm rupture increases relative to aneurysm size although some small aneurysms occasionally rupture and some large do not (6, 8). AAAs larger than 5.5.cm show an almost exponential increase of risk of rupture and therefore require surgical repair (1, 41). The management of small aneurysm (4.0 – 5.5 cm in diameter) is much more controversial. Several large-scale trials like the Unites Kingdom Small Aneurysm Trial (UKSAT) and the Aneurysm Detection and Management (ADAM) Veterans Affairs Cooperative Study showed no survival benefit of patients undergoing preventive surgical repair compared to patients getting regular surveillance imaging (42-46).
Two different surgical approaches for aneurysm repair are currently available: open surgery and endovascular repair. Open surgery includes an abdominal or flank incision followed by opening of the aneurysm sac and interposition of a synthetic graft while vessels above and below the AAA are controlled (6). Endovascular repair represents a less invasive technique which can be performed percutaneously with the patient under local anesthesia. A covered stent is intraluminal introduced through the femoral and iliac arteries and functions as a sleeve passing through the aneurysm sac, anchoring above and below the aneurysm in the normal aorta and iliac arteries (6). Patients undergoing endovascular repair show a reduced hospitalization time, shorter recovery time and return to baseline functional capacity and less blood loss compared to patients with open surgery. Furthermore, numerous studies showed significantly higher rates of short-term morbidity and mortality (1 to 3 years) of endovascular therapy although both techniques are associated with similar long term mortality (8 to 10 years) (6, 36, 47-49). Due to these advantages, endovascular repair is currently performed in more than 75% of patients undergoing aneurysm repair. However, some patients do not have an appropriate aortic anatomy for endovascular repair because of insufficient size of iliac vessels or a too short aortic neck above the AAA so that the stent could not be anchored (6).

The probably most certain therapeutic approach to decrease the rate of AAA expansion is the reduction of risk factors. Tobacco smoking represents the main risk factor for AAA prevalence, incidence and progression. More than 90% of AAA patients have a history of smoking and several studies showed a significant correlation between continued smoking and increased aneurysm growth rate (50). Additionally, preclinical and clinical studies suggest that constant exercise can increase the abdominal aortic blood flow which may inhibit AAA expansion and may also reduce other cardiovascular events in AAA patients (51). The occurrence of AAAs is

furthermore thought to be associated with hypertension or hypercholesterolemia which suggests the control of these coexisting conditions with medications to reduce the incidence of cardiovascular events including aneurysm expansion although there is limited data available to support this hypothesis (see below) (6).

A management option for patients with small to medium-sized aneurysms that are not surgically treated represents medical therapy. Because of the central role of matrix metalloproteinases in aneurysm development, pharmacologic inhibition of these proteases has gained in research interest. Doxycycline, a tetracycline analogue and nonspecific MMP inhibitor, was shown to effectively reduce MMP activity and could inhibit AAA formation and progression in various rodent models (52). So far, no clinical trial has shown any benefit of doxycycline therapy in AAA patients so far (53-55) although the results of a new large placebo-controlled, double-blinded clinical trial testing doxycycline for inhibition of growth of small AAAs are currently under evaluation (56). A further antibiotic therapy with roxithromycin, a macrolide, was tested in two clinical randomized studies and showed a significant reduction of the expansion rate of small AAAs (57, 58). In the context of AAAs, macrolide antibiotics are not only applied due to their effects on MMP-expression but also due to their antibacterial effects. In this context the bacterium *Chlamydia pneumoniae* has been identified in the aneurysmatic aortic wall as well as infection with *C. pneumoniae* has been associated with faster expansion rate (1, 59).

Statins (hydroxymethylglutaryl coenzyme A reductase inhibitors) represents a further class of medications for AAA therapy. Besides their cholesterol-lowering effects, a reduced expression of various inflammatory molecules, including MMP-2 and MMP-9, has been shown in preclinical and clinical studies (2, 60, 61). A meta-analysis of 13 observational studies investigating the influence of statins on the growth rate of AAAs demonstrated a significant preventive effect on small aneurysm growth (62). In contrast, a larger study by Ferguson *et al.* including 652 patients with small AAAs, revealed no association between statin prescription and AAA expansion (63). Nevertheless, there is evidence, that statin treatment reduces perioperative and long-term mortality as well as postoperative complications after AAA surgery so that a routine statin treatment of patients with small AAAs should be implemented (64).

The use of beta-blockers, e.g. propranolol, to inhibit AAA expansion by lowering the arterial blood pressure was successfully investigated in various rodent studies. However, three big clinical trials failed to find a significant effect on the progression of AAAs in over 1000 patients (50). Furthermore, there is still no proof of a significant correlation between blood pressure and aneurysm growth whereas a current meta-analysis could show a correlation between blood pressure and AAA rupture rate (65, 66). Nevertheless, due to certain comorbidities, including

hypertension, coronary heart disease or chronic heart disease, there is still a valid indication for therapy with beta-blockers in patients with AAAs (1).
Other medications which have been successfully tested in animal studies and, therefore, might protect from AAA progression represent angiotensin-converting enzyme (ACE) inhibitors and angiotensin-II type 1 (AT1)-receptor antagonists as well as angiotensin-II type 2 (AT2)-receptor agonists. By downregulation of the expression of adhesion molecules and proinflammatory cytokines as well as by decreasing degradation of ECM proteins, AAA progression was prevented in different experimental mouse and rat models (1, 67-70). However, the clinical data regarding a therapeutic effect of ACE- or AT1-receptor inhibitors or AT2-receptor agonists are controversial and until today, there is no clear evidence that these medications can limit AAA progression in patients (1, 51).
In summary, no medication is currently in the guidelines for reducing AAA enlargement. On the other hand, the results of several ongoing large clinical trials using different kinds of medical therapies are still pending and numerous new therapeutic approaches are investigated in preclinical studies (71). Therefore, pharmacological treatment of AAAs could play a key role in aneurysm prevention and therapy in future.

1.1.4 Small animal models of AAA

For the investigation of crucial pathogenic factors of aneurysm development and new approaches regarding aneurysm therapy, animal models still provide the method of choice. The basic premise of animal models of human diseases is the imitation of cellular and biochemical characteristics in the development and progression of the disease. In the case of AAAs, animal models recapitulate several facts of the human disease including aortic medial degeneration, inflammation, thrombus formation and rupture (72).

Especially mice have become dominant in biomedical research due to numerous advantages that include their small size, great comparability because of well-documented genetic backgrounds and the ability to create genetically engineered variants (72). The most commonly used mouse models of AAA are chemically induced by elastase, calcium chloride or angiotensin-II (Ang II).
The infusion of porcine pancreatic elastase (PPE) into the infrarenal segment of the abdominal aorta has been initially established in rats (73) and has been modified for mice by Pyo and colleagues (74). 14 days after elastase perfusion a significant dilation of the aortic wall and extensive destruction of the elastic lamina together with a pronounced inflammatory infiltration was shown. Using this model, the role of matrix metalloproteinases MMP-9 and MMP-12 in the mural elastin destruction could be revealed as well as the potential of doxycycline as AAA

therapy (74, 75). In the following years, the model of elastase perfusion was also applied to rabbit and pig models (76, 77).

The periaortic incubation of calcium chloride *via* a soaked gauze or direct placement of a concentrated solution between the aortic renal branches leads to a progressive increase in aortic diameter by 2 to 4 weeks after incubation in mice (78, 79). Furthermore, a structural disruption of the medial aortic wall, as well as inflammatory responses, has been shown. In contrast to elastase infusion, the periaortic incubation of calcium chloride does not cause an immediate aortic dilatation due to mechanical manipulation (72). This experimental AAA model was also introduced in rats, rabbits and pigs, often applied in combination with PPE perfusion (80-82).

The most commonly used mouse model of AAA represents the infusion of angiotensin-II developed by Daugherty *et al.* (83). Ang II is delivered at doses of 500 to 1000 ng/kg/min *via* osmotic minipumps (Figure 3A) which are subcutaneously implanted in the dorsal neck region (Figure 2B, C).

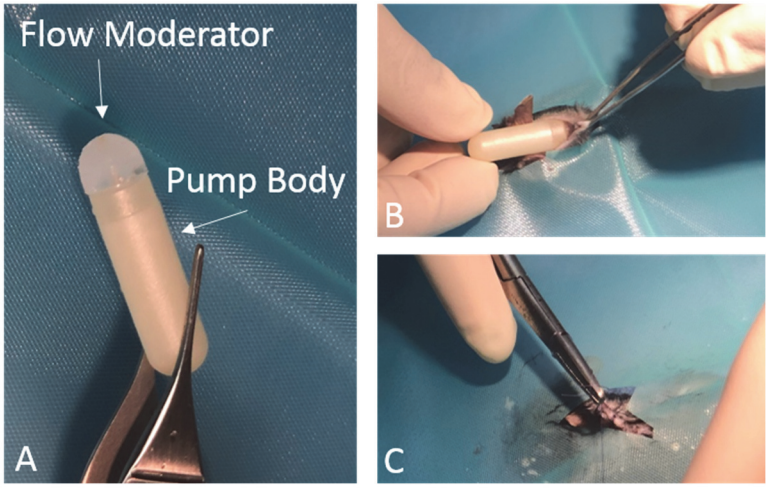

Figure 2: MRI compatible osmotic minipump implantation. After preparation of a subcutaneous tunnel in the dorsal neck region, the osmotic minipump is inserted gently through the skin incision (B). After pump insertion, the skin incision is sutured (C).

Within 28 days after implantation, AAAs spontaneously develop in the suprarenal region of the abdominal aorta (Figure 3). The earliest changes are already visible at 1 to 4 days of Ang II infusion including disruption of medial elastic fibers at the sites of macrophage accumulation. Beyond 14 days of Ang II infusion, increased deposition of extracellular matrix in regions of former medial disruption and a reendothelization of the dilated lumen is shown. This animal model also includes the possible rupture of the aortic wall, causing a fatal abdominal hemorrhage in at least 10% of the mice. Although the administration of the vasoactive peptide Ang II was first thought to raise the blood pressure, several studies demonstrated that the arterial blood pressure was not altered by Ang II infusion in both anaesthetized and conscious

mice. However, an increase in blood pressure does not appear to account for the development of AAAs (72). Another characteristic of these mice is the enhanced propensity for AAA development in male mice showing an incidence almost twice that of females, while the reasons for this gender difference have not been defined yet (84). An important difference between human AAAs and those formed in Ang II-infused mice represents the location in the infrarenal versus suprarenal region. Currently, the mechanisms of AAA location in human disease and in this mouse model are still unknown (85). The majority of Ang II infusion studies have used hyperlipidemic mice, either low-density lipoprotein receptor knockout (LDL-/-) or apolipoprotein-E knockout (ApoE-/-) mice. ApoE represents a ligand for receptors that clear remnants of chylomicrons and very low-density lipoproteins from the blood. Therefore, a lack of ApoE causes an accumulation of cholesterol-rich remnants in plasma resulting in a 5 time higher plasma cholesterol in ApoE-/- mice (86). The absence of functional LDL receptors leads to an accumulation of cholesterol-rich lipoproteins in plasma as well, leading to a 7 to 9-fold increase in LDL (87). However, it was recently reported that AAAs can also develop in wild-type C57BL/6 which represents the background strain of the hyperlipidemic mice, although the incidence of AAAs was much lower (72).

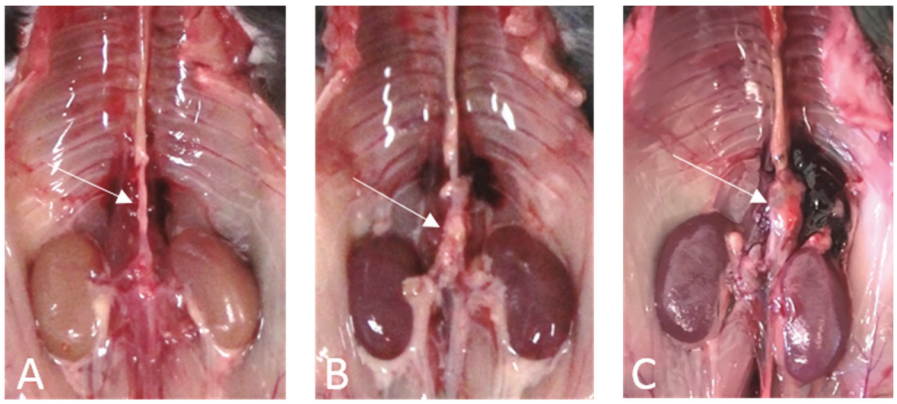

Figure 3: Abdominal aortic aneurysms (arrow) formed in response to angiotensin-II (Ang II) in male ApoE-/- mice after 2 weeks (B) resp. 4 weeks (C) of Ang II infusion; control mouse infused with NaCl for 4 weeks (A).

1.2 Magnetic resonance imaging (MRI)

The use of magnetic resonance imaging (MRI) for medical investigations has provided a huge step forward in the field of diagnosis, especially with the avoidance of exposure to ionizing radiation. Due to decreasing costs and a rising availability, MR imaging is becoming more and more omnipresent in clinical practice (88).

1.2.1 Principles of MRI

Atomic nuclei consist of protons and neutrons which have a positive charge. Certain nuclei spin around their own axes including hydrogen as the most frequently used nucleus for MRI as well as carbon-13, sodium and phosphorus. This spin induces a magnetic moment, generating a local magnetic field with north and south poles. Normally, these tiny magnets are randomly distributed but when submitted to a strong, external magnetic field (B_0), the nuclei align either parallel with or perpendicular to this external field. The parallel alignment represents a lower energy state whereas the perpendicular alignment represents a higher energy state. To produce a measurable signal, the precessing spins have to be excited by a second radiofrequency (RF) magnetic field B_1 which is applied perpendicular to B_0 in short pulses of a certain frequency (Larmor frequency). Following the RF signal, the protons absorb the energy and transit to the higher level of the perpendicular state and the spins are “whipped” to precess in phase. As a result, the net magnetization flips 90° to a transverse plane, rotating around B_0 at the Larmor frequency. This rotating magnetization induces a voltage that can be detected by a receiver coil which is placed around the animal or patient. When the RF frequency transmitter is switched off, the protons will transit back to the low energy levels, seeking the equilibrium state. The time required for the signal to return to the equilibrium is defined as the relaxation time (TR). There are two different types of relaxation processes. The longitudinal relaxation presents the process of realignment to the external magnetic field and is described by the relaxation time T1. T1 is defined as the time which is required for the system to recover to 63% of its initial signal value after the RF pulse has been applied. Water has a rather long T1 value (3000-5000 ms) and therefore appears dark on T1-weighted images, while fat has a short T1 value (260 ms) and appears bright. T1 can be manipulated by varying the repetition time which represents the time between the RF pulses. TR, therefore, determines how much longitudinal magnetization can recover between two pulses. The transverse relaxation is also called spin-spin relaxation and is characterized by the relaxation time T2. It describes the signal decrease due to the dephasing process of the spins induced by local magnetic inhomogeneities and spin-spin interactions. The time it takes for this dephasing to decay the signal to 37% of the original value is called T2 relaxation time which is always shorter than T1. On T2-weighted images fluids like water, urine or cerebrospinal fluid appear bright. The amount of transverse relaxation is controlled by the echo time (TE) which represents the time between the initial RF excitation and the acquisition of the signal. The contrast between different soft tissues in MRI is superb by visualizing the differences in T1 and T2 of different tissues (88-90). Another MRI sequence represents T2*-weighted imaging, also considered as “observed” or “effective” T2. T2* is always less than or equal to T2 and results from the

inhomogeneities of the magnetic field. T2*-weighted imaging is primarily used for the detection of deoxygenated hemoglobin, methemoglobin or hemosiderin in lesions or tissues which become hypointense in this sequence. Therefore pathologic conditions like cerebral hemorrhage, hemorrhage in tumor or thrombosed aneurysm can be depicted (91).

A common clinical MRI scanner consists of the main magnet, gradient magnets, radiofrequency coils which transmit and/or receive the MRI signal, and associated signal processing equipment. A cryogenic superconducting magnet produces a static, stable, spatially homogeneous magnetic field, operating at 0.5 to 3 Tesla (T). Compared to that, the Earth's magnetic field is at 0.00005 T. To conduct such huge currents the magnet has to be cooled close to the temperature of 0 K usually *via* immersion in liquid helium. Most of the currently available MRI scanners operate at a field strength of 1.5 or 3 T. Higher field strengths provide an improved signal to noise ratio (SNR), higher spectral, spatial, and temporal resolution, and improved quantification resulting in a reduced imaging time (88, 90).

1.2.2 MRI of abdominal aortic aneurysms

MRI allows an accurate anatomical visualization of AAAs as well as the evaluation of thrombus and blood flow in the aorta. The use of MRI in AAA diagnosis has been demonstrated in patients with aortic aneurysm and aortic dissection about almost a decade ago. Magnetic resonance angiography was shown to be as sensitive as CT angiography or even more sensitive in the detection of endoleaks following endovascular repair (92). The development of imaging techniques that discriminate flowing spins in blood from those in stationary tissue, allows the visualization of a hemodynamic flow (93). Therefore, even without the application of contrast agents, MRA provides valuable anatomical and morphological information about AAAs and can, therefore, be used in patients suffering from possible contrast medium-related adverse reactions including renal failure, contrast-induced nephropathy or allergic reactions (92). The time-of-flight (TOF) method represents one MRA method and is based on the idea that T1 of flowing water is effectively shorter than T1 of stationary water. This could be explained by the fact that stationary spins are saturated by the radiofrequency excitation but in a flow these spins are constantly replaced by fresh spins with full magnetization, increasing thereby the signal. On the resulting MR images, blood appears bright while stationary tissue appears dark (Figure 4).

In combination with gadolinium (Gd)-based contrast agents, MRA has become an even more valuable tool in the depiction of vascular structures (93, 94). Current contrast-enhanced MRA uses conventional Gd-contrast agents which are administered intravenously and subsequently distributed *via* the whole cardiovascular system. This however results in a very short imaging

acquisition window that is available to assure an adequate arterial contrast in the vessel of interest. This limitation of contrast-enhanced MRA could be overcome by further optimization of injection protocols and particularly by the development and investigation of new molecular contrast agents (94, 95).

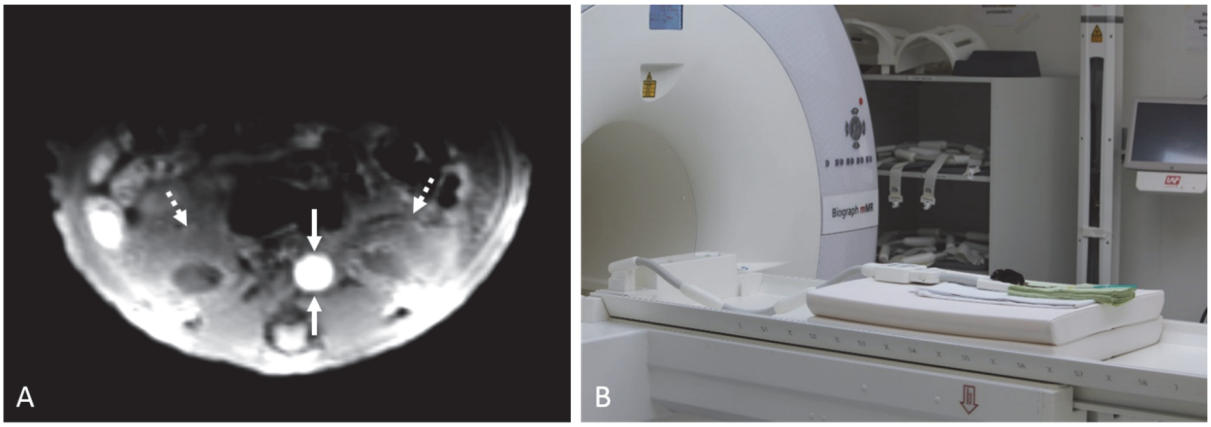

Figure 4: Magnetic resonance imaging of a male mouse A: Angiography of an experimental AAA (white arrows) in a male ApoE-knockout mouse at the level of the kidneys (white dotted arrows). B: Clinical 3 Tesla Siemens system. The mouse is positioned in a prone position on a microscope single loop coil (47 mm).

1.3 Molecular MR imaging

Molecular imaging represents a new multidisciplinary field in which the produced images reflect physiological and pathological cellular and molecular pathways within living organisms. Biological processes can not only be characterized but also quantified at a cellular and subcellular level (96). Concerning abdominal aneurysms, molecular MRI represents a new approach for diagnosis and characterization of the aneurysmal wall. Currently, the aortic diameter is the only determining parameter for the prediction of AAA rupture and the resulting management of the patient. Nevertheless, mounting clinical data show that AAA size is not a reliable marker. Patients with AAAs of identical size often demonstrate significant differences in morbidity, mortality and response to treatment. In addition, the management of medium-sized AAAs still remains challenging. Molecular marker reflecting aortic wall destruction or inflammatory activity could therefore substantially improve the identification of patients for different interventions rather than relying on the aortic diameter alone (92, 97).

1.3.1 Molecular imaging probes

By taking the advantages of the traditional diagnostic imaging technique, molecular imaging introduces molecular imaging agents or probes, which specifically bind a target or biomarker of interest e.g. receptors or enzymes while retaining long enough in the system to be detected.

A molecular probe usually consists of a signal agent and a targeting moiety, connected by a linker. The targeting moiety could be any targeting ligand like peptides, antibodies or nanoparticles. As signal agents for MR imaging, magnetically active elements are used, including gadolinium(III) chelates and iron oxide particles (98). Gadolinium-based contrast agents are currently by far the most often used contrast agents in clinical practice and research. Free Gd ions have a biological half-life of several weeks and are primary cleared from blood by the kidneys and liver and therefore offer sufficient time to obtain high-quality images. Due to the toxic nature of free the gadolinium ions, it is necessary to bind the ion in a complex with a multidentate ligand, such as 1,4,7,10-tetraazacyclododecane-N, N', N'', N'''-tetraacetic acid (DOTA), to shield the ion from biological processes (Figure 5) (99). Gd complexes shorten the observed T1 relaxation time resulting in T1 contrast enhancement. In contrast, the use of iron oxide particles increases the T2 contrast by shortening the T2 relaxation time. Small (SPIO) and ultra-small superparamagnetic iron oxide (USPIO) particles are readily phagocytized by cells of the reticuloendothelial system like active macrophages and thus act as a marker for inflammatory processes (92). Similar to other pharmaceuticals, efficacy and safety are two of the most important considerations for molecular probes. Furthermore, a high binding affinity and specificity to the target, high sensitivity and high stability *in vivo* are essential for clinical translation. To provide a high imaging quality and high contrast ratio, the imaging probe should show a high uptake and slow wash-out in target tissue as well as a low uptake and fast clearance from normal organs. Currently, there are several promising molecular probes under investigation in preclinical and clinical studies but the development of novel desirable molecular probes with clinical applicability remains challenging (98).

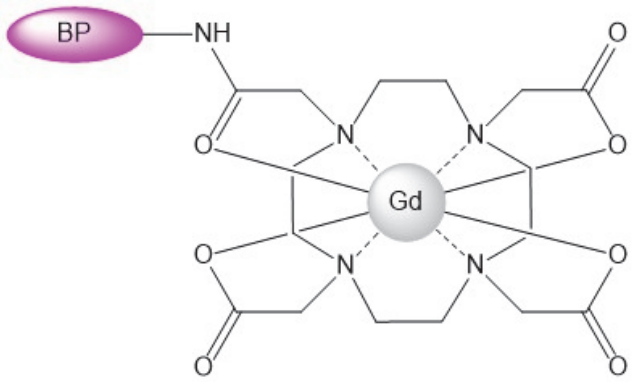

Figure 5: Structure of a gadolinium-based contrast agent consisting of DOTA connected to a variable binding part (BP), which binds the target.

1.3.2 Preclinical molecular MR imaging

Several preclinical studies investigated the potential of molecular MRI, using mainly small animal models. There are various different biomarkers of interest, based on the present understanding of the pathogenesis of AAAs. Especially the degradation of ECM proteins (e.g. elastin and collagen), as well as inflammatory processes, including the accumulation of macrophages, the release of cytokines (e.g. interleukins) and ECM degrading enzymes (MMPs), represent promising targets for tracking aneurysm progression or evaluating the effects of potential therapeutics (97).

For the characterization of the temporal progression of experimental AAAs, Klink *et al.* used a paramagnetic/fluorescent micellar nanoparticles functionalized with a collagen-binding protein (CNA-35) for molecular MRI of collagen. AAAs were induced in male C57BL/6 mice *via* a combination of Ang II infusion and transforming growth factor β neutralization. The intravenous injection of CNA-35 micelles after 4 weeks of Ang II infusion resulted in a significant higher MR signal enhancement in the aneurysmal wall compared to non-specific micelles. Histological analysis demonstrated a clear co-localization of CNA-35 with type I collagen. To proof the predictive value of molecular MRI, it was tested whether molecular MRI can discriminate between stable AAA lesions and aneurysms that are prone to severely progress or rupture. CNA-35 micelles enhanced molecular MRI was performed at day 5 and 15 after the onset of AAA. Stable aneurysms were associated with increased expression of collagen fibers in the aortic wall and high CNA-35 uptake while ruptured AAAs showed a significant collagen degradation and low CNA-35 uptake (100, 101).

Due to the crucial role of elastin fragmentation during the development and progression of AAAs, a molecular elastin-specific MRI probe was recently tested in several studies. Using different small animal models, including Ang II-infused ApoE-/- mice and a mice model of Marfan syndrome ($Fbn1^{C1039G/+}$), it was possible to image and quantify the decrease of elastin content within the aortic wall (102, 103). In male ApoE-/- mice, the specific rupture site of aortic elastic laminae could be visualized even before the dilation of the aorta (103). This elastin-specific probe offers, therefore, the potential to detect and quantify alterations of the aortic wall before aortic dilatation occurs. Furthermore, this probe was already successfully tested in a swine model of coronary injury for detection and quantification of vascular remodeling (104).

To evaluate the potential of ultra-small and small superparamagnetic iron oxide particles as a marker of activated monocytes and macrophages, different studies were performed especially using Resovist®, a SPIO, and ferumoxtran-10, an USPIO. Both were tested in an Ang II infusion ApoE-/- mouse model with MR imaging performed directly after particle injection and 24h post-injection. A significantly reduced signal intensity was evident primarily along the

aneurysm shoulder and outer layer of AAA in correspondence with regions of macrophage infiltration, indicating acute inflammatory processes within the aortic wall (105, 106).
Matrix metalloproteinases are further potential markers of inflammation in AAA formation and progression. MMPs were successfully targeted in an elastase-induced AAA rat model using the molecular probe P947. Rats showing a significant increase in MR signal following P947 injection also showed high levels of pro-MMP-9 and pro-MMP-2 in the aortic media. In addition, the area of contrast enhancement on MRI images was clearly co-localized with the fluorescence generated by MMPs in the AAA inflammatory area, as detected by *ex vivo* analysis (101, 107).

1.3.3 Clinical molecular MR imaging

Clinical studies with AAA patients are of high importance and indispensable for the introduction of molecular imaging into clinical practice. Special attention has been recently paid to the use of MRI in combination with iron oxide particles in a clinical setting (101).
Two clinical studies with overall 43 AAA patients demonstrated the potential of USPIO particles to detect focal inflammation within the aneurysmal wall. 25-36 hours following USPIO administration, T2* weighted MR imaging enabled the visualization and quantification of particle accumulation in the aortic wall. Furthermore, patients were followed-up to evaluate the predictive value of the molecular MRI. Patients who have shown the highest mural USPIO uptake, demonstrated a 3-fold higher AAA growth rate compared to those with lower particle uptake, despite having similar aortic diameters (108, 109). Therefore these studies proof once again that the aneurysm diameter is limited as a prognostic factor for the prediction of aneurysm expansion (101). Another study investigating SPIOs in AAA patients showed similar results. The decrease of MR T2* signal intensity as a result of SPIO phagocytosis by macrophages in the aneurysmal wall correlated strongly with levels of leucocyte infiltration and MMP-9 (101, 110). In 2017 the first prospective multicenter observational cohort study was published, investigating over 300 patients with AAAs using USPIO-enhanced MRI and consequent monitoring and clinical follow-up for ≥ 2 years. This prospective clinical study was the largest and the first to demonstrate that USPIO-enhanced MRI identifies cellular inflammation and predicts the rate of aneurysm expansion as well as the future risk of abdominal aortic aneurysm rupture or repair (111).

In contrast to iron oxide particles, gadolinium-based probes or other nanoparticles have not been tested so far in a clinical setting due to relatively high regulatory hurdles (101).

2 Aims and Objectives of the Thesis

The aim of this thesis is the evaluation of *in vivo* molecular MR imaging for the analysis of an AAA mouse model, by verifying three hypotheses:

Hypothesis 1: Magnetic resonance imaging using an elastin-specific imaging probe in combination with iron oxide particles enables the diagnosis and characterization of different stages of abdominal aortic aneurysms in a mouse model.

Hypothesis 2: Information from a combined application of both molecular probes, enables a reliable prediction of aortic rupture.

Hypothesis 3: Molecular MR imaging using an elastin-specific imaging probe enables the early visualization and quantification of therapeutic effects of the interleukin-1β inhibitor 01BSUR on aneurysm development.

3 Publication I

Concurrent Molecular Magnetic Resonance Imaging of Inflammatory Activity and Extracellular Matrix Degradation for the Prediction of Aneurysm Rupture

Short title: Brangsch et al; Molecular MRI of Aneurysms

Authors: Julia Brangsch[1,2] ,DVM, Carolin Reimann[1,2],DVM, Jan O. Kaufmann[1,3,4], MSc, Lisa C. Adams[1], MD, David C. Onthank[5], PhD, Christa Thöne-Reineke[2],DVM, Simon P. Robinson[5],PhD, Rebecca Buchholz[6], MSc, Uwe Karst[6], PhD, Rene M. Botnar[7,8,9], PhD, Bernd Hamm[1], MD, Marcus R. Makowski[1,7,8], MD

[1]Charité – Universitätsmedizin Berlin, corporate member of Freie Universität Berlin, Humboldt-Universität zu Berlin, and Berlin Institute of Health, Charitéplatz 1, 10117 Berlin, Germany
[2]Department of Veterinary Medicine, Institute of Animal Welfare, Animal Behavior and Laboratory Animal Science, Freie Universität Berlin, Königsweg 67, Building 21, 14163 Berlin, Germany
[3]Federal Institute for Materials Research and Testing (BAM), Division 1.5 Protein Analysis, Richard-Willstätter-Str. 11, 12489 Berlin, Germany
[4]Humboldt-Universität zu Berlin, Department of Chemistry, Brook-Taylor-Str. 2, 12489 Berlin, Germany
[5]Lantheus Medical Imaging, North Billerica, Massachusetts, USA, 331 Treble Cove Road, USA
[6]Institute of Inorganic and Analytical Chemistry, Westfälische Wilhelms-Universität Münster, Corrensstr. 30, 48149 Münster, Germany
[7]King's College London, School of Biomedical Engineering and Imaging Sciences, United Kingdom, St Thomas' Hospital Westminster Bridge Road, London SE1 7EH, United Kingdom
[8]BHF Centre of Excellence, King's College London, United Kingdom, Denmark Hill Campus, 125 Coldharbour Lane, London SE5 9NU, United Kingdom
[9]Escuela de Ingeniería, Pontificia Universidad Católica de Chile, Santiago, Chile.

Journal: Circulation: Cardiovascular Imaging 019;12:e008707, ©2019 American Heart Association, Inc., received November 23, 2018; accepted January 18, 2019.

DOI: https://doi.org/10.1161/CIRCIMAGING.118.008707

Key Words: aneurysm, extracellular matrix, inflammation, macrophage, magnetic resonance imaging

Abstract

Background: Molecular magnetic resonance imaging is a promising modality for the characterization of abdominal aortic aneurysms (AAAs). The combination of different molecular imaging biomarkers may improve the assessment of the risk of rupture. This study investigates the feasibility of imaging inflammatory-activity and extracellular-matrix-degradation by concurrent dual-probe molecular MRI in an AAA-mouse-model.

Methods: Osmotic minipumps with a continuous infusion of Ang II (angiotensin II; 1000ng/[kg·min]) to induce AAAs were implanted in apolipoprotein-deficient-mice (N=58). Animals were assigned to two groups. In group 1 (longitudinal-group, n =13), imaging was performed once after 1 week with a clinical dose of a macrophage-specific iron oxide based-probe (ferumoxytol, 4 mgFe/kg, surrogate marker for inflammatory activity) and an elastin-specific gadolinium-based probe (0.2 mmol/kg, surrogate-marker for extracellular matrix degradation). Animals were then monitored with death as end-point. In group 2 (week-by-week-group), imaging with both probes was performed after 1, 2, 3, and 4 weeks (n=9 per group). Both probes were evaluated in 1 magnetic resonance session.

Results: The combined assessment of inflammatory activity and extracellular matrix degradation was the strongest predictor of AAA-rupture (sensitivity 100%; specificity 89%; area under curve, 0.99). Information from each single probe alone resulted in lower predictive accuracy. In vivo measurements for the elastin- and iron oxide probe were in good agreement with ex vivo histopathology (Prussian blue stain: R^2=0.96, P<0.001; Elastica van Giesson stain: R^2=0.79, P<0.001). Contrast-to-noise-ratio measurements for the iron oxide and elastin-probe were in good agreement with inductively coupled mass spectroscopy (R^2=0.88, R^2=0.75, P<0.001) and laser ablation coupled to inductively coupled plasma-mass spectrometry.

Conclusion: This study demonstrates the potential of the concurrent assessment of inflammatory activity and extracellular matrix degradation by dual-probe molecular magnetic resonance imaging in an AAA mouse model. Based on the combined information from both molecular probes, the rupture of AAAs could reliably be predicted.

Clinical Perspective

Abdominal aortic aneurysms (AAAs) are the third leading cause of death after myocardial infarction and stroke in the group of cardiovascular diseases. The incidence of AAAs has been continuously increasing, currently occurring in 3-4% of men aged over 65 years. Although there are several causes leading to aneurysm formation, including trauma or connective-tissue diseases, most AAAs are still categorized as ‘non-specific’. Regardless of the cause, progressive dilatation of the aortic-wall can result in AAA rupture, with a mortality rate of >90%. Molecular MRI is a promising modality for the characterization of abdominal aortic aneurysms. The combination of different molecular imaging biomarkers may improve the assessment of the risk of rupture. This study demonstrates the potential of the concurrent assessment of inflammatory activity and extracellular-matrix degradation by dual-probe molecular MRI in an experimental mouse model of AAA. Based on the combined information from both molecular probes the rupture of AAAs could reliably be predicted, with higher accuracy compared to each probe alone. The combined in vivo quantification of these biomarkers in one imaging session may be useful to improve the in vivo characterization of AAAs.

Introduction

Abdominal aortic aneurysms (AAAs) are the third leading cause of death after myocardial infarction and stroke in the group of cardiovascular diseases.[1] The incidence of AAAs has been continuously increasing, currently occurring in 3-4% of men aged over 65 years.[2] Although there are several causes leading to aneurysm formation, including trauma or connective-tissue diseases, most AAAs are still categorized as 'non-specific'.[2] Regardless of the cause, progressive dilatation of the aortic-wall can result in AAA rupture, with a mortality rate of >90%.[3]

Formation, progression, and rupture of AAAs involve two key processes, which are inseparably connected: inflammation and extracellular-matrix (ECM) degradation, including the breakdown of elastic fibers. Both processes represent a key factor for the clinical outcome of AAAs.[4] During the initial phase of aortic aneurysm development, proinflammatory cells accumulate within the medial wall and produce cytokines and proteases leading to degradation, and dilatation of the aortic-wall.[5] The breakdown of ECM proteins in the aortic-wall, especially elastin and collagen, leads to an inability of the vessel wall to withstand the pulsating intraluminal pressure.[4] The stronger the inflammatory process and the more pronounced the degradation of ECM proteins, the higher the probability of AAA rupture.[6]

For the diagnosis of AAAs in clinical practice, CT, magnetic resonance imaging (MRI), or ultrasound-based angiographic techniques are still the reference standard. Besides aortic diameter, there is currently no established biomarker available for the evaluation of risk of aortic rupture.[2] In the past several years, molecular MRI has been successfully used for the visualization of proinflammatory cells and ECM proteins for the evaluation of AAAs.[7-10] However, the merits of a combined assessment of inflammatory activity and ECM degradation in 1 MRI examination has not been evaluated so far.

The aim of the present study was to test the feasibility and predictive value of concurrent multitarget dualprobe molecular MRI for the *in vivo* characterization of AAAs in an experimental mouse model. Iron oxide particles were used for the visualization of the inflammatory activity whereas an elastin-specific gadoliniumbased probe was used to visualize ECM degradation.

Methods

The data that support the findings of this study are available from the corresponding author on reasonable request.

Animal experiments

All procedures were performed according to the guidelines and regulations of the Federation of Laboratory Animal Science Associations and the local Guidelines and Provisions for Implementation of the Animal Welfare Act. Male ApoE-knockout (B6.129P2-ApoE^{tm1Unc}/J) were obtained from the Research Institute of Experimental Medicine at the Charité Berlin. For aneurysm induction, osmotic minipumps (Alzet model 2004, Durect Corp) were implanted subcutaneously in the dorsal neck region at the age of 8 weeks (n=36). For up to 28 days, Ang II (angiotensin II) was continuously infused with a rate of 1000 ng/(kg·min). Sham-operated ApoE$^{-/-}$mice (n=9) delivered saline over a course of 28 days, serving as the control group. In group 1 (longitudinal study, n=13), the first day of imaging included imaging before and after the administration of 0.2 mmol/kg of an elastin-specific contrast agent. After the second magnetic resonance (MR) scan, a clinical dose (4 mg Fe/kg) of ferumoxytol was administered. After 24 hours, MRI was repeated, including imaging before and after the administration of 0.2 mmol/kg of an elastin-specific contrast agent (Figure 1A). Animals were then followed up for 4 weeks with death as end point, to evaluate the potential of both probes for the prediction of aneurysm rupture. In group 2 (week-by-week study), imaging was performed after 1, 2, 3, and 4 weeks (n=9 per group) of Ang II infusion after administration of both probes (Figure 1B). *Ex vivo* analysis (histology, immunohistochemistry, inductively coupled mass spectroscopy (ICP-MS), and laser ablation coupled to inductively coupled plasma-mass spectrometry) was performed after the final scan of each week (n=9 per week) to correlate in vivo with ex vivo results. As control, 9 ApoE$^{-/-}$ mice were implanted with osmotic minipumps primed with sodium chloride. Please refer to the Data Supplement for further details.

Gadolinium-based elastin-specific contrast agent

The elastin-specific probe (ESMA; Lantheus Medical Imaging, North Billerica, MA) is composed of the D-amino-acid homophenylalanine, which is linked to a gadolinium-diethylenetriaminepentaacetic acid (Gd-DTPA) complex.[11,12] Ex vivo measurements obtained a longitudinal relaxivity for the agent bound to mice aortas of 8.65±0.42 mmol/L^{-1} s^{-1} at 3 T.[11] This probe has already been introduced in different previous studies in the context of aortic aneurysm[7,10,13] as well as atherosclerosis.[11,12] In this study, a clinical dose of 0.2 mmol/kg was used and administered via the tail vein on day 1 and 2 of MR imaging.

Iron oxide-based macrophage-specific agent

Iron oxide particles lead to a strong decrease in T1 and T2/ T2* relaxation time and therefore to a signal void in the corresponding MR images.[14] In this study, we used ferumoxytol (Feraheme, AMAG Pharmaceuticals, Waltham, MA), an ultrasmall superparamagnetic iron oxide particle.[15] With a relative size of 30 nm, the iron particles are phagocytized by cells of the mononuclear phagocyte system. Ferumoxytol shows a prolonged blood-pool-phase with a plasma half-life of 14 to 21 hours and delayed intracellular uptake.[14] Therefore, MR imaging was performed 24 hours after administration of a clinical dose (4 mg Fe/kg) via the tail vein.

In Vivo MR Experiments

For all imaging sessions, a clinical 3T Siemens system (Biograph, Siemens Healthcare Solutions, Erlangen, Germany) and a clinical approved single loop coil (47 mm) were used. For details on the T1-weighted and T2*-weighted sequences please refer to the Data Supplement.

Assessment of MRI signal

Assessment of the gadolinium-based elastin-specific probe on T1-weighted sequences

All resulting MR images were analyzed using OsiriX (version 7.1, OsiriX foundation). Morphometric measurements were conducted on high-resolution MRI images. For signal measurements, regions-of-interest were defined as areas of signal enhancement, which were colocalized with areas of aneurysmal aortic tissue. For these areas, the contrast-to-noise ratio (CNR) was calculated as follows: CNR = (combined vessel wall and aneurysmal aortic tissue signal – blood signal) / SD signal (noise). Noise was defined as the SD in pixel intensity from a region-of-interest placed in the background air anterior to the aorta.

Quantification of iron oxide on T2*-weighted sequences

The aortic aneurysm areas were assessed by comparison (subtraction) of precontrast T2*-weighted MR images before iron oxide injection and images 24 hours postinjection. Using identical window and level settings, the areas of signal void within the regions-of-interest (mm2) were measured. Identical 2-dimensional segmentation parameters were used to establish areas semiautomatically.

Histological analysis of aortic aneurysms and aortic aneurysm morphometry

Histological analysis is provided in Data Supplement.

Immunofluorescence analysis

Immunofluorescence analysis is provided in the Data Supplement.

ICP-MS and element specific bioimaging using laser ablation coupled to inductively coupled plasma-mass spectrometry

ICP-MS and Element Specific Bioimaging is provided in Data Supplement.

Competition experiments

Details on competition experiments are provided in the Data Supplement.

Statistical Analysis

Values are specified as mean±SD. For the comparison of continuous variables, a Student *t* test (unpaired, 2-tailed) was applied. Sensitivities and specificities of imaging measurements were compared with survival data of the animals (the reference standard). Linear regression was applied to determine the relationship between in vivo and the ex vivo measurements. A $P < 0.05$ was considered to indicate a statistically significant difference.

Results

For details on the study setup please see Figure 1. In sham-operated mice (n=9), which served as control-group and received a continuous saline-infusion for 28 days, AAA development was not observed (Figure 1 and 2).

Concurrent molecular MRI of inflammatory activity and ECM degradation for the prediction of aneurysm rupture (group 1, longitudinal group)

To evaluate the potential of multitarget MRI as a prognostic tool for aneurysm rupture, a longitudinal investigation of ApoE$^{-/-}$ mice was performed (group 1, longitudinal group, n=13). After 1 week of Ang II infusion, the administration of the iron oxide particles resulted in an 85% larger signal void on T2*-weighted images (P=0.004) in animals suffering subsequent deadly aneurysm rupture (n=4) compared with animals which survived (n=9; Figures 3A, 4A, and 4B). Based on the signal void resulting from the iron oxide particles, AAA rupture could be predicted with a sensitivity of 80%, a specificity of 89% (cutoff 0.565), and an area under the curve of 0.91 (Figure 3B). This finding suggests that the accumulation of proinflammatory macrophages within the aneurysmal wall represents a novel imaging biomarker for aneurysm rupture.

After 1 week of Ang II infusion, the elastin-specific MR probe in animals, which died of aneurysm rupture, showed an 84% lower CNR (P=0.03) on T1-weighted images compared with surviving animals (Figures 3A, 4A, and 4B). Based on the signal from the elastin-specific probe, AAA rupture could be predicted with a sensitivity of 80%, a specificity of 78% (cutoff 0.59), and an area under the curve of 0.82 (Figure 3C). This observation suggests that the breakdown of elastic fibers within the aneurysmal wall also represents a novel imaging biomarker for aneurysm rupture.

The combined assessment of the iron oxide particles and elastin-specific probe demonstrated the highest accuracy for the prediction of aneurysm rupture with a sensitivity of 100%, a specificity of 89% and an area under the curve of 0.99 (Figure 3D), compared with each parameter alone.

Concurrent imaging of inflammatory activity and ECM degradation for the characterization of different stages of aortic aneurysms (group 2, week-by-week-group)

Ang II infusion resulted in an average increase of 81% in the aortic diameter after 7 days, of 250% after 14 days and of 276% after 28 days (Figure I in the Data Supplement).

In early-stage aneurysms, 1 week after Ang II infusion, the degradation of elastic laminae with an associated dissection of elastic fibers could be observed in *vivo*, using the elastin-specific probe and *ex vivo* with histology showing a dilation of the aortic lumen and the formation of an intramural hematoma in 70% of the mice. Simultaneously, an increasing MR signal void in the area of the aortic wall was observed based on the accumulation of the iron oxide particles and *ex vivo* histology. Between 2 and 3 weeks following Ang II infusion, further degradation of elastic fibers was observed, being associated with an additional increase in aortic diameter (Figure 5A1-7). Additionally, an increased inflammatory response was observed, which involved the infiltration of macrophages.

In late-stage aneurysms, 4 weeks after Ang II infusion, strong ECM remodeling at the rupture site was observed characterized by expression of elastic fibers *in vivo* and *ex vivo* (Figure 5B1-5B7).

T2-weighted MR imaging for the assessment of macrophage-specific iron oxide particles*

Before the administration of the macrophage-specific iron oxide particles, a bright circular lumen was observed on cross-sectional T2*-weighted images of the abdominal-aorta in all Ang II- infused and saline-infused mice. Twenty-four hours after ferumoxytol-injection, a significant MRI signal loss on T2* sequences could be observed in the aneurysmal aortic-wall of mice treated with Ang II infusion (Figure 5B3), whereas no significant MRI signal changes were found in control mice (Figure 2A3). The area of MRI signal void was localized in the aneurysmal wall close to dissection site and the area increased with AAA progression up to 4 weeks. *In vivo* MRI measurements showed a strong correlation with *ex vivo* analysis of Prussian blue-stained iron particles on histological sections ($y=0.11x+0.17$; $R^2=0.96$; $P<0.001$, Figure IIA in the Data Supplement).

T1-weighted MR imaging for the assessment of the gadolinium-based elastin-specific probe

A low CNR was measured in the aortic-wall on all MR scans before to the administration of the elastin-specific probe in Ang II- infused and saline-infused mice. After the administration of the elastin-specific agent, a significant increase ($P<0.001$) in CNR in the aneurysmal aortic wall was measured (Figure 5B2). These findings correlated with *ex vivo* measurements of elastic fiber density on histological sections using the Elastica van Gieson staining ($y=0.09x+5.37$; $R^2=0.79$, $P<0.001$, Figure IIB in the Data Supplement).

Influence of the iron oxide particles on the visualization of the gadolinium-based elastin-specific probe and vice versa

CNR measurements on T1-weighted images before and 24 hours after the administration of iron oxide particles were performed in a subgroup (n=9), showing a strong correlation between CNR measurements at both days ($y=0.96x+0.27$; $R^2=0.99$; Figure IIIA in the Data Supplement). No significant difference (P=0.18) was measured between the 2 days, indicating that the iron oxide particles did not affect the visualization and quantification of the elastin-specific probe on T1-weighted-scans. In addition, 24 hours after the administration of the iron oxide particles, T2*-weighted-imaging was performed before and 45 minutes after the administration of the elastin-specific probe. Measurements on T2*-weighted images before and after the administration of the gadolinium-based probe showed a strong correlation ($y=1.03x-0.01$; $R^2=0.97$; Figure IIIB in the Data Supplement) and no significant difference (P=0.88) between both time points.

Correlation of in vivo measurements of the elastin-specific probe with ex vivo histology

To investigate the spatial distribution of elastic fibers in aortic aneurysms, histological sections were stained with the Elastica van Giesson staining, and the percentage of elastic fibers in relation to the overall adventitial area was determined. Histological ex vivo measurements were in good correlation with in vivo T1-weighted MR sequences using the elastin-specific probe ($y=0.09x+5.37$; $R^2=0.79$, Figure IIB in the Data Supplement).

Correlation of in vivo measurements of iron oxide particles with ex vivo histology and immunohistochemistry

Immunofluorescence staining with an anti-CD68 monoclonal antibody as tissue macrophage marker was used to evaluate macrophage accumulation in the aneurysmal tissue (Figure 5A7and 5B7). Perls Prussian blue staining and CD68-staining of adjacent histological sections confirmed the colocalization of macrophages and iron oxide particles (Figure IVA in the Data Supplement). A strong correlation was found between areas positive for CD68 and Prussian blue-stained areas in relation to the overall adventitial area ($y=1.03x+0.80$; $R^2=0.98$; Figure IVB in the Data Supplement). Additionally, a strong correlation was measured between the area of signal void on in vivo T2* sequences after the administration of the iron oxide particles and the ex vivo Prussian blue stain ($y=0.11+ 0.17$; $R^2=0.96$).

Gadolinium concentration by ICP-MS

Measurements by ICP-MS were performed in 12 mice (n=3 mice per time point and n=3 control mice). *In vivo* CNR measurements correlated strongly with *ex vivo* measured gadolinium concentrations by ICP-MS (Figure IIC in the Data Supplement). Also, a significant correlation between *in vivo* T2* measurements and *ex vivo* measured iron ions content by ICP-MS was observed (Figure IID in the Data Supplement).

Spatial localization of the gadolinium-based elastin-specific probe and iron oxide particles using laser coupled mass spectrometry

The spatial distribution of gadolinium and iron ions within the aneurysmal wall was visualized using laser ablation coupled to inductively coupled plasma-mass spectrometry. Sections of AAAs after 4 weeks of Ang II infusion (n=3) showed a strong co-localization of gadolinium with elastic fibers (Figure 6A3 and 6A4). Additionally, a clear colocalization of iron oxide particles with Prussian blue positive areas and macrophages (CD68) was demonstrated (Figure 6A5 and 6A6).

Competition experiments

The specific binding of the elastin probe was shown by an *in vivo* competition experiment in 3 mice (n=3) after 4 weeks of Ang II infusion. After the injection of a 10-fold higher dose of the nonparamagnetic europium-labeled elastin-specific probe, a significant decrease of CNR was observed compared with the administration of the gadolinium-labeled elastin-specific agent alone (Figure 6B).

Discussion

This study demonstrates the potential of the concurrent assessment of inflammatory activity and ECM degradation by dual-probe molecular MRI in an experimental mouse model of AAA. Based on the combined information from both molecular probes, the rupture of AAAs could be reliably predicted, with higher accuracy compared with each probe alone. The concurrent *in vivo* quantification of these biomarkers in 1 imaging session could be useful to improve the *in vivo* characterization of AAAs.

Molecular MRI for the characterization of aortic aneurysms

Even though the pathophysiology of AAAs is not fully elucidated yet, inflammation was shown to be a key process in AAA development. Especially macrophages play a central role by secreting inflammatory cytokines and proteases, such as MMPs (matrix-metalloproteinases).[4] In this context, the degradation of the ECM is another key biological process for AAA progression, including the breakdown of cross-linked elastin and collagen. The loss of medial elastin fibers due to increased degradation by different enzymes is thought to be the initiating event of AAA development.[16] Ongoing elastin degradation leads to reduced stability of the aortic wall.[16]

Inflammatory activity and ECM degradation represent promising *in vivo* biomarkers to improve the characterization of aneurysms and prediction of aortic rupture. Previous studies have shown that the application of the gadolinium-based elastin-specific probe, which was also used in the present study, allows the *in vivo* visualization of changes in elastin composition of the aortic-wall at different stages of aortic aneurysms.[7,17] Because of the shortening of the T1 relaxation times, gadolinium-based probes are visualized as a bright signal on T1-weighted sequences and can therefore be distinguished from iron oxide particles, which appear as signal void on T2/T2*-weighted sequences.

About iron oxide particles, several preclinical and clinical studies demonstrated the potential for imaging of macrophage activity in the aneurysmal wall.[9,18] Especially the MA3RS study (MRI Using Ultrasound Superparamagnetic Particles of Iron Oxide to Predict Clinical Outcome in Patients Under Surveillance for Abdominal Aortic Aneurysms) demonstrated that iron oxide particle enhanced MRI could identify aortic wall inflammation in patients with AAAs and predicts the rate of aneurysm growth and clinical outcome.[19]

In the late phase (12-24 h, uptake macrophages) iron oxide particles cause a local decrease in T2/T2* relaxation time, which corresponds to a signal void in the MR images. In a clinical

setting, patients with pronounced iron oxide particle accumulation within the aneurysmal wall, showed a 3-fold higher AAA growth rate compared to those with significantly lower particle uptake, despite having similar aneurysm diameters.[18] In contrast, in the early phase (blood pool phase) iron oxide particles lead to a significant shortening of the T1 relaxation time and can therefore also be used for the visualization of the vascular system in this initial phase.

Concurrent molecular MRI of inflammatory activity and ECM degradation for the prediction of aneurysm rupture

To our knowledge, this is the first study to show the feasibility of a dual-probe approach in a concurrent MR imaging session. In the present study, animals suffering subsequent deadly aneurysm rupture, showed a significantly higher MR signal void in the aneurysm wall *in vivo* after 1 week of Ang II infusion, compared with animals which survived. In our study, the iron oxide particles enabled the prediction of AAA rupture with a sensitivity of 80% and a specificity of 89%. This finding suggests that the accumulation of proinflammatory macrophages visualized by MRI within the aneurysmal wall represents a predictive marker for aneurysm rupture.

Regarding the ECM, after 1 week of Ang II infusion, a significantly stronger breakdown of elastic fibers in the aneurysmal wall was observed by MRI after one week of Ang II infusion in animals suffering subsequent deadly aneurysm rupture compared with animals which survived. The elastin-specific probe enabled the prediction of AAA rupture with a sensitivity of 80% and a specificity of 78%. This observation suggests that the breakdown of elastic fibers within the aneurysmal wall also represents a predictive imaging biomarker for aneurysm rupture.

Even though these 2 key processes, inflammatory activity, and ECM degradation, are inseparably linked, they represent 2 independent processes during the development and potential rupture of AAAs. Although one process reflects the cellular component, the other comprises the ECM component of AAA development. If both processes overlap or occur simultaneously, the formation of aortic aneurysm is most likely. In this study, we could show that the combined assessment of both imaging probes demonstrated the highest accuracy for the prediction of aneurysm rupture with a sensitivity of 100% and a specificity of 89%. These findings underline that there is an additional and independent value of each parameter to the other and that the combined MR based assessment of both processes improves the risk of rupture prediction in AAAs.

Translational potential of this study

For a potential clinical application of concurrent imaging with 2 different MR probes in 1 imaging session, it is of high importance that there is no influence of the iron-based probe on the visualization and quantification of the gadolinium-based probe and vice versa. As part of this study, we could demonstrate that the iron oxide-based probe does not affect the visualization and quantification of the elastin-specific probe on T1-weighted scans. We could also show that the gadolinium-based probe does not affect the visualization and quantification of the iron oxide-based probe on T2*-weighted scans.

This study has further advantages in clinical translation. The iron oxide-based agent ferumoxytol is approved by the Food and Drug Administration for the treatment of iron deficiency anemia in adults and is currently used as an MRI agent in a clinical setting. Both agents in this study were administered at a clinical dose. Despite using an ultrahigh field preclinical MR scanner for small animals, imaging was performed using a clinical 3 T MR scanner. Therefore, relaxation, rotational correlation, and signal properties can be directly translated to human application. Additionally, molecular size and composition, as well as clearance of the gadolinium-based probe, are comparable to contrast agents already used in clinical practice.[11]

Mouse model used in this study

The small animal model used in this study is one of the most commonly used AAA mouse models. In this model, AAAs develop spontaneously without the need for surgical intervention. The infusion of Ang II into male ApoE-deficient mice leads to a reproducible formation of AAAs in the suprarenal region.[20] The formation of AAAs in this model recapitulates several facets of human disease including inflammation, thrombus formation, and rupture.[21]

Study limitations

One main difference between human AAAs and those formed in Ang II infused mice is that in ApoE$^{-/-}$ mice, AAAs develop in the suprarenal region.[6,20] In addition, AAAs in human disease are generally not caused by dissection or intramural hematoma. Aortic dissections often lead on to the development of aneurysms but the vast majority of AAAs have a different pathophysiology**.** Ferumoxytol is not clinically approved for the assessment of aortic aneurysms and has to be used off-label with care because of potential risk of complement

activation. The elastin-specific-agent is also not approved for clinical use. The safety profile of both agents in combination has to be investigated before this approach can be translated into a patient setting. Regarding the use of ferumoxytol, it is not fully elucidated whether iron oxide uptake in the spleen does induce inflammatory macrophages that are then recruited to the inflammatory site. It was also suggested that iron oxide particles can be used to increase the M1 to M2 ratio in cancers with potential therapeutic benefit.[22] These effects have to be thoroughly studied before a translation into a patient setting.

Conclusion

This study demonstrates the potential of the concurrent assessment of inflammatory activity and ECM degradation by dual-probe molecular MRI in an experimental mouse model of AAA. Based on the combined information from both molecular probes the rupture of AAAs could reliably be predicted, with higher accuracy compared with each probe alone. The combined *in vivo* quantification of these biomarkers in one imaging session may be useful to improve the *in vivo* characterization of AAAs.

References

1. Krishnan A, Yadav K, Kaur M, Kumar R. Epidemiology to public health intervention for preventing cardiovascular diseases: the role of translational research. Indian J Med Res. 2010;132:643-50.

2. Sakalihasan N, Limet R, Defawe OD. Abdominal aortic aneurysm. Lancet. 2005;365(9470):1577-89.

3. Thompson RW, Geraghty PJ, Lee JK. Abdominal aortic aneurysms: basic mechanisms and clinical implications. Curr Probl Surg. 2002;39(2):110-230.

4. Hellenthal FA, Buurman WA, Wodzig WK, Schurink GW. Biomarkers of AAA progression. Part 1: extracellular matrix degeneration. Nat Rev Cardiol. 2009;6(7):464-74.

5. Shimizu K, Mitchell RN, Libby P. Inflammation and cellular immune responses in abdominal aortic aneurysms. Arterioscler Thromb Vasc Biol. 2006;26(5):987-94.

6. Saraff K, Babamusta F, Cassis LA, Daugherty A. Aortic dissection precedes formation of aneurysms and atherosclerosis in angiotensin II-infused, apolipoprotein E-deficient mice. Arterioscler Thromb Vasc Biol. 2003;23(9):1621-6.

7. Botnar RM, Wiethoff AJ, Ebersberger U, Lacerda S, Blume U, Warley A, et al. In Vivo Assessment of Aortic Aneurysm Wall Integrity Using Elastin-Specific Molecular Magnetic Resonance Imaging. Circulation: Cardiovascular Imaging. 2014;7(4):679-89.

8. Turner GH, Olzinski AR, Bernard RE, Aravindhan K, Boyle RJ, Newman MJ, et al. Assessment of macrophage infiltration in a murine model of abdominal aortic aneurysm. J Magn Reson Imaging. 2009;30(2):455-60.

9. Yao Y, Wang Y, Zhang Y, Li Y, Sheng Z, Wen S, et al. In Vivo Imaging of Macrophages during the Early-Stages of Abdominal Aortic Aneurysm Using High Resolution MRI in ApoE(−/−) Mice. PLoS ONE. 2012;7(3):e33523.

10. Makowski MR, Preissel A, von Bary C, Warley A, Schachoff S, Keithan A, et al. Three-dimensional imaging of the aortic vessel wall using an elastin-specific magnetic resonance contrast agent. Invest Radiol. 2012;47(7):438-44.

11. Makowski MR, Wiethoff AJ, Blume U, Cuello F, Warley A, Jansen CH, et al. Assessment of atherosclerotic plaque burden with an elastin-specific magnetic resonance contrast agent. Nat Med. 2011;17(3):383-8.

12. Onthank D, Yalamanchili P, Cesati R, Lazewatsky J, Azure M, Hayes M, et al. Abstract 1914: BMS753951: A Novel Low Molecular Weight Magnetic Resonance Contrast Agent Selective For Arterial Wall Imaging. Circulation. 2007;116(Suppl 16):II_411-II_2.

13. von Bary C, Makowski M, Preissel A, Keithahn A, Warley A, Spuentrup E, et al. MRI of coronary wall remodeling in a swine model of coronary injury using an elastin-binding contrast agent. Circ Cardiovasc Imaging. 2011;4(2):147-55.

14. Toth GB, Varallyay CG, Horvath A, Bashir MR, Choyke PL, Daldrup-Link HE, et al. Current and potential imaging applications of ferumoxytol for magnetic resonance imaging. Kidney International. 2017;92(1):47-66.

15. Knobloch G, Colgan T, Wiens CN, Wang X, Schubert T, Hernando D, et al. Relaxivity of Ferumoxytol at 1.5 T and 3.0 T. Investigative Radiology. 2018;53(5):257-63.

16. Daugherty A, Cassis LA. Mechanisms of abdominal aortic aneurysm formation. Curr Atheroscler Rep. 2002;4(3):222-7.

17. Okamura H, Pisani LJ, Dalal AR, Emrich F, Dake BA, Arakawa M, et al. Assessment of elastin deficit in a Marfan mouse aneurysm model using an elastin-specific magnetic resonance imaging contrast agent. Circ Cardiovasc Imaging. 2014;7(4):690-6.

18. Richards JM, Semple SI, MacGillivray TJ, Gray C, Langrish JP, Williams M, et al. Abdominal aortic aneurysm growth predicted by uptake of ultrasmall superparamagnetic particles of iron oxide: a pilot study. Circ Cardiovasc Imaging. 2011;4(3):274-81.

19. Investigators MRS. Aortic Wall Inflammation Predicts Abdominal Aortic Aneurysm Expansion, Rupture, and Need for Surgical Repair. Circulation. 2017;136(9):787-97.

20. Daugherty A, Manning MW, Cassis LA. Angiotensin II promotes atherosclerotic lesions and aneurysms in apolipoprotein E-deficient mice. J Clin Invest. 2000;105(11):1605-12.

21. Cassis LA, Gupte M, Thayer S, Zhang X, Charnigo R, Howatt DA, et al. ANG II infusion promotes abdominal aortic aneurysms independent of increased blood pressure in hypercholesterolemic mice. Am J Physiol Heart Circ Physiol. 2009;296(5):H1660-5.

22. Zanganeh S, Hutter G, Spitler R, Lenkov O, Mahmoudi M, Shaw A, et al. Iron oxide nanoparticles inhibit tumour growth by inducing pro-inflammatory macrophage polarization in tumour tissues. Nat Nanotechnol. 2016;11(11):986-94.

Acknowledgements

The elastin-specific contrast agent was provided by Lantheus Medical Imaging, North Billerica, MA. We are thankful for performed inductively coupled mass spectroscopy by Andy Cakebread, Mass Spectrometry Facility, King's College London, the London Metallomics Facility funded by the Wellcome Trust (grant reference 202902/Z/16/Z).

Sources of Funding

This study was funded by the Deutsche Forschungsgemeinschaft (DFG, German Research Foundation) – CRC 1340/1 2018, B01, MA 5943/3-1/4-1/9-1 and the British Heart Foundation (BHF) program grant - RG/12/1/29262. Dr Adams is grateful for her participation in the Berlin Institute of Health (BIH) Charité - Junior Clinician Scientist Program funded by the Charité – Universitaetsmedizin Berlin and the Berlin Institute of Health.

Disclosures

None.

Figure Legends

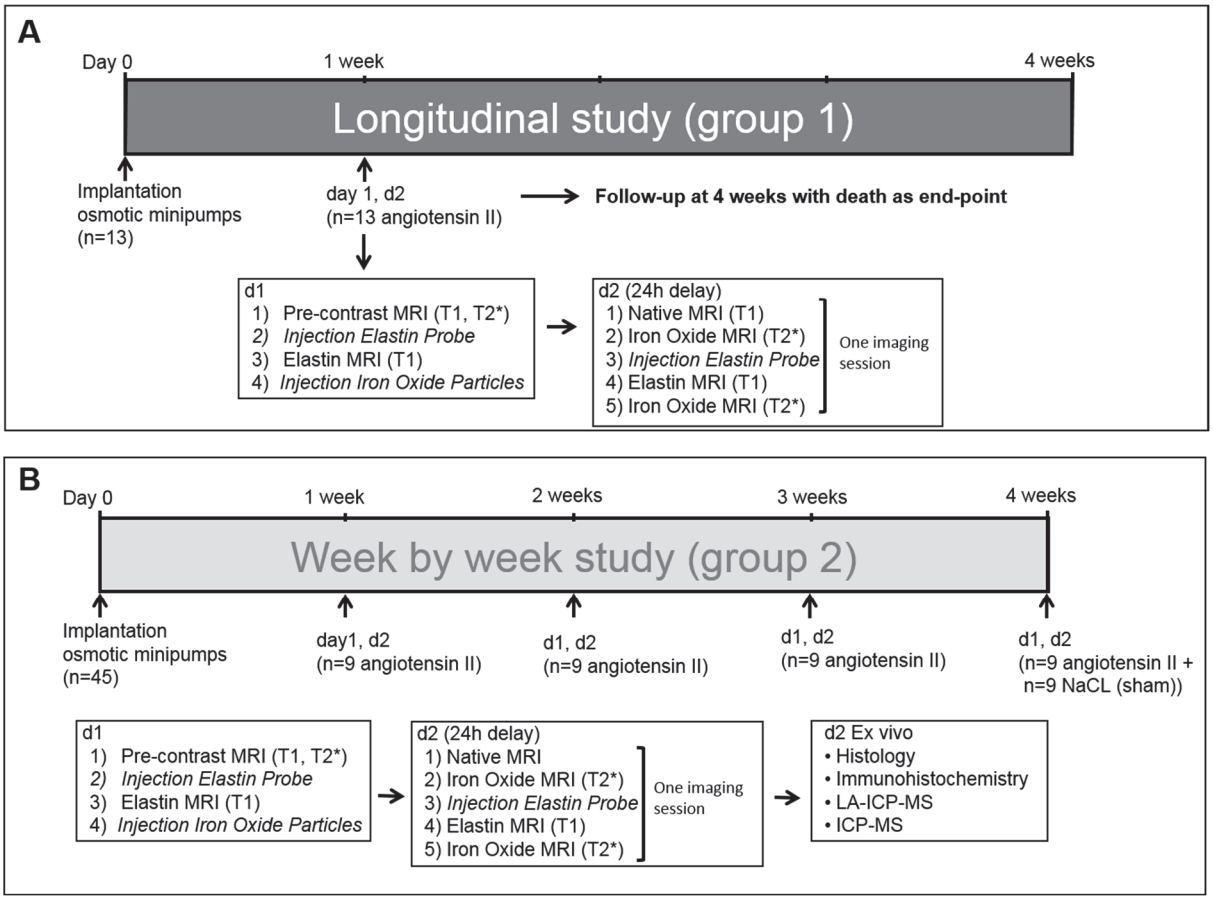

Figure 1. Experimental setup.

A: In group 1 (longitudinal study), imaging in 1 magnetic resonance (MR) session was performed only once after 1 week (n =13) with a clinical dose of macrophage-specific iron oxide particles (ferumoxytol, 4 mg Fe/kg, surrogate marker for inflammatory activity) and an elastin-specific gadolinium-based (0.2 mmol/kg, surrogate marker for extracellular matrix degradation). Animals were then followed up until week 4 with death as end point. B: In group 2 (week-by-week study), imaging was performed after 1, 2, 3 and 4 weeks (n=9 per group) of Ang II (angiotensin II) infusion after administration of both probes. Both probes were evaluated in 1 MR session. *Ex vivo* analysis was performed after the final scan of each week to correlate *in vivo* with *ex vivo* results.

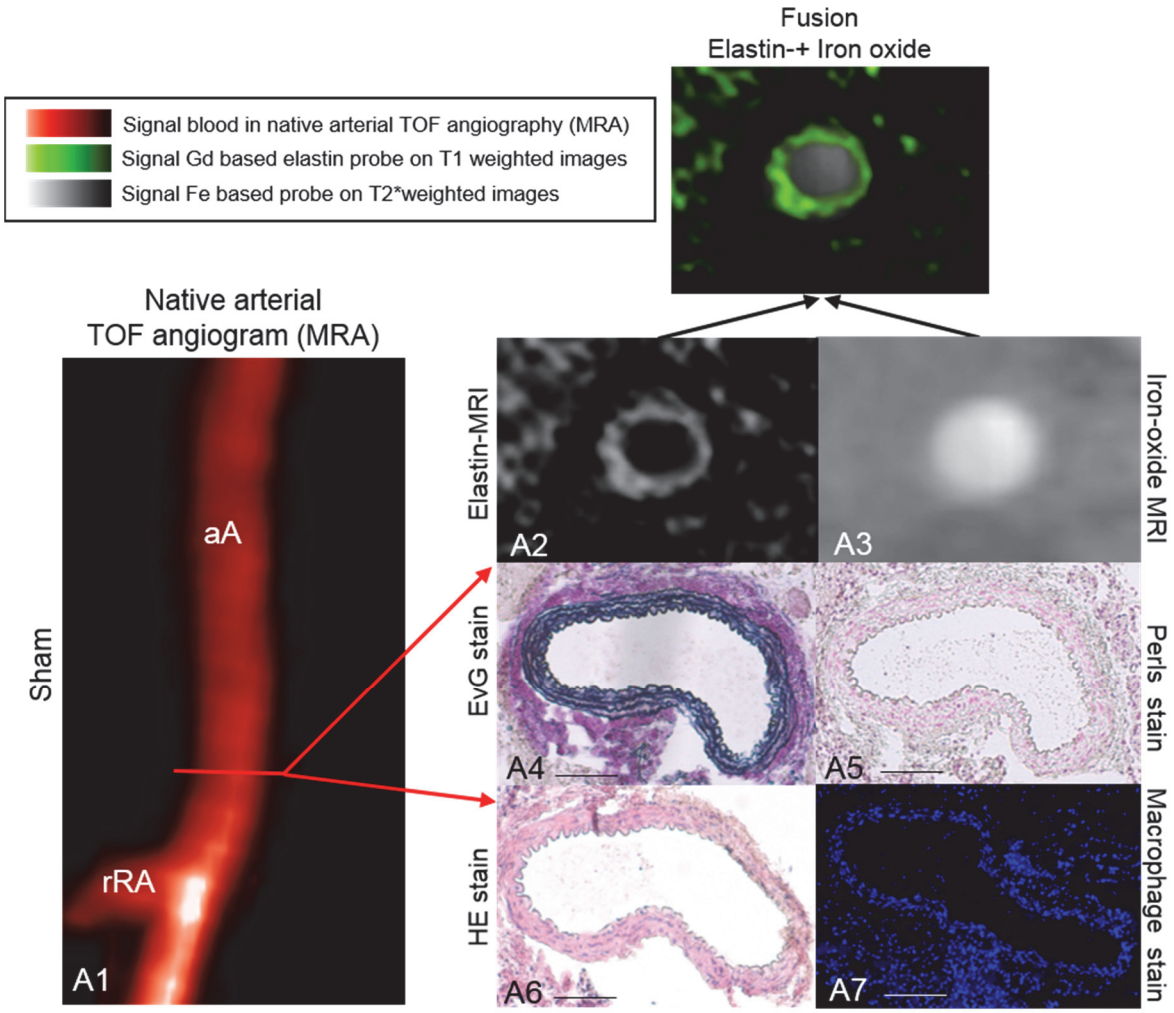

Figure 2. *In vivo* dual-probe molecular magnetic resonance imaging (MRI) and *ex vivo* assessment of the abdominal aorta in sham-operated mice.

A1, Time-of-flight angiogram showing the suprarenal abdominal aorta (aA), including the right renal-artery (rRA), of an ApoE$^{-/-}$ mouse after 4 weeks of saline infusion. The red line indicates the orientation of subsequently performed transverse MRI sequences and corresponding histological sections. **A2** and **A3**, No pathological changes of the aortic-wall were observed *in vivo* using the elastin-specific probe on the T1-weighted sequences (**A2**) and iron oxide particles on the T2*-weighted sequences (**A3**) or on corresponding *ex vivo* histology (**A4-A7**). To highlight the anatomic correlation of both probes, an automatic image fusion was performed (black arrows). Scale bars represent 100 µm. HE, hematoxylin-eosin staining; MRA, magnetic resonance-angiography; and TOF, arterial time-of-flight.

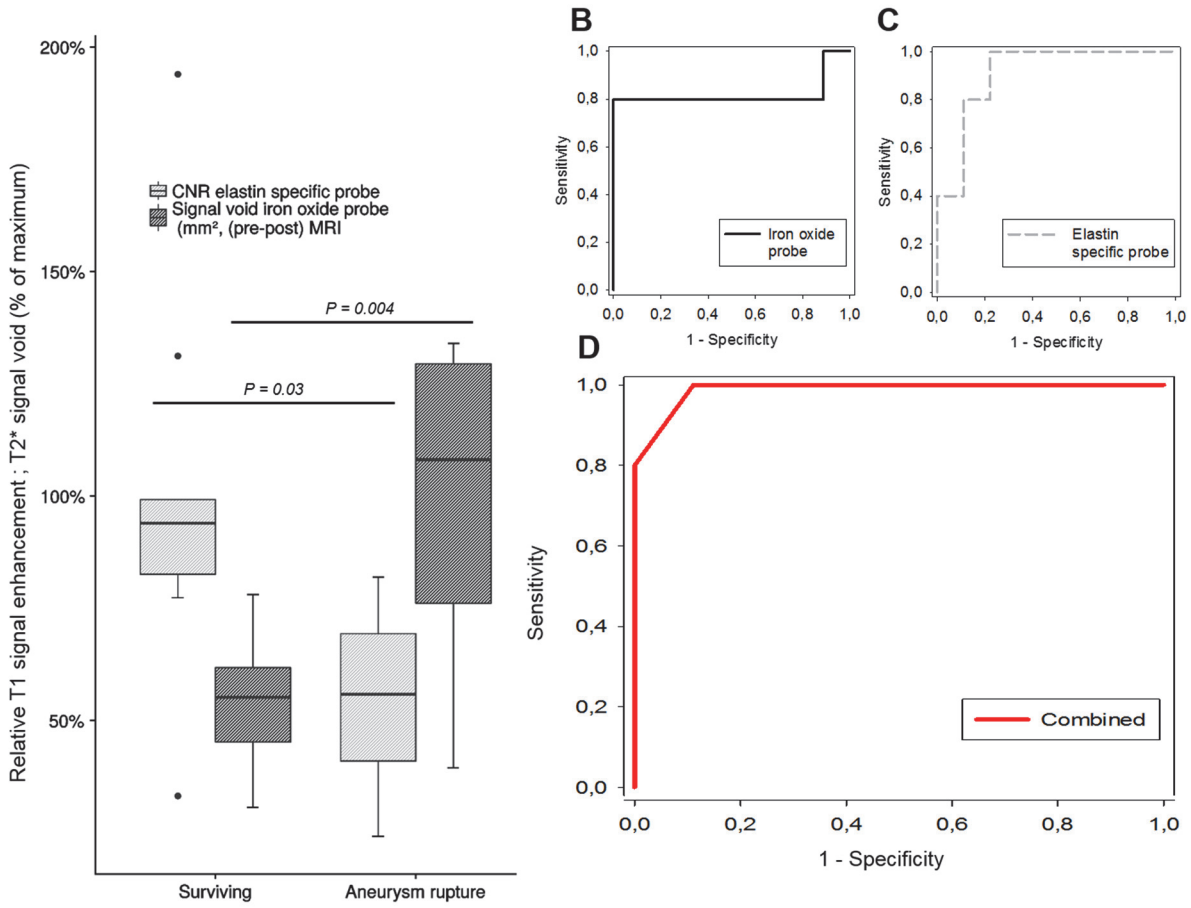

Figure 3. Diagnostic accuracy of molecular magnetic resonance imaging (MRI) of inflammatory activity and extracellular matrix degradation for the prediction of aneurysm rupture.

A, In animals suffering from aortic rupture, MRI with both probes demonstrated an elevated macrophage activity (P=0.004) and significantly lower elastin content (P=0.03) of the aneurysmal wall, compared with those surviving. **B**, Based on the MR signal void resulting from the iron oxide particles, abdominal aortic aneurysm (AAA) rupture could be predicted with a sensitivity of 80%, a specificity of 89%. **C**, Based on the signal from the elastin-specific probe, AAA rupture could be predicted with a sensitivity of 80%, a specificity of 78%. **D**: The combined assessment of both imaging probes demonstrated the highest accuracy for the prediction of aneurysm rupture with a sensitivity of 100%, a specificity of 89%. CNR indicates contrast-to-noise ratio.

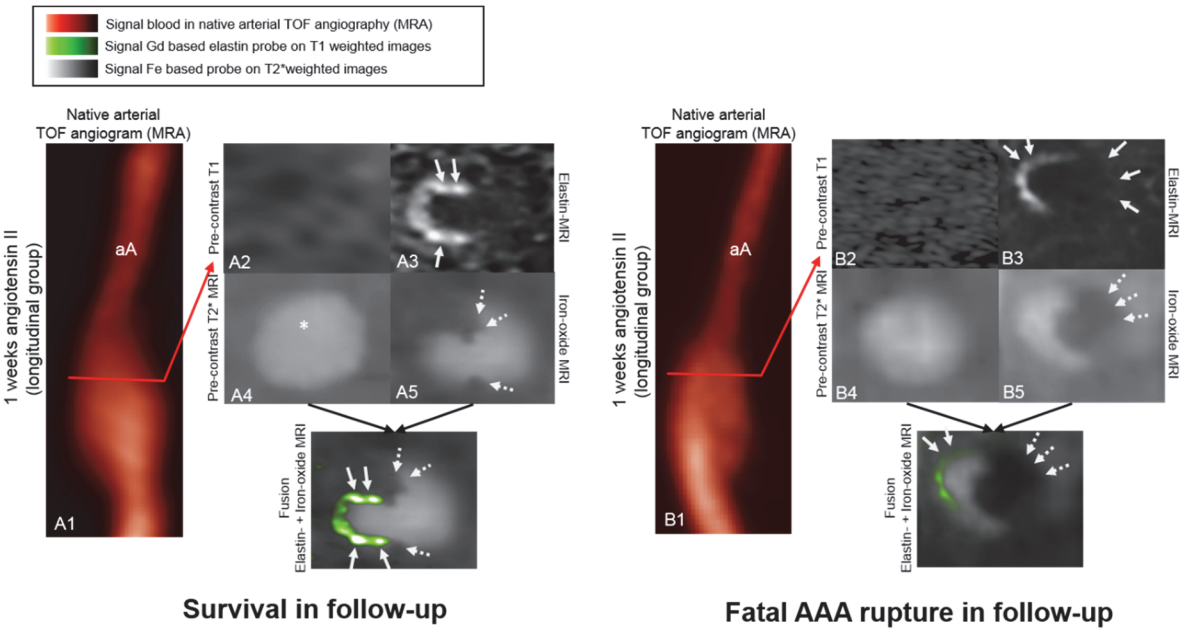

Figure 4. *In vivo* dual-probe molecular magnetic resonance imaging (MRI) of inflammatory activity and extracellular matrix degradation in animals with a stable aortic aneurysm and in animals with a fatal aortic rupture (longitudinal-group).

A1 and **B1**, Time-of-flight angiograms showing a comparable suprarenal abdominal-aorta (aA; no significant difference in maximum size, P=0.78) of 1 male ApoE$^{-/-}$ mouse surviving (**A1**) and 1 suffering from fatal aneurysm rupture (**B1**). **A2** and **B2,** Precontrast T1-weighted magnetic resonance (MR) scans show no relevant signal of the aortic aneurysm prior to the administration of the elastin-specific probe. **A4** and **B4**, A bright circular lumen/aortic aneurysm can be observed before the administration of the iron oxide particles. **A3** and **B3**, In the surviving animal (**A4**), a strong enhancement of the elastin-specific probe in the ruptured aortic wall is visualized, indicating only a minor breakdown of elastic fibers. In the animal, which suffered a fatal aneurysm rupture (**B4**), only a weak enhancement from the elastin-specific probe can be seen, indicating a pronounced breakdown of elastic fibers. **A5** and **B5**, In the surviving animal (**A5**), a minor signal void resulting from the accumulation of iron oxide particles in the ruptured aortic wall is visualized. In the animal, which suffered a fatal aneurysm rupture (**B5**), a strong signal void resulting from the iron oxide particles is visualized, indicating a pronounced influx of proinflammatory macrophages. The black arrows highlight the fusion of the elastin and iron oxide MR images to indicate the spatial relation of the different processes to each other. The solid arrows indicate the signal from the elastin-specific probe; the dotted arrows indicate the signal void resulting from the accumulation of the iron oxide particles. AAA indicates abdominal aortic aneurysm; MRA, MR angiography; and TOF: time-of-flight.

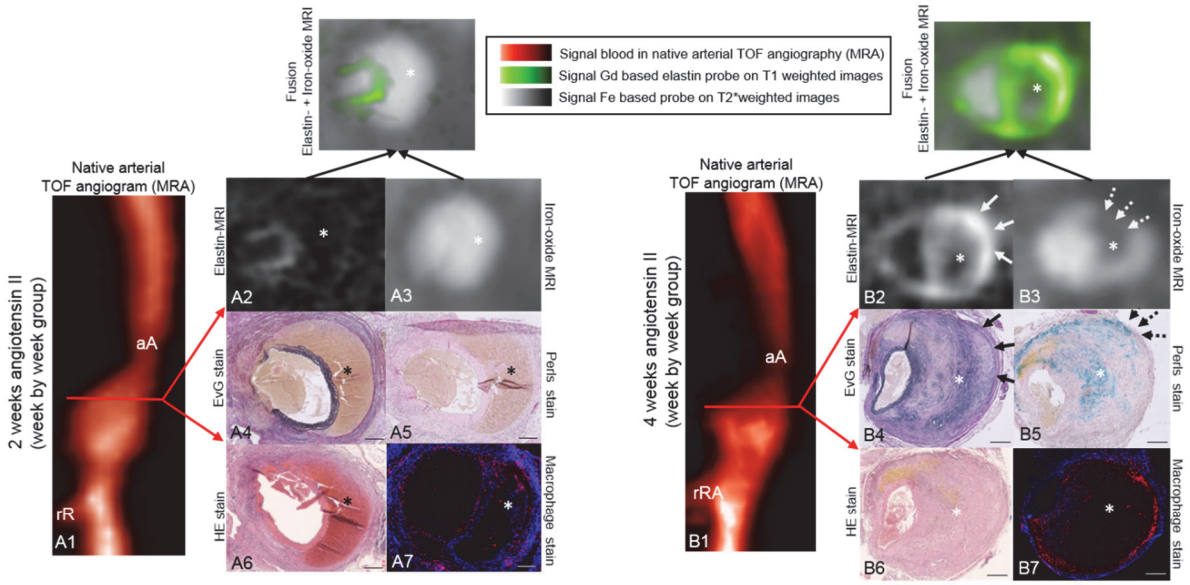

Figure 5. *In vivo* dual-probe molecular magnetic resonance imaging (MRI) of inflammatory activity and extracellular matrix degradation during the development of aortic aneurysms (week-by-week-group).

A1 and **B,** Time-of-flight angiograms show the suprarenal abdominal-aorta (aA), including the right renal-artery (rRA), of a male ApoE$^{-/-}$ mouse after 2 weeks (**A1**) and 4 weeks (**B1**) of Ang II (angiotensin II) infusion. **A2**, On T1-weighted sequences, a weak signal enhancement resulting from the elastin-specific probe in the aneurysmal wall was observed after 2 weeks of Ang II infusion. **B2**, After 4 weeks of Ang II- infusion, a strong remodeling of the rupture site by an expression of elastic fibers was observed *in vivo* by MRI after the administration of the elastin-specific probe. **A3**, Only a minor signal void resulting from the iron oxide particles on T2* sequences was be appreciated after 2 weeks of Ang II infusion. **B3**, The most pronounced signal void was observed after 4 weeks of Ang II infusion reflecting an increased macrophage infiltration into the aneurysmal wall (white dotted arrows). **A4-7** and **B4-7,** *Ex vivo* histological measurements using Perls Prussian blue staining and immunofluorescence for macrophage accumulation confirmed the *in vivo* findings. The solid arrows indicate the signal from the elastin-specific magnetic resonance (MR) probe; the dotted arrows indicate the signal void resulting from the accumulation of the iron oxide particles. Scale bars represent 200 µm. *Area of the thrombus. EvG indicates Elastica van Gieson; HE, hematoxylin-eosin staining; MRA, magnetic-resonance-angiography; and TOF, arterial time-of-flight.

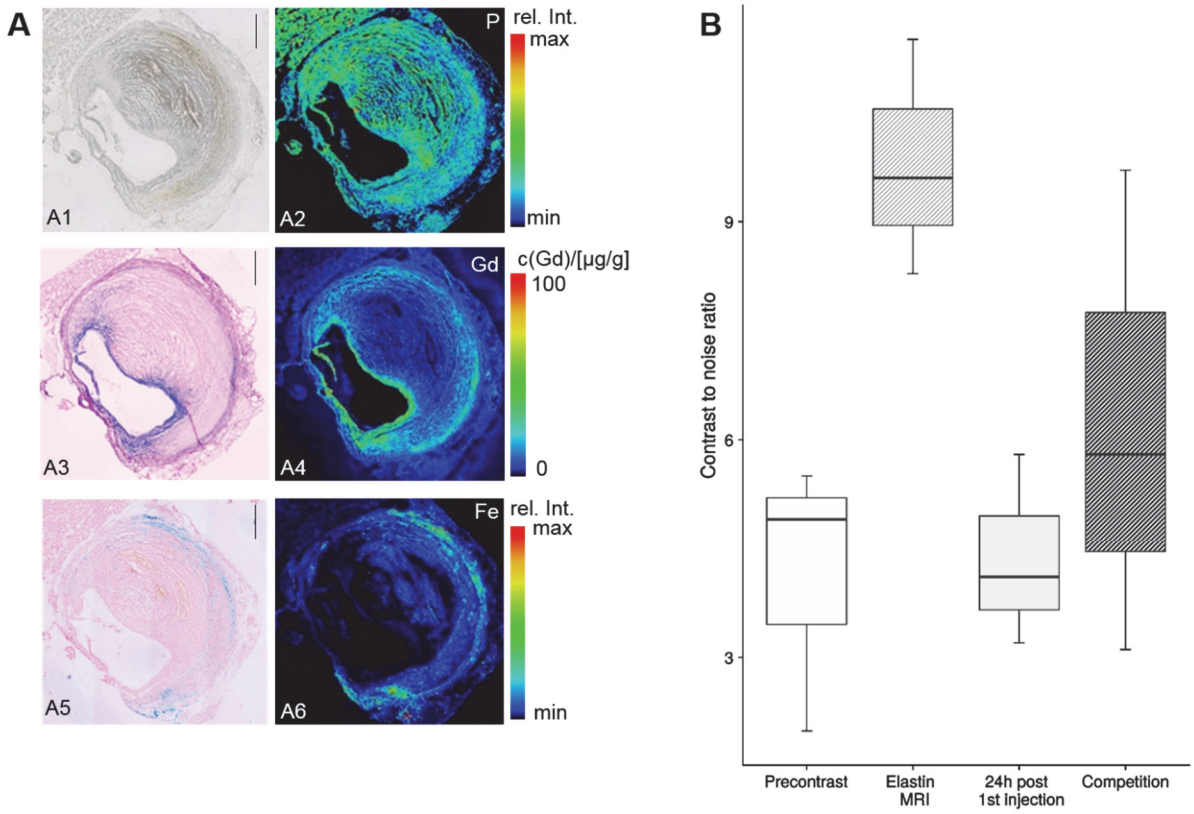

Figure 6. Spatial localization of the elastin-specific gadolinium-based probe and the iron oxide particles in aortic aneurysms using Laser Ablation Inductively Coupled Mass Spectrometry (LA-ICP-MS) and competition experiments.

A1 and **A2**, To get an anatomical overview of the histological AAA sections, the phosphorus distribution was measured using LA-ICP-MS. **A3** and **A4**, LA-ICP-MS confirmed the *in vivo* measurements with the visualization of the elastin-specific gadolinium-based probe in the aneurysmal wall. A colocalization of gadolinium accumulation (**A4**) with the elastic fibers in the Elastica van Giesson stain was also demonstrated (**A3**). **A4** and **A5**, LA-ICP-MS confirmed accumulation of the iron oxide particles in the aneurysmal wall. Additionally, the co-localization of iron accumulation (**A6**) and areas positive for Perls Prussian blue staining (**A5**) was demonstrated. Scale bars represent 500 µm. **B**: For the competition experiments, a significant decrease in the contrast-to-noise ratio compared to the administration of the gadolinium labeled elastin-specific agent alone was shown. MRI indicates magnetic resonance imaging.

Concurrent Molecular Magnetic Resonance Imaging of Inflammatory Activity and Extracellular Matrix Degradation for the Prediction of Aneurysm Rupture

Supplemental Material

Supplemental Methods

Animal experiments

Animal care and housing, as well as all procedures, were performed according to the guidelines and regulations of the Federation of Laboratory Animal Science Associations (FELASA) and the local Guidelines and Provisions for Implementation of the Animal Welfare Act. All animals were maintained under barrier conditions, administered a standard laboratory diet and provided water ad libitum. Male ApoE-knockout (B6.129P2-ApoEtm1Unc/J) were obtained from the Research Institute of Experimental Medicine at the Charité Berlin. At the age of eight weeks (n=45), osmotic minipumps (Alzet model 2004, Durect Corp) were implanted subcutaneously in the dorsal neck region. For up to 28 days angiotensin II (Ang II) was continuously infused with a rate of 1000 ng/kg/min (n=36). Sham-operated mice (n=9) delivered saline over a course of 28 days, serving as the control group. One, two, three and four weeks following minipump implantation, MR imaging was performed. At each time point, nine animals (n=9) were scanned within a 48 hours imaging session. The first imaging session included imaging prior to and following the administration of 0.2 mmol/kg of an elastin-specific contrast agent (ESMA, Lantheus Medical Imaging, North Billerica, Massachusetts, USA). Following the second MR scan, a clinical dose (4 mg Fe/kg) of ferumoxytol (Feraheme® AMAG Pharmaceuticals®) was administered. After 24 hours MRI was repeated including imaging prior to and following the administration of 0.2 mmol/kg of an elastin-specific contrast agent. Prior to MRI, animals were anesthetized by an intraperitoneal injection of a combination of Medetomidine (500 µg/kg), Fentanyl (50 µg/kg), and Midazolam (5 mg/kg). Following the first imaging session, anesthesia was antagonized using a combination of Atipamezole (2.5 mg/kg), Naloxone (1200 µg/kg), Flumazenil (500 µg/kg), leading to an accelerated recovery time. Following the second imaging session, mice were sacrificed and exsanguinated by arterial perfusion of saline. The aorta including the right renal artery and the last pair of intercostal arteries was excised for histological examinations, ICP-MS and Laser-ICP-MS. Animals developing no abdominal aneurysm were excluded from the study (n=10).

In vivo MR Experiments

For all imaging sessions, a clinical 3T Siemens system (Biograph, Siemens Healthcare Solutions, Erlangen, Germany) and a clinical single loop coil (47 mm, Siemens Healthcare Solutions, Erlangen, Germany) were used. To avoid rapid cooling during the imaging, body temperature (37 °C) of the mice was monitored using an MR-compatible heating system (Model 1025, SA Instruments Inc, Stony Brook, NY). Following anesthesia injection, the

animals were positioned in a prone position on the microscope (47 mm in diameter) single loop coil. To establish a venous access for the administration of the contrast agents into the tail vein, a small diameter tube with an attached 30G cannula was used.

Elastin imaging using T1-weighted sequences

The imaging protocol included the following sequences. For an anatomical overview and localization of the abdominal aorta, low-resolution three-dimensional gradient echo scout scan was performed followed by an arterial 2D TOF angiography (two-dimensional time-of-flight angiography) in transverse orientation for specific visualization of the aorta. Both sequences were performed using the following imaging parameters: Imaging matrix = 960, field of view = 200×200 mm, slice thickness = 0.35 mm, inplane spatial resolution = 0.166 mm (reconstructed 0.15 mm), flip angle = 90 °, repetition time (TR) sequence = 35 ms and echo time (TE) 4,4 ms. From the arterial time-of-flight dataset, a maximum intensity projection (MIP) was generated for display of an arterial angiogram of the abdominal aorta and abdominal aortic aneurysms (AAAs), to plan the subsequent contrast-enhanced sequences. The inversion recovery scan to visualize the gadolinium-based contrast agent was preceded by a 2D TI scout sequence planned perpendicular to the abdominal aorta, which was used to determine the optimal inversion time (TI) for blood signal nulling. Imaging parameters of the TI scout sequence included: FOV = 180 mm, matrix = 750, in plane spatial resolution = 0.24 x 0.24 mm, slice thickness = 1 mm, TR between subsequent IR pulses = 1000 ms, and °. Imaging parameters of the high-resolution 3D inversion FLASH sequence scan employed for visualization of gadolinium-based molecular probe were: FOV = 50 mm, matrix = 416, inplane spatial resolution = 0.12 x 0.12 mm, slice thickness = 0.3 mm, slices = 56, TR/TE = 10.1/7.0 ms, TR between subsequent IR pulses = 1000 ms, and flip angle = 30°.

Iron oxide imaging using T2-weighted sequences*

Imaging parameters for the T2* weighted sequences in this study included a field of view 150x150 mm; matrix 832; in-plane spatial resolution 0.18 x 0.18 mm; slice thickness 0.3 mm; TR/TE 15/4 ms; flip angle 20; averages and 42 slices.

Competition experiments

In three ApoE$^{-/-}$ mice (n=3) in vivo competition experiments were performed four weeks following minipump implantation. MR imaging was performed within a 48 hours imaging session. On the first day, the animals were imaged prior to and following the administration of the elastin-specific probe via the tail vein. After 24 hours imaging was performed prior to and following the administration of a tenfold higher dose of the non-paramagnetic europium-labeled elastin-specific MR probe. Subsequently, the elastin-specific probe was administered at a clinical dose of 0.2 mmol/kg and MR imaging was performed after 20 minutes.

Histological analysis of aortic aneurysms and aortic aneurysm morphometry

For correlation of in vivo and ex vivo MRI data, histological analysis was performed in the same region of the abdominal aorta that was imaged. Following surgical excision, aortic aneurysms tissues were processed overnight in MorFFFix® (Morphisto, Frankfurt am Main, Germany) and embedded in paraffin for sectioning. The sections (5 µm) were stained for Miller's Elastica van Gieson stain (EvG) to visualize the elastic fibers and for Perls' Prussian blue stain to visualize the iron ions. Hematoxylin and Eosin (HE) staining were additionally performed. Resulting histological slices were examined and photographed using a light microscope (Observer Z1, Carl Zeiss Microscopy GmbH, Jena, Germany). Digitized images of EvG, Perl's Prussian blue and immunofluorescence sections were used for morphological measurements. Computer-assisted image-analysis (ImageJ software, Version 1.51) was used for measurement of morphometry as well as for quantification of the adventitial area. The adventitia, media, intima, and lumen of the vessel (including the aneurysm) were defined as adventitial area as previously described (7). To measure the %EvG stain area per adventitial area, the color profile of the normal elastic laminae in the media was set as a reference standard. All structures with this specific color profile within the adventitial area were automatically segmented and resulting areas were recorded. By dividing the segmented area by the overall adventitial area, the %EvG stain area per adventitial area was determined. The same procedure was used to measure the %Perl Prussian blue iron oxide stain per adventitial area, including the segmentation of all areas positive for Perls Prussian blue staining.

Immunofluorescence analysis

Immunofluorescence staining was performed for evaluation of localization and density of macrophages. Abdominal aortic tissues were embedded in OCT compound and cut at -20 °C into 10 µm cryosections and immediately mounted on SuperFrost Plus adhesion slides (Thermo Scientific). Sections were incubated overnight at 4°C with a monoclonal CD68 antibody (Rat anti-Mouse CD68, clone FA-11, Bio-Rad, 1:100) diluted in Dako REALTM Antibody Diluent (Dako, Denmark). Subsequently, slides were washed two times with PBS (pH=7.4). For visualization of macrophages, slides were incubated with polyclonal secondary antibody AlexaFluor 568 (Goat anti Rat IgG, Thermo Fisher Scientific, Germany, 1:200) for one hour, followed by counterstaining and mounting using Roti®-Mount FlourCare (Carl Roth, Germany).

Elemental bioimaging by means of laser ablation coupled to inductively coupled plasma-mass spectrometry (LA-ICP-MS)

Abdominal aortic aneurysms were cut at -20 °C into 10 µm cryosections and immediately mounted on SuperFrost Plus adhesion slides (Thermo Scientific). The LA-ICP-MS analysis was performed with a LSX 213 G2+ laser system (CETAC Technologies, Omaha, USA) equipped with a two volume HelEx II cell connected via Tygon tubing to an ICPMS-2030 (Shimadzu, Kyoto, Japan). Samples were ablated via line-by-line scan with a spot size of 15 µm, a scan speed of 30 µm/s and 800 mL/min He as transport gas. The analysis was performed in collision gas mode with He as collision gas and 100 ms integration time for the five analyzed isotopes 31P, 57Fe, 64Zn, 158Gd and 160Gd. For the quantification of Gd, matrix-matched standards based on gelatin were used. Nine gelatin standards (10% w/w) including a blank, were spiked with different Gd concentrations ranging from 1 to 5.000 µg/g. Averaged intensities of the scanned lines of the standards showed a good linear correlation with a regression coefficient R^2=0.9999 within this concentration range. Limit of detection (LOD) and limit of quantification (LOQ), calculated with the 3σ- and 10σ-criteria, were 8 ng/g and 28 ng/g Gd. The quantification and visualization were performed with an in-house developed software (WWU Münster, Münster, Germany).

Figure Legends

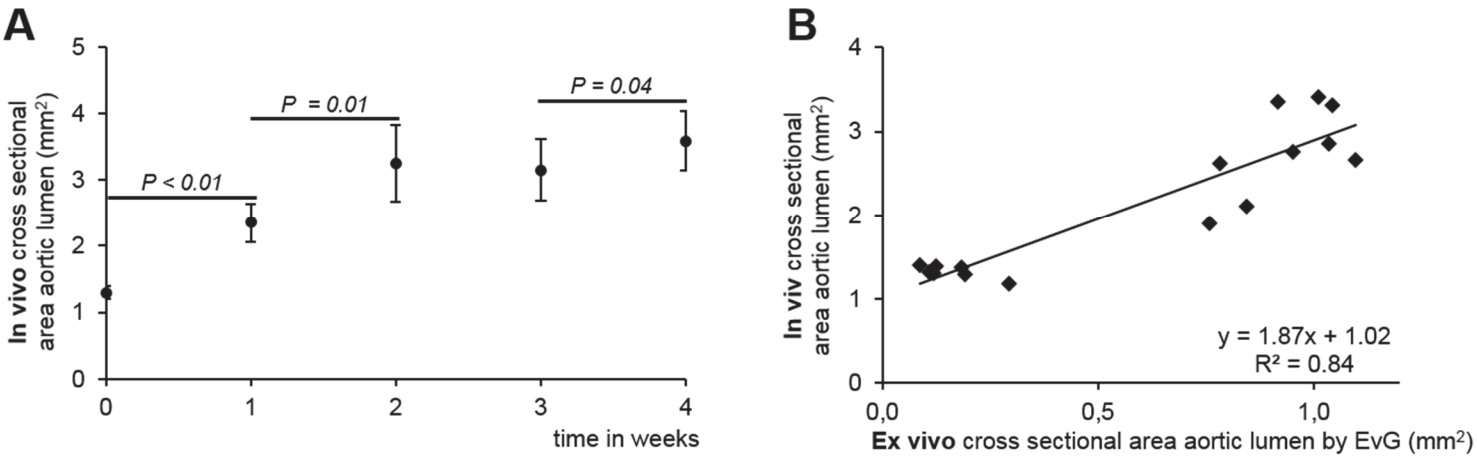

Supplemental Figure I. In vivo and ex vivo assessment of abdominal aortic aneurysms and thrombus cross-sectional area (week-by-week-group).

A, On in vivo MR imaging, an increase in cross-sectional areas of the aortic lumen size (P≤ 0.05) was observed over the 4-week time course of angiotensin II infusion reflecting the development of AAAs in this mouse model. **B**, In vivo MR measurements of the aortic dilation correlated strongly with ex vivo measurements on histological Pruss van Gieson (EvG) stained sections.

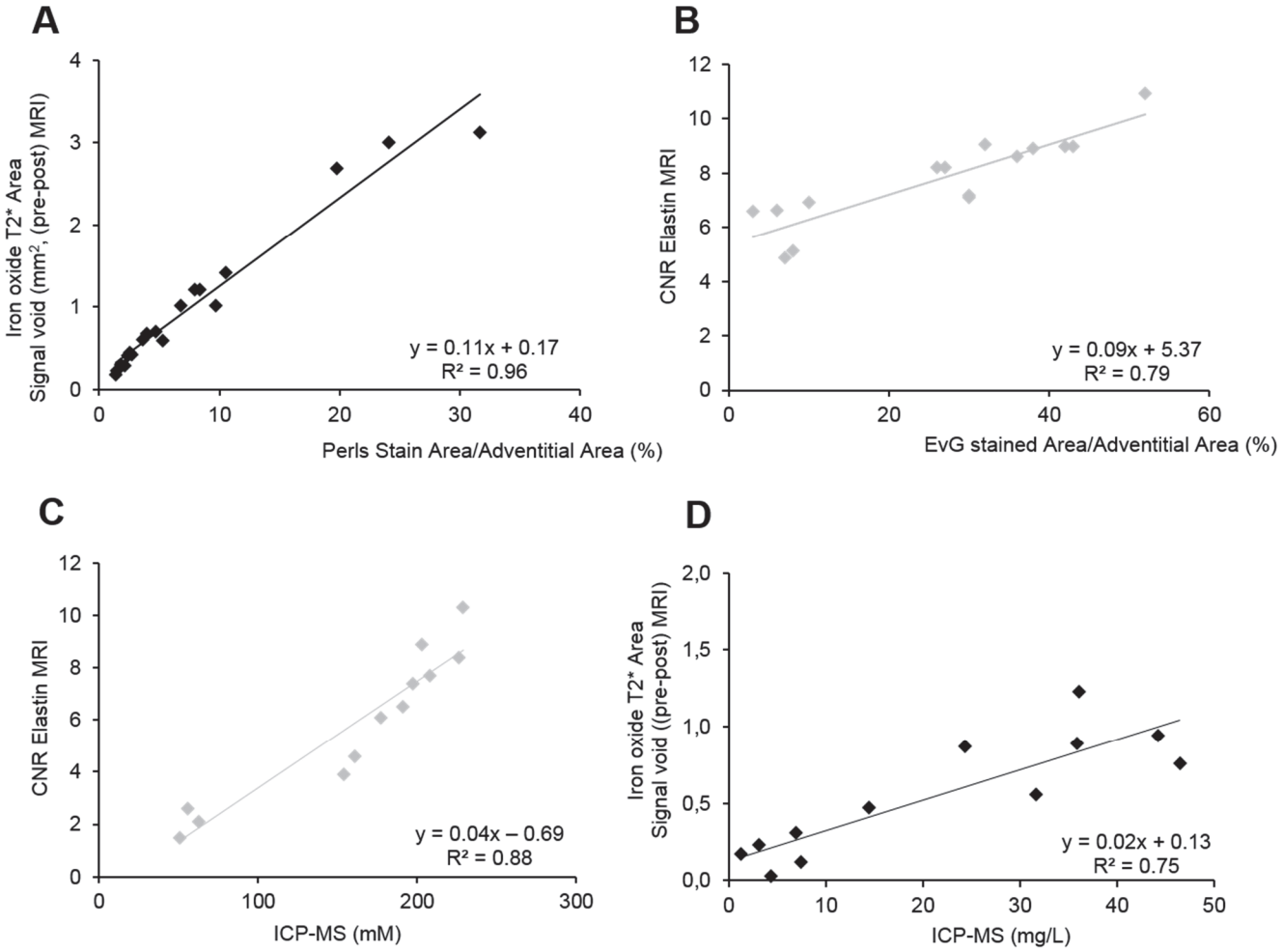

Supplementary Figure II. Correlation of in vivo MRI signal measurements derived from both molecular probes and ex vivo histology.

A, In vivo measured areas of signal void due to iron oxide particle accumulation correlated strongly with histological measurements on Perls Prussian blue-stained sections. **B**, In vivo CNR measurements after the administration of the elastin specific probe showed a strong correlation with ex vivo Elastica van Gieson (EvG) staining on corresponding histological sections. **C**, Results from ICP-MS for gadolinium showed a strong correlation with in vivo CNR measurements following the administration of the elastin specific probe. **D**, A strong correlation was also observed between ICP-MS for iron and the signal-void on the T2*-weighted-sequences following the administration of the iron oxide particles. Overall, these measurements indicate a good agreement between in vivo and ex vivo measurements of the iron oxide particles and the elastin specific probe. CNR: Contrast to noise ratio; ICP-MS: Inductively coupled mass spectroscopy.

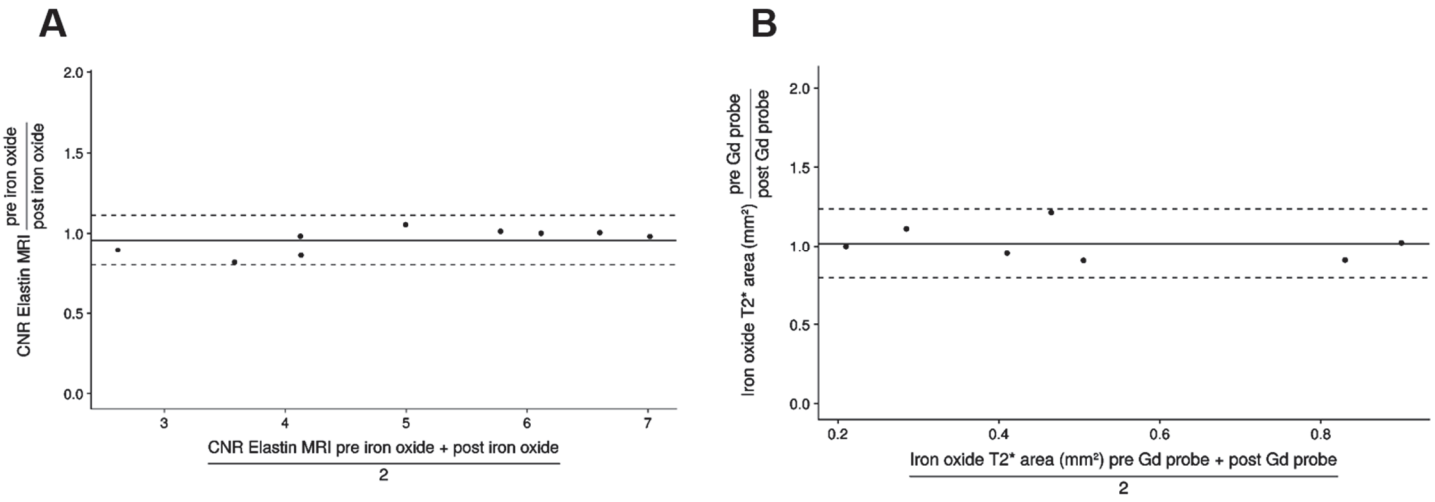

Supplementary Figure III. Effect of the iron oxide particles and the gadolinium-based elastin-specific probe on the visualization of each other.

A, To investigate the influence of iron oxide particles on the assessment of the elastin-specific agent, T1-weighted imaging was performed on day one prior to the administration of the iron oxide particles and 24 hours following the administration of the iron oxide particles. A strong correlation of CNR measurements between both days was shown. ICC=0.98 **B**, T2*-weighted imaging was performed on day two prior to and following the administration of the elastin-specific probe to investigate the influence of the gadolinium-based probe on the assessment of the iron oxide particles. The measurements on T2*-weighted images prior to and following the administration of the gadolinium-based probe demonstrated a strong correlation. ICC=0.98
CNR: contrast-to-noise-ratio.

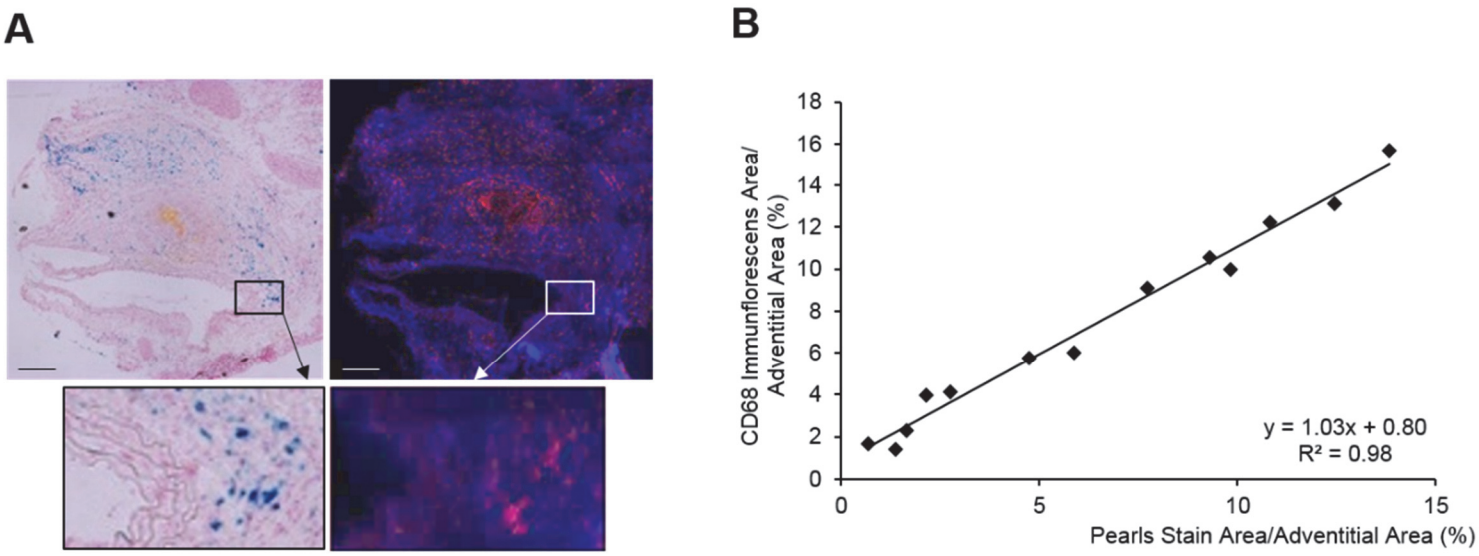

Supplemental Figure IV. Ex vivo immunofluorescence measurements.

A, Perls Prussian blue staining (left) and CD68 staining (right) of adjacent histological sections confirmed the colocalization of macrophages and iron oxide particles (magnifications). **B**, Areas positive for CD68 correlated strongly with Perls Prussian blue stained areas. Scale bars represent 200 µm.

4 Publication II

Molecular MR-imaging for the noninvasive quantification of the anti-inflammatory effect of targeting interleukin-1β in a mouse model of aortic aneurysm

Authors: Julia Brangsch[1,2], Carolin Reimann[1,2], Jan Ole Kaufmann[1,3,4], Lisa Christine Adams[1], David Onthank[5], Christa Thöne-Reineke[2], Simon Robinson[5], Marco Wilke[3], Michael Weller[3], Rebecca Buchholz[6], Uwe Karst[6], Rene Botnar[7,8,9,10], Bernd Hamm[1], Marcus Richard Makowski[1,7,9,11]

[1]Charité – Universitätsmedizin Berlin, corporate member of Freie Universität Berlin, Humboldt-Universität zu Berlin, and Berlin Institute of Health, Department of Radiology, Charitéplatz 1, 10117 Berlin, Germany

[2]Department of Veterinary Medicine, Institute of Animal Welfare, Animal Behavior and Laboratory Animal Science, Freie Universität Berlin, Königsweg 67, Building 21, 14163 Berlin, Germany

[3]Federal Institute for Materials Research and Testing (BAM), Division 1.5 Protein Analysis, Richard-Willstätter-Str. 11, 12489 Berlin, Germany

[4]Humboldt-Universität zu Berlin, Department of Chemistry, Brook-Taylor-Str. 2, 12489 Berlin, Germany

[5]Lantheus Medical Imaging, North Billerica, Massachusetts, USA, 331 Treble Cove Road, USA

[6]Institute of Inorganic and Analytical Chemistry, Westfälische Wilhelms-Universität Münster, Corrensstr. 30, 48149 Münster, Germany

[7]King's College London, School of Biomedical Engineering and Imaging Sciences, United Kingdom, St Thomas' Hospital Westminster Bridge Road, London SE1 7EH, United Kingdom

[8]Wellcome Trust / EPSRC Centre for Medical Engineering, King's College London

[9]BHF Centre of Excellence, King's College London, United Kingdom, Denmark Hill Campus, 125 Coldharbour Lane, London SE5 9NU, United Kingdom

[10]Escuela de Ingeniería, Pontificia Universidad Católica de Chile, Santiago, Chile.

[11]Klinikum rechts der Isar, Technical University Munich, Department of Diagnostic and Interventional Radiology, Ismaninger Str. 22, 81675 Munich

Journal: Molecular Imaging, ©2020 SAGE Publications Inc., received April 17, 2020; accepted August 28, 2020.

DOI: https://doi.org/10.1177/1536012120961875

Molecular MR-imaging for the noninvasive quantification of the anti-inflammatory effect of targeting interleukin-1β in a mouse model of aortic aneurysm

Abstract

Background: Molecular-MRI is a promising imaging modality for the diagnosis and monitoring of abdominal aortic aneurysms (AAAs). Interleukin-1β (IL-1β) represents a new therapeutic tool for AAA- treatment, since pro-inflammatory cytokines are key-mediators of inflammation in aneurysms. This study investigates the potential of molecular-MRI to evaluate therapeutic effects of an anti-IL-1β-therapy on AAA-formation in a mouse-model.

Methods: Osmotic minipumps were implanted apolipoprotein-deficient-mice (N=27). One group (Ang-II + 01BSUR group, n=9) was infused with angiotensin-II (Ang-II) for 4 weeks and received an anti-murine IL-1β antibody (01BSUR) 3 times. One group (Ang-II group, n=9) was infused with Ang-II for 4 weeks but received no treatment. The control-group (n=9) was infused with saline and received no treatment. MR-imaging was performed using an elastin-specific gadolinium-based probe (0.2 mmol/kg).

Results: Mice of the Ang-II + 01BSUR group showed a lower aortic-diameter compared to mice of the Ang-II group and control mice ($p<0.05$). Using the elastin-specific probe, a significant decrease in elastin-destruction was observed in mice of the Ang-II group. In vivo MR measurements correlated well with ex vivo histopathology ($y=0.34x-13.81$, $R^2=0.84$, $p<0.05$), ICP-MS ($y=0.02x+2.39$; $R^2=0.81$, $p<0.05$) and LA-ICP-MS. Immunofluorescence and western-blotting confirmed a reduced IL1-β expression.

Conclusions: Molecular MRI enables the early visualization and quantification of the anti-inflammatory-effects of an IL-1β inhibitor in a mouse-model of AAAs. Responders and non-responders could be identified early after the initiation of the therapy using molecular-MRI.

Keywords

animal models of disease, cardiovascular

Molecular MR-imaging for the noninvasive quantification of the anti-inflammatory effect of targeting interleukin-1β in a mouse model of aortic aneurysm

Introduction

Abdominal aortic aneurysms (AAAs) affect 3-4% of men over the age of 65 and account annually for over 15,000 deaths.[1] If unrecognized or untreated, the progressive dilation of the aortic wall can lead to AAA rupture. Therefore, a high clinical need for noninvasive medical therapies of AAAs exists. The inhibition of progressive aortic dilation via a pharmacological approach could represent a substantial advancement for patients, especially as invasive therapy or surgery can be associated with severe complications. As antibody-based therapies are associated with substantial costs it would be benefical to differentiate therapy responders from non-responders early after the initiation of the therapy.

Although the initiating events are not fully elucidated yet, inflammation was shown to be a major contributing factor to AAA formation and progression.[2] AAA formation is characterized by proinflammatory cell infiltration, including monocytes and macrophages, the release of cytokines and proteases and breakdown of extracellular matrix (ECM) proteins.[2-5] Especially, the destruction of medial elastin and collagen (type I and III) causes an ongoing reduction of the stability of the aortic wall leading to an increasing inability to withstand the high intraluminal pressure.[6-7]

Interleukin-1β (IL-1β) represents a gatekeeper for inflammation and contributes substantially to the progressive destruction of aortic ECM proteins during AAA development.[8] Different preclinical and clinical studies demonstrated significantly increased levels of IL-1β in AAAs compared to healthy aortas. Therefore, the disruption of the inflammatory pathway via IL-1β neutralization represents a promising novel therapeutic target for the treatments of AAAs.[9-12]

In clinical practice, diagnosis and monitoring of AAAs include computed tomography (CT), magnetic resonance imaging (MRI) or ultrasound. Currently, there is no established biomarker available for the characterization of aortic aneurysms since the aortic diameter alone was shown to be not a reliable diagnostic and prognostic parameter for AAAs.[13,14] Molecular MRI using probes that visualize extracellular-matrix proteins for the assessment of AAAs presents a promising new approach for aneurysm diagnosis and monitoring.[15-17] Elastin-specific molecular MRI allows an in vivo visualization and quantification of changes in elastin composition of the aortic wall and offers, therefore, the potential for noninvasive characterization of AAAs.[14,18,19]

In this study, we investigated the feasibility of molecular MRI for the early visualization and quantification of the effects of the interleukin-1β inhibitor 01BSUR in a mouse model of AAAs with the overall aim to differentiate responders from non-responders early after the initiation of the therapy.

Methods

Animal experiments

Eight-week-old male ApoE-knockout (B6.129P2-ApoE^{tm1Unc}/J) mice were obtained from the Research Institute of Experimental Medicine at the Charité Berlin. Three groups (N=27) of ApoE-/- mice underwent subcutaneous implantation of osmotic minipumps (Alzet model 2004, Durect Corp). To determine the effect of the interleukin-1β on AAA progression, nine mice (n=9, Ang-II + 01BSUR group) were continuously infused with angiotensin-II with a rate of 1000 (ng/kg)/min for 28 days and were injected subcutaneously (s.c.) with 0.3 mg 01BSUR (Novartis, Basel, Switzerland) three times: on the day of minipump implantation (day 0), 7 days and 14 days after minipump implantation (Figure 1). In addition, one group of mice (Ang-II group, n=9) was also continuously infused with angiotensin-II for 28 days but received no treatment after minipump implantation. A control group of nine mice (n=9) received saline instead of AngII via the osmotic minipump for 28 days and received also no treatment. For MR imaging, animals were anaesthetized by an intraperitoneal injection of a combination of Medetomidine (500 µg/kg), Fentanyl (50 µg/kg), and Midazolam (5 mg/kg). MRI was then performed prior to and following the administration of 0.2 mmol/kg of an elastin-specific contrast agent (ESMA, Lantheus Medical Imaging, North Billerica, Massachusetts, USA). For ex vivo analysis, mice were sacrificed and exsanguinated by arterial perfusion of saline and the aorta including the right renal artery and the last pair of intercostal arteries was excised.

All procedures were performed according to the guidelines and regulations of the Federation of Laboratory Animal Science Associations (FELASA) and the local Guidelines and Provisions for Implementation of the Animal Welfare Act.

Interleukin-1β Inhibitor 01BSUR

The Ang-II + 01BSUR group (n=9) received 01BSUR (Novartis, Basel, Switzerland), an interleukin-1β inhibitor. This IgG2a/k monoclonal mouse antibody highly binds to IL-1β (dissociation constant (K_D) = 302 pM) and shows a half-life of 14 days.[9] By neutralizing the cytokine IL-1β, this antibody may reduce the pro-inflammatory and tissue-degrading activities of IL-1 β resulting in a reduced development and progression of a variety of acute and chronic inflammatory diseases.[20] 01BSUR has already been introduced in several preclinical studies in the context of aortic aneurysms[9] as well as aortic calcification[21] or collagen-induced arthritis using different rodent models.[20]

Mice were treated three times with 0.3 mg (0.9 mg per mice in total) 01BSUR starting on the day of minipump implantation (day 0) followed by injections (s.c.) after 7 and 14 days. The

used dose in this study is equivalent to the clinically approved dose of canakinumab used in the CANTOS study.[22]

Gadolinium-based elastin-specific contrast agent

The gadolinium-based elastin-specific contrast agent (ESMA, Lantheus Medical Imaging, North Billerica, Massachusetts, USA) has a small molecular weight of 856 g/mol. Showing a short blood half-life and the highest uptake within the aorta 30 to 45 minutes following the administration (13.2 ± 2.3% ID g^{-1}) the agent is then predominant cleared by the renal system.[23,24] A longitudinal relaxivity of 8.65 ± 0.42 mM^{-1} s^{-1} at 3 Tesla was reported for the agent bound to mice aortas.[23] Due to the small molecular weight, short blood half-life, renal clearing and relaxivity, the elastin-specific contrast agent used in this study is comparable to other clinically used gadolinium-based contrast agents, including gadobuterol (Gadovist®, Bayer AG, Leverkusen Germany) and gadofosveset (Vasovist®, Bayer AG, Leverkusen Germany). This probe has already been validated and used for the visualization and characterization of elastin in the context of atherosclerosis[23,24] and aortic aneurysms.[18,19,25] In this study, a clinical dose of 0.2 mmol/kg was used.

***In Vivo* MR Experiments including MR angiography**

All animals (N=27) were imaged 4 weeks after osmotic minipump implantation (Figure 1). A clinical 3T Siemens system (Biograph, Siemens Healthcare Solutions, Erlangen, Germany) equipped with a clinical single loop coil (47 mm, Siemens Healthcare Solutions, Erlangen, Germany) was used for the imaging session. Following anesthesia injection, venous access for the administration of the contrast agent into the tail vein was established using a small diameter tube with an attached 30G cannula. Animals were then positioned in a prone position on the microscope (47 mm in diameter) single loop coil. The body temperature (37 °C) of the mice was monitored using an MR-compatible heating system (Model 1025, SA Instruments Inc, Stony Brook, NY) to avoid rapid cooling.

The elastin imaging was performed as described previously.[14] For an anatomical overview and localization of the abdominal aorta, low-resolution three-dimensional gradient echo scout scan was performed followed by an arterial 2D TOF angiography (two-dimensional time-of-flight angiography) in transverse orientation for specific visualization of the aorta. Both sequences were performed using the following imaging parameters: Imaging matrix = 960, field of view = 200×200 mm, slice thickness = 0.35 mm, in plane spatial resolution = 0.166 mm (reconstructed 0.15 mm), flip angle = 90 °, repetition time (TR) sequence = 35 ms and echo time (TE) 4,4 ms. From the arterial time-of-flight dataset, a maximum intensity projection (MIP)

was generated for display of an arterial angiogram of the abdominal aorta and abdominal aortic aneurysms, to plan the subsequent contrast-enhanced sequences. The inversion recovery scan to visualize the gadolinium-based contrast agent was preceded by a 2D TI scout sequence planned perpendicular to the abdominal aorta, which was used to determine the optimal inversion time (TI) for blood signal nulling. Imaging parameters of the TI scout sequence included: FOV = 180 mm, matrix = 750, in plane spatial resolution = 0.24 x 0.24 mm, slice thickness = 1 mm, TR between subsequent IR pulses = 1000 ms, and flip angle = 15°. Imaging parameters of the high-resolution 3D inversion FLASH sequence scan employed for visualization of gadolinium-based molecular probe were: FOV = 50 mm, matrix = 416, in plane spatial resolution = 0.12 x 0.12 mm, slice thickness = 0.3 mm, slices = 56, TR/TE = 10.1/7.0 ms, TR between subsequent IR pulses = 1000 ms, and flip angle = 30°.

Assessment of magnetic resonance imaging signal

Morphometric measurements were conducted on high–resolution MRI images using OsiriX (version 7.1, OsiriX foundation) as previously described. [14] Regions of interests (ROIs) were defined as areas of signal enhancement, which were co-localized with areas of aneurysmal aortic tissue. For these areas, the contrast-to-noise-ratio (CNR) was calculated as follows: CNR = (Combined vessel wall and aneurysmal aortic tissue signal – blood signal) / standard deviation signal (noise). Noise was defined as the standard deviation in pixel intensity from a ROI placed in the background air anterior to the aorta.

Histological analysis of aortic aneurysms and aortic aneurysm morphometry

For histological analysis, aortic tissue was processed overnight in MorFFFix® (Morphisto, Frankfurt am Main, Germany). The aortas were embedded in paraffin and cut into 5 µm thick serial sections. Miller's Elastica van Gieson stain (EvG) was performed for visualization of elastic fibers. Additionally, Hematoxylin and Eosin (HE) staining was performed. For morphological measurements, histological slices were photographed using a light microscope (Keyence BzX800) and analyzed using computer-assisted image analysis (ImageJ software, Version 1.51) to determine the %EvG stain area per adventitial area as previously described.[14,18]

Immunofluorescence analysis

Immunofluorescence staining was performed to visualize interleukin-1β within the aortic wall. After embedding in OCT compound, abdominal aortic tissues were cut at -20 °C into 10 µm thick serial cryosections. Sections were treated with polyclonal IL-1β antibody (Rabbit anti-Mouse IL-1 beta, Bio-Rad 1:100, 1 hour at room temperature) followed by a polyclonal secondary antibody AlexaFluor 568 (Donkey anti Rabbit IgG, Thermo Fisher Scientific, Germany, 1:200, 1 hour at room temperature) each diluted in Dako REAL™ Antibody Diluent (Dako, Denmark). Counterstaining and mounting were performed using Roti®-Mount FluorCare (Carl Roth, Germany).

Western immunoblot analysis

To evaluate the levels of IL-1β and CD68 in the aortic wall of the Ang-II + 01BSUR group and Ang-II group, Western immunoblot analysis was performed. Aortic tissues (n=3 per group) were homogenized and solubilized in RIPA buffer (pH=7.4). The protein concentration was determined using UV-spectrometry at 280 nm (Evolution 220 UV-Visible Spectrometer, Thermo Scientific™). 5 mg/ml total protein per lane diluted in SDS loading buffer was loaded onto 4-12% Tris-Glycine Gels (ServaGel TG Prime Vertical Tris-Glycine Gel 4-12%). Proteins were separated by SDS-PAGE (Hoefer SE260). To assure equal amounts of total protein loaded per lane, GAPDH was used as loading control. Due to the identical molecular weights of the targeted proteins CD68 and GAPDH, two gels were run simultaneously. Proteins were transferred to PVDF membranes using Trans-Blot Turbo RTA transfer kit (Bio-Rad). Primary antibodies (Rabbit anti-Mouse IL-1β, Bio-Rad 1:500; Rabbit anti-Mouse CD68, antibodies.com, 1:500; Rabbit anti-Mouse GAPDH, Invitrogen 1:1000) were detected using a secondary HRP-labeled antibody (Goat anti-Rabbit IgG (H/L): HRP, Bio-Rad 1:1000) and SeramunBlau® blotting substrate (Seramun Diagnostica GmbH). Protein bands were quantified by ImageJ (Version 1.51).

Inductively Coupled Mass Spectroscopy (ICP-MS)

For a reproducible measurement of the local gadolinium concentration, ICP-MS was performed. Aortic tissue samples (n=3 per group) were digested overnight in 70% nitric acid at 37 °C. For ICP-MS analysis samples were diluted with deionized water. A standard curve was acquired for the concentration of gadolinium for each analysis.

Element specific bioimaging using laser ablation (LA) coupled to inductively coupled plasma-mass spectrometry (LA-ICP-MS)

LA-ICP-MS was performed as described previously.[14] Aneurysms were cut into 10 µm cryosections at -20 °C and mounted on SuperFrost Plus adhesion slides (Thermo Scientific). The LA-ICP-MS analysis was performed using an LSX 213 G2+ laser system (CETAC Technologies, Omaha, USA) which was equipped with a two-volume HelEx II cell connected via Tygon tubing to an ICPMS-2030 (Shimadzu, Kyoto, Japan). With a spot size of 10 µm samples were ablated via line-by-line scan using a scan speed of 30 µm/s and 800 mL/min He as transport gas. The analysis was performed in collision gas mode with He as collision gas, with 50 ms integration time for the analyzed isotopes ^{31}P, ^{57}Fe, and ^{64}Zn and 75 ms integration time for the two Gd isotopes ^{158}Gd and ^{160}Gd. Matrix-matched standards based on gelatin were used for the quantification of Gd. Nine gelatin standards (10% w/w) including a blank, were spiked with different Gd concentrations (1 to 500 µg/g). Averaged intensities of the scanned lines of the standards were in good linear correlation with a regression coefficient R2=0.998 within this concentration range. Limit of detection (LOD) and limit of quantification (LOQ), calculated with the 3σ- and 10σ-criteria, were 16 ng/g and 54 ng/g Gd. The quantification and visualization were performed using in-house developed software (WWU Münster, Münster, Germany).

Statistical Analysis

Values are specified as mean ± standard deviation. An unpaired, two-tailed Student's t-test was applied for the comparison of continuous variables. Linear regression was applied to determine the relationship between in vivo and the ex vivo measurements. P-value < 0.05 was considered to indicate a statistically significant difference.

Results

Overall 27 mice (N=27) were included until the end point of the study. Figure 1 summarizes the detailed study setup including the different groups of mice.

MR angiographic measurements for the assessment of the area of the aortic lumen

The angiography of the mice of the control group (ApoE-/- mice after 4 weeks of saline infusion, n=9) showed a non-dilated aortic lumen. The continuous Ang-II infusion in mice (n=9) resulted in a significantly enlarged aortic lumen and dilatation of the aortic wall in the suprarenal region (Figure 2A). AngII-infused mice treated three times with 01BSUR (n=9) showed a substantially lower aortic diameter in vivo and ex vivo compared to mice without 01BSUR treatment ($p<0.05$) (Figure 2B, C). No significant difference in aortic diameter could be observed in vivo and ex vivo between the control group and Ang-II + 01BSUR group ($p>0.05$) (Figure 2B, C). In vivo measurements were in good agreement with ex vivo measurements of the cross-sectional area on histological sections ($y=2.38x-1.17$, $R^2=0.89$; $p<0.05$, Figure 2D).

Molecular MRI for the noninvasive assessment of the effects of IL-1β inhibitor 01BSUR on AAA formation

ApoE-/- mice (n=9) developed extensive aortic aneurysm after 4 weeks of AngII-infusion as described previously including infiltration of inflammatory cells and ECM remodeling.[14] Using the elastin-specific probe, a strong expression of elastin within the aortic wall could be observed in vivo in these mice due to a strong remodeling of the extracellular matrix (ECM) especially in the areas of former elastic fiber dissection. In contrast, 01BSUR treatment reduced the impact of Ang-II on elastin levels, prevent the destruction of elastic fibers within the aortic wall and therefore the development of abdominal aortic aneurysms (Figure 3). The control group receiving saline, showed no pathological changes of the aortic wall.

T1-weighted MR imaging for the assessment of the gadolinium-based elastin-specific probe

Prior to the administration of the elastin-specific MR probe, a low contrast-to-noise-ratio was measured in the aortic wall of all three groups. A significant ($p<0.05$) increase in CNR in the aortic wall was measured for mice receiving Ang-II, Ang-II + 01BSUR and the control mice following the administration of the elastin-specific agent (Figure 4A). The Ang-II group showed a strong signal enhancement in the area of the aneurysmal wall due to extracellular matrix remodeling by expression of elastic fibers in the area of former disruption of the internal elastic lamina. The Ang-II + 01BSUR group showed a significantly weaker signal enhancement in the

aortic wall indicating an absence of aortic rupture and prevention of AAA formation. In vivo measurements correlated with ex vivo histological measurements of elastic fiber density using Elastica van Gieson staining ($y=0.34x-13.81$, $R^2=0.85$; $p<0.05$, Figure 4B).

Correlation of in vivo measurements of the elastin specific probe with ex vivo histology

For ex vivo measurements on histological sections, the Elastica van Giesson (EvG) staining was used to assess the amount and distribution of elastic fibers in the aortic wall (Figure 3A4, B4). The Ang-II group showed the development of aortic aneurysms due to the dissection of internal elastic fibers. After 4 weeks of AngII-infusion a strong remodeling of the aortic wall was observed at these areas. Due to this compensatory repair process, a significant increase in elastic fibers in both, in vivo and ex vivo measurements was observed in mice of the AngII-group. A good correlation was shown between ex vivo histological measurements and in vivo measurements using the elastin-specific probe ($y=0.34x-13.81$ $R^2=0.85$; Figure 4B).

Expression of IL-1β in the aortic wall by Immunofluorescence and Western Blot

For the evaluation of the expression of IL-1β within the aortic wall, Western Blot analysis and immunofluorescence staining of histological sections were performed. Western Blot analysis of the abdominal aorta (n=3 per group) showed a significantly lower expression of IL-1β within the aortic wall in mice treated with 01BSUR compared with the AngII group (Figure 5A, B). These results were confirmed by histological analysis which also showed a significant decrease in IL-1β expression around the aorta after 01BSUR treatment (Figure 6).

In addition, to evaluate the effects of 01BSUR on macrophage recruitment and accumulation, Western Blot analysis and immunofluorescence CD68 staining of adjacent histological slices were performed. Mice of the AngII group demonstrated extensive macrophage staining and a significant higher expression of CD68 whereas mice treated with 01BSUR had trivial macrophage staining (Figure 6) and lower CD68 expression in Western Blot analysis (Figure 5A, C). Furthermore, immunofluorescence microscopy showed that IL-1β clearly co-localized with macrophages within the aortic wall (Figure 6). These findings are consistent with 01BSUR suppressing inflammatory processes in aneurysm development.

Spatial localization of the gadolinium-based elastin-specific probe using laser coupled mass spectrometry (LA-ICP-MS)

LA-ICP-MS was performed to visualize the spatial distribution of gadolinium within the aortic wall. Sections of the aortic wall from mice of the Ang-II + 01BSUR group (n=3) and AngII group (n=3) after 4 weeks of AngII-infusion showed a strong co-localization of targeted gadolinium with elastic fibers (Figure 7A, B).

Gadolinium concentration by inductively-coupled mass spectrometry (ICP-MS)

For determination of the concentration of gadolinium from the elastin-specific contrast agent in the aortic wall, inductively coupled mass spectrometry (ICP-MS) was performed in 9 mice (n=3 of each group). A strong correlation of in vivo CNR measurements and ex vivo measured gadolinium concentrations by ICP-MS was shown ($y=0.02x+2.39$; $R^2=0.81$, $p<0.05$) (Figure 7C).

Discussion

This study demonstrates the potential of molecular elastin specific MRI to evaluate the effect of disrupting IL-1β signaling on AAA formation in ApoE-/- mice. Using an elastin-specific probe, the development of an abdominal aneurysm, as well as the response to therapy, could reliably be visualized in one imaging session after 4 weeks of AngII-infusion. This non-invasive in vivo visualization and quantification by molecular MRI could improve the early evaluation of response to therapy in patients and could help to identify responders and non-responders early after initiation of the therapy.

Ex vivo histology and Western Blot analysis confirmed a reduction of inflammatory processes and IL-1β expression within the aortic wall due to the 01BSUR treatment. Further ex vivo examination by LA-ICP-MS and ICP-MS proved the specific binding of the molecular probe and correlated well with in vivo MR measurements.

Role of IL-1β during AAA formation

Inflammation has been shown to be a key process in AAA formation and progression including several different cytokines and proinflammatory cells. Interleukin-1β is one of the key mediators of inflammation and previous studies demonstrated its critical role in experimental aortic aneurysm development.[8,10,26] Furthermore, IL-1β was found to be elevated 4-fold in human AAAs compared to healthy aortas while circulating IL-1β is increased by nearly 10-fold in AAA patients.[11,12,27,28] By inducing the production of matrix metalloproteinases (MMPs) in fibroblastic cells and macrophages, including MMP-9, a protease with high elastolytic activity, IL-1β contributes crucially to the progressive destruction of aortic ECM proteins during AAA formation and progression.[27,29] Especially the loss of medial elastin fibers is thought to be the initiating event of aneurysm development.[30] Therefore, IL-1β antagonism represents a promising approach for AAA treatment by disruption of the inflammatory pathway.

There are several pharmacological agents targeting the IL-1β pathway, including direct antibodies to IL-1β or IL-1 receptor (IL-1R). Although IL-1β neutralization was once thought to be predominantly limited to the treatment of autoimmune and chronic inflammatory diseases, including gout, rheumatoid arthritis or type 2 diabetes, the role of IL-1β in cardiovascular diseases has gained more and more in importance.[31]

Anakinra, a commercially available recombinant human IL-1R antagonist, has previously been evaluated in an experimental abdominal and thoracic aortic aneurysms model. Johnston et al. treated C57Bl/6 mice following elastase aortic perfusion with escalating doses of anakinra.[10,26] Significant protection against AAA progression was shown in mice treated with anakinra 3 or

7 days following AAA initiation and furthermore mice treated prior to elastase exposure showed a dose-dependent decrease in maximal aortic dilation. This study indicates that IL-1β is critical for both the initiation and progression of experimental AAAs. A major clinical limitation of this study represents the application of anakinra at a dose of 100 (mg/kg)/day which exceeds the dosage approved for patient by 100-fold.

The direct inhibition of IL-1β using the monoclonal antibody 01BSUR was also recently assessed in different mouse models including Kawasaki Disease, renal inflammation and AAAs.[9,32,33] Isoda et al. showed that treatment with 01BSUR decreased AngII-induced AAAs in IL-1 Ra-deficient mice.[9] Histological analyses were performed after 28 days of AngII-infusion and revealed decreased degeneration of smooth muscle cells, elastic fibers and a decreased accumulation of inflammatory cells. These findings are consistent with the current study. Moreover, in our study, the effects of 01BSUR treatment were not only evaluated by ex vivo histology but more importantly by noninvasive in vivo molecular MR imaging.

Molecular MRI for the noninvasive assessment of treatment of aortic aneurysms

For the diagnosis and evaluation of AAAs, MRI using molecular probes for the visualization of extracellular matrix proteins has shown potential in experimental studies in the last several years. Native MR imaging enables solely the assessment of the aortic diameter which may be an unreliable marker for the risk of rupture and expansion rate and therefore the inflammatory status of aortic aneurysm.[34,35]

The gadolinium-based elastin-specific probe used in the present study allows the in vivo visualization of the elastin remodeling of the aortic wall at different stages of aortic aneurysms which has been shown by our research group[14] and others.[18,36] In our current study we showed that the use of this probe enables the early in vivo evaluation and quantification of AAAs and furthermore the response to the anti-inflammatory treatment with 01BSUR.

To our knowledge, this study represents the first molecular MRI study on the in vivo effects of anti-inflammatory therapy of experimental AAAs.

Translational potential of this study

Currently, there are no widely accepted medical options available to reduce or slow AAA progression. The recommended treatment paradigm includes monitoring of disease progression eventually followed by surgical intervention of AAAs larger than 55 mm while the management of asymptomatic medium-sized AAAs (40–55 mm) remains still controversial.[37,38] Therefore, there is a tremendous need for medical therapy for the treatment of patients with abdominal aneurysms.

A fully human monoclonal antibody directed against IL-1β, canakinumab, was previously presented following investigation in a large phase 3 trial for the prevention of recurrent myocardial infarction.[22] The anti-inflammatory therapy at a dose of 150 mg every 3 months led to a significantly lower rate of recurrent cardiovascular events than placebo, independent of lipid-level lowering, in patients with previous myocardial infarction. In addition, a phase IIb trial investigating canakinumab treatment in high-risk diabetic patients demonstrated a significant dose-dependent reduction in various major inflammatory biomarkers (C - reactive protein, IL-6 and fibrinogen).[39] These data support the potential of this novel therapeutic option for several inflammatory cardiovascular diseases, including AAAs. Regarding clinical translation in our present study, mice were treated with the clinically approved dose of an anti-IL-1β antibody as used within the CANTOS study. Using molecular MRI in addition to the evaluation of an anti-inflammatory therapy of cardiovascular diseases, responders and non-responders could be identified early after the initiation of the therapy. Such an approach could be helpful to identify the most suited patient collective, which response to treatment early after the initiation of the therapy. Additionally, this could help to identify patient collectives which would benefit from a potentially increased dose and reduce the costs as only responders would be continuously treated.

Another advantage of this study regarding clinical translation includes the use of a clinical 3 Tesla MR scanner. Since we have not used an ultrahigh field preclinical MR scanner for small animals, relaxation, rotational correlation, and signal properties can be directly translated into a clinical setting. Furthermore, the elastin-specific probe used in this study, is comparable to contrast agents already used in clinical practice, regarding molecular size and composition, as well as blood clearance and was administered at a clinical dose.[23]

Mouse model used in this study

In the small animal model used in this study, AngII-infused male apolipoprotein deficient mice develop suprarenal AAAs spontaneously without the need for surgical intervention.[40] The formation of AAAs in this murine model and humane aneurysm formation have numerous commonalities, including medial elastic fiber degeneration, inflammatory processes and thrombus formation.[41,42] AngII-infusion promotes macrophage infiltration, MMP activation as well as an increased release of cytokines, including IL-1β.[43,44]

Study limitations

The selected therapy with 01BSUR did not only reduce but prevent the formation of AAA in our current study. Therefore, a reduction in aneurysm size or inflammation within the aortic wall following AAA diagnosis with molecular MRI could not be evaluated. To further evaluate the feasibility of molecular imaging using an elastin-specific contrast agent for the monitoring of AAA therapy, a modified study design will be necessary, for example including a therapy onset after induction auf aneurysms. Consequently, more studies are needed, also to prove a possible translation into a clinical setting of AAA therapy monitoring using molecular MRI. Another limitation of the present study represents the used mouse model. Although it closely models human AAA formation, the murine AAAs develop in the suprarenal region, whereas in humans AAAs develop preferentially in the infrarenal region.[40] Furthermore, the elastin-specific probe used in this study is currently not approved for clinical use and a safety profile has to be investigated before translation into a patient setting.

Conclusions

Molecular MRI enables the early visualization and quantification of the anti-inflammatory effects of the IL-1β inhibitor 01BSUR in an ApoE-/- mouse model of AAAs. Responders and non-responders might be identified early after the initiation of the therapy using molecular MRI.

Funding

The author(s) disclosed receipt of the following financial support for the research, authorship, and/or publication of this article: This study was funded by the Deutsche Forschungsgemeinschaft (DFG, German Research Foundation) - Projektnummer 372486779 - SFB 1340; MA 5943/3-1/4-1/9-1 and the BHF program grant - RG/12/1/29262. LCA is grateful for her participation in the Berlin Institute of Health (BIH) Charité–Junior Clinician Scientist Program funded by the Charité–Universitaetsmedizin Berlin and the Berlin Institute of Health. The interleukin-1β inhibitor 01BSUR was provided by Novartis, Basel, Switzerland. The elastin-specific contrast agent was provided by Lantheus Medical Imaging, North Billerica, Massachusetts, USA. The authors are thankful for performed ICP-MS by Andy Cakebread, Mass Spectrometry Facility, King's College London, the London Metallomics Facility funded by the Wellcome Trust (grant reference 202902/Z/16/Z).

Contributions

J.B. performed and analyzed the animal and *ex vivo* experiments and wrote the manuscript. M.R.M. and C.T.-R. designed and supervised the study. R.B. and U.K. designed and carried out the LA-ICP-MS experiments. D.C.O. and S.P.R. provided the elastin-specific contrast agent. J.O.K., C.R., M.W., M.G.W. participated in *ex vivo* experiments and reviewed the manuscript. L.C.A., R.M.B. and B.H. reviewed and commented on the manuscript.

Declaration of Conflict of Interests

The author(s) declared no potential conflict of interest with respect to the research, authorship, and/or publication of this article.

References

1. Benjamin EJ, Muntner P, Alonso A, Bittencourt MS, Callaway CW, Carson AP, et al. Heart Disease and Stroke Statistics—2019 Update: A Report From the American Heart Association. Circulation. 2019;139(10):e56-e528.

2. Shimizu K, Mitchell RN, Libby P. Inflammation and cellular immune responses in abdominal aortic aneurysms. Arterioscler Thromb Vasc Biol. 2006;26(5):987-94.

3. Anidjar S, Dobrin PB, Eichorst M, Graham GP, Chejfec G. Correlation of inflammatory infiltrate with the enlargement of experimental aortic aneurysms. J Vasc Surg. 1992;16(2):139-47.

4. Brophy CM, Reilly JM, Smith GJ, Tilson MD. The role of inflammation in nonspecific abdominal aortic aneurysm disease. Ann Vasc Surg. 1991;5(3):229-33.

5. Freestone T, Turner RJ, Coady A, Higman DJ, Greenhalgh RM, Powell JT. Inflammation and matrix metalloproteinases in the enlarging abdominal aortic aneurysm. Arterioscler Thromb Vasc Biol. 1995;15(8):1145-51.

6. Hellenthal FA, Buurman WA, Wodzig WK, Schurink GW. Biomarkers of AAA progression. Part 1: extracellular matrix degeneration. Nat Rev Cardiol. 2009;6(7):464-74.

7. Farand P, Garon A, Plante GE. Structure of large arteries: orientation of elastin in rabbit aortic internal elastic lamina and in the elastic lamellae of aortic media. Microvasc Res. 2007;73(2):95-9.

8. Dinarello CA. A clinical perspective of IL-1β as the gatekeeper of inflammation. European Journal of Immunology. 2011;41(5):1203-17.

9. Isoda K, Akita K, Kitamura K, Sato-Okabayashi Y, Kadoguchi T, Isobe S, et al. Inhibition of interleukin-1 suppresses angiotensin II-induced aortic inflammation and aneurysm formation. Int J Cardiol. 2018;270:221-7.

10. Johnston WF, Salmon M, Su G, Lu G, Stone ML, Zhao Y, et al. Genetic and pharmacologic disruption of interleukin-1β signaling inhibits experimental aortic aneurysm formation. Arterioscler Thromb Vasc Biol. 2013;33(2):294-304.

11. Juvonen J, Surcel HM, Satta J, Teppo AM, Bloigu A, Syrjala H, et al. Elevated circulating levels of inflammatory cytokines in patients with abdominal aortic aneurysm. Arterioscler Thromb Vasc Biol. 1997;17(11):2843-7.

12. Pearce WH, Sweis I, Yao JS, McCarthy WJ, Koch AE. Interleukin-1 beta and tumor necrosis factor-alpha release in normal and diseased human infrarenal aortas. J Vasc Surg. 1992;16(5):784-9.

13. Richards JM, Semple SI, MacGillivray TJ, Gray C, Langrish JP, Williams M, et al. Abdominal aortic aneurysm growth predicted by uptake of ultrasmall superparamagnetic particles of iron oxide: a pilot study. Circ Cardiovasc Imaging. 2011;4(3):274-81.

14. Brangsch J, Reimann C, Kaufmann JO, Adams LC, Onthank DC, Thöne-Reineke C, et al. Concurrent Molecular Magnetic Resonance Imaging of Inflammatory Activity and Extracellular Matrix Degradation for the Prediction of Aneurysm Rupture. Circulation: Cardiovascular Imaging. 2019;12(3):e008707.

15. Turner GH, Olzinski AR, Bernard RE, Aravindhan K, Boyle RJ, Newman MJ, et al. Assessment of macrophage infiltration in a murine model of abdominal aortic aneurysm. J Magn Reson Imaging. 2009;30(2):455-60.

16. Yao Y, Wang Y, Zhang Y, Li Y, Sheng Z, Wen S, et al. In vivo imaging of macrophages during the early-stages of abdominal aortic aneurysm using high resolution MRI in ApoE mice. PLoS One. 2012;7(3):e33523.

17. Klink A, Heynens J, Herranz B, Lobatto ME, Arias T, Sanders HM, et al. In vivo characterization of a new abdominal aortic aneurysm mouse model with conventional and molecular magnetic resonance imaging. J Am Coll Cardiol. 2011;58(24):2522-30.

18. Botnar RM, Wiethoff AJ, Ebersberger U, Lacerda S, Blume U, Warley A, et al. In Vivo Assessment of Aortic Aneurysm Wall Integrity Using Elastin-Specific Molecular Magnetic Resonance Imaging. Circulation: Cardiovascular Imaging. 2014;7(4):679-89.

19. Makowski MR, Preissel A, von Bary C, Warley A, Schachoff S, Keithan A, et al. Three-dimensional imaging of the aortic vessel wall using an elastin-specific magnetic resonance contrast agent. Invest Radiol. 2012;47(7):438-44.

20. Geiger T, Towbin H, Cosenti-Vargas A, Zingel O, Arnold J, Rordorf C, et al. Neutralization of interleukin-1 beta activity in vivo with a monoclonal antibody alleviates collagen-induced arthritis in DBA/1 mice and prevents the associated acute-phase response. Clin Exp Rheumatol. 1993;11(5):515-22.

21. Awan Z, Denis M, Roubtsova A, Essalmani R, Marcinkiewicz J, Awan A, et al. Reducing Vascular Calcification by Anti-IL-1β Monoclonal Antibody in a Mouse Model of Familial Hypercholesterolemia. Angiology. 2016;67(2):157-67.

22. Ridker PM, Everett BM, Thuren T, MacFadyen JG, Chang WH, Ballantyne C, et al. Antiinflammatory Therapy with Canakinumab for Atherosclerotic Disease. New England Journal of Medicine. 2017;377(12):1119-31.

23. Makowski MR, Wiethoff AJ, Blume U, Cuello F, Warley A, Jansen CH, et al. Assessment of atherosclerotic plaque burden with an elastin-specific magnetic resonance contrast agent. Nat Med. 2011;17(3):383-8.

24. Onthank D, Yalamanchili P, Cesati R, Lazewatsky J, Azure M, Hayes M, et al. Abstract 1914: BMS753951: A Novel Low Molecular Weight Magnetic Resonance Contrast Agent Selective For Arterial Wall Imaging. Circulation. 2007;116(suppl_16):II_411-II_2.

25. von Bary C, Makowski M, Preissel A, Keithahn A, Warley A, Spuentrup E, et al. MRI of coronary wall remodeling in a swine model of coronary injury using an elastin-binding contrast agent. Circ Cardiovasc Imaging. 2011;4(2):147-55.

26. Johnston WF, Salmon M, Pope NH, Meher A, Su G, Stone ML, et al. Inhibition of interleukin-1β decreases aneurysm formation and progression in a novel model of thoracic aortic aneurysms. Circulation. 2014;130(11 Suppl 1):S51-S9.

27. Newman KM, Jean-Claude J, Li H, Ramey WG, Tilson MD. Cytokines that activate proteolysis are increased in abdominal aortic aneurysms. Circulation. 1994;90(5 Pt 2):II224-7.

28. Abdul-Hussien H, Hanemaaijer R, Kleemann R, Verhaaren BF, van Bockel JH, Lindeman JH. The pathophysiology of abdominal aortic aneurysm growth: corresponding and discordant inflammatory and proteolytic processes in abdominal aortic and popliteal artery aneurysms. J Vasc Surg. 2010;51(6):1479-87.

29. Pyo R, Lee JK, Shipley JM, Curci JA, Mao D, Ziporin SJ, et al. Targeted gene disruption of matrix metalloproteinase-9 (gelatinase B) suppresses development of experimental abdominal aortic aneurysms. J Clin Invest. 2000;105(11):1641-9.

30. Daugherty A, Cassis LA. Mechanisms of abdominal aortic aneurysm formation. Curr Atheroscler Rep. 2002;4(3):222-7.

31. Dinarello CA. Interleukin-1 in the pathogenesis and treatment of inflammatory diseases. Blood. 2011;117(14):3720-32.

32. Hashimoto Y, Fukazawa R, Nagi-Miura N, Ohno N, Suzuki N, Katsube Y, et al. Interleukin-1beta Inhibition Attenuates Vasculitis in a Mouse Model of Kawasaki Disease. Journal of Nippon Medical School. 2019;86(2):108-16.

33. Kitamura K, Isoda K, Akita K, Okabayashi Y, Kadoguchi T, Shimada K, et al. Abstract 11695: An Anti-Interleukin-1β Antibody Suppresses Both Angiotensin II-induced Renal Inflammation and Hypertension. Circulation. 2017;136(suppl_1):A11695-A.

34. Golledge J, Tsao PS, Dalman RL, et al. Circulating markers of abdominal aortic aneurysm presence and progression. Circulation 2008; 118: 2382-2392. 2008/12/03. DOI: 10.1161/CIRCULATIONAHA.108.802074.

35. Hong H, Yang Y, Liu B, et al. Imaging of Abdominal Aortic Aneurysm: the present and the future. Curr Vasc Pharmacol 2010; 8: 808-819. 2010/02/26. DOI: 10.2174/157016110793563898.

36. Okamura H, Pisani LJ, Dalal AR, Emrich F, Dake BA, Arakawa M, et al. Assessment of Elastin Deficit in a Marfan Mouse Aneurysm Model Using an Elastin-Specific Magnetic Resonance Imaging Contrast Agent. Circulation: Cardiovascular Imaging. 2014;7(4):690-6.

37. Rooke TW, Hirsch AT, Misra S, Sidawy AN, Beckman JA, Findeiss LK, et al. 2011 ACCF/AHA Focused Update of the Guideline for the Management of Patients With Peripheral Artery Disease (updating the 2005 guideline): a report of the American College of Cardiology Foundation/American Heart Association Task Force on Practice Guidelines. J Am Coll Cardiol. 2011;58(19):2020-45.

38. Sakalihasan N, Limet R, Defawe OD. Abdominal aortic aneurysm. Lancet. 2005;365(9470):1577-89.

39. Ridker PM, Howard CP, Walter V, Everett B, Libby P, Hensen J, et al. Effects of interleukin-1beta inhibition with canakinumab on hemoglobin A1c, lipids, C-reactive protein, interleukin-6, and fibrinogen: a phase IIb randomized, placebo-controlled trial. Circulation. 2012;126(23):2739-48.

40. Daugherty A, Manning MW, Cassis LA. Angiotensin II promotes atherosclerotic lesions and aneurysms in apolipoprotein E-deficient mice. J Clin Invest. 2000;105(11):1605-12.

41. Daugherty A, Cassis LA. Mouse models of abdominal aortic aneurysms. Arterioscler Thromb Vasc Biol. 2004;24(3):429-34.

42. Cassis LA, Gupte M, Thayer S, Zhang X, Charnigo R, Howatt DA, et al. ANG II infusion promotes abdominal aortic aneurysms independent of increased blood pressure in hypercholesterolemic mice. Am J Physiol Heart Circ Physiol. 2009;296(5):H1660-5.

43. Longo GM, Xiong W, Greiner TC, Zhao Y, Fiotti N, Baxter BT. Matrix metalloproteinases 2 and 9 work in concert to produce aortic aneurysms. J Clin Invest. 2002;110(5):625-32.

44. Ishibashi M, Egashira K, Zhao Q, Hiasa K, Ohtani K, Ihara Y, et al. Bone marrow-derived monocyte chemoattractant protein-1 receptor CCR2 is critical in angiotensin II-induced acceleration of atherosclerosis and aneurysm formation in hypercholesterolemic mice. Arterioscler Thromb Vasc Biol. 2004;24(11):e174-8.

Figure Legends

Fig. 1

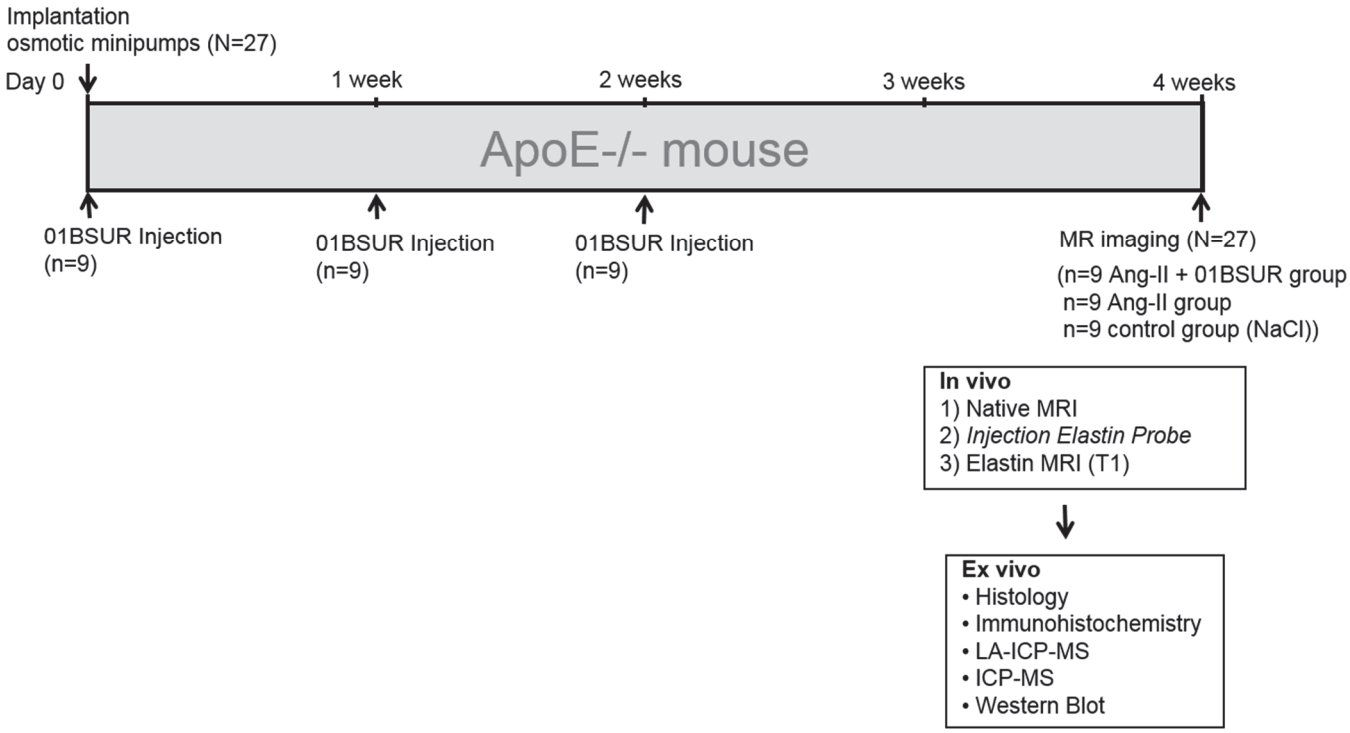

Figure 1: Experimental setup

Nine mice (n=9, Ang-II + 01BSUR group) were injected subcutaneously (s.c.) with 0.3 mg of 01BSUR three times: on the day of minipump implantation (day 0), 7 days and 14 days after minipump implantation. The angiotensin-II group (n=9) and the control group received no treatment after minipump implantation. MR imaging with a clinical dose of an elastin-specific gadolinium-based (0.2 mmol/kg) of all three groups was performed 28 days following minipump implantation.

Fig. 2

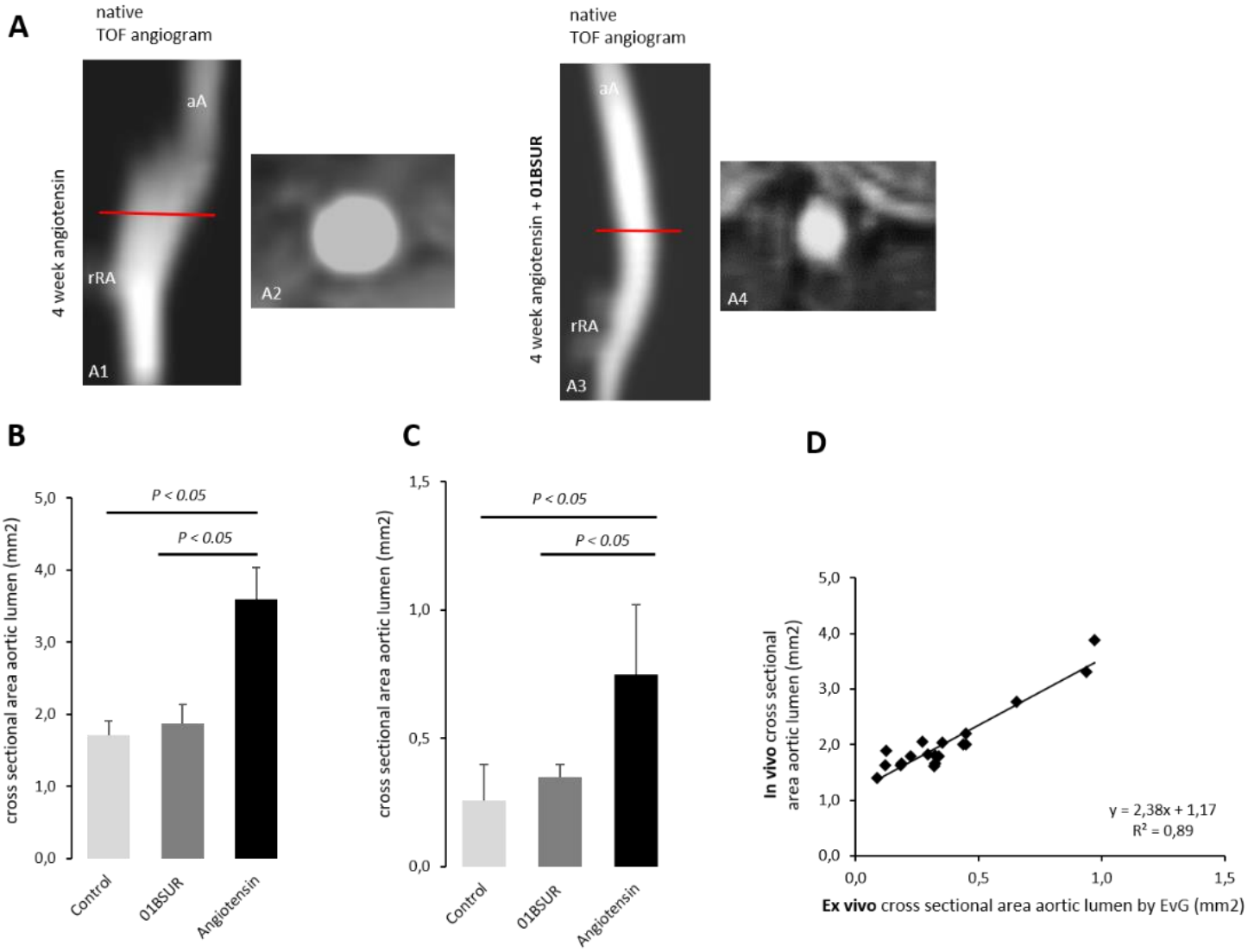

Figure 2: In vivo and ex vivo assessment of the aortic cross-sectional area

The Time-of-flight (TOF) angiogram of the suprarenal part of the abdominal aorta 4 weeks after continuous infusion of angiotensin II showed a strong dilatation of the aortic lumen (A1, A2) whereas a non-dilated aortic lumen was observed in mice treated with 01BSUR (A3, A4). On in vivo cross-sectional area measurements (B) and ex vivo histological measurements (C) a significant increase in cross-sectional areas of the aortic lumen size was observed in untreated mice after 4 weeks of angiotensin II infusion, reflecting development of AAAs in these mice in contrast to mice treated with 01BSUR. There was no significant difference in the cross-sectional area of the aortic lumen size between the Ang-II + 01BSUR group and the control group. In vivo MR measurements of the aortic diameter correlated strongly with ex vivo measurements on histological Elastica van Gieson (EvG) stained sections (D). aA: suprarenal abdominal-aorta; rRA: right renal-artery.

Fig. 3

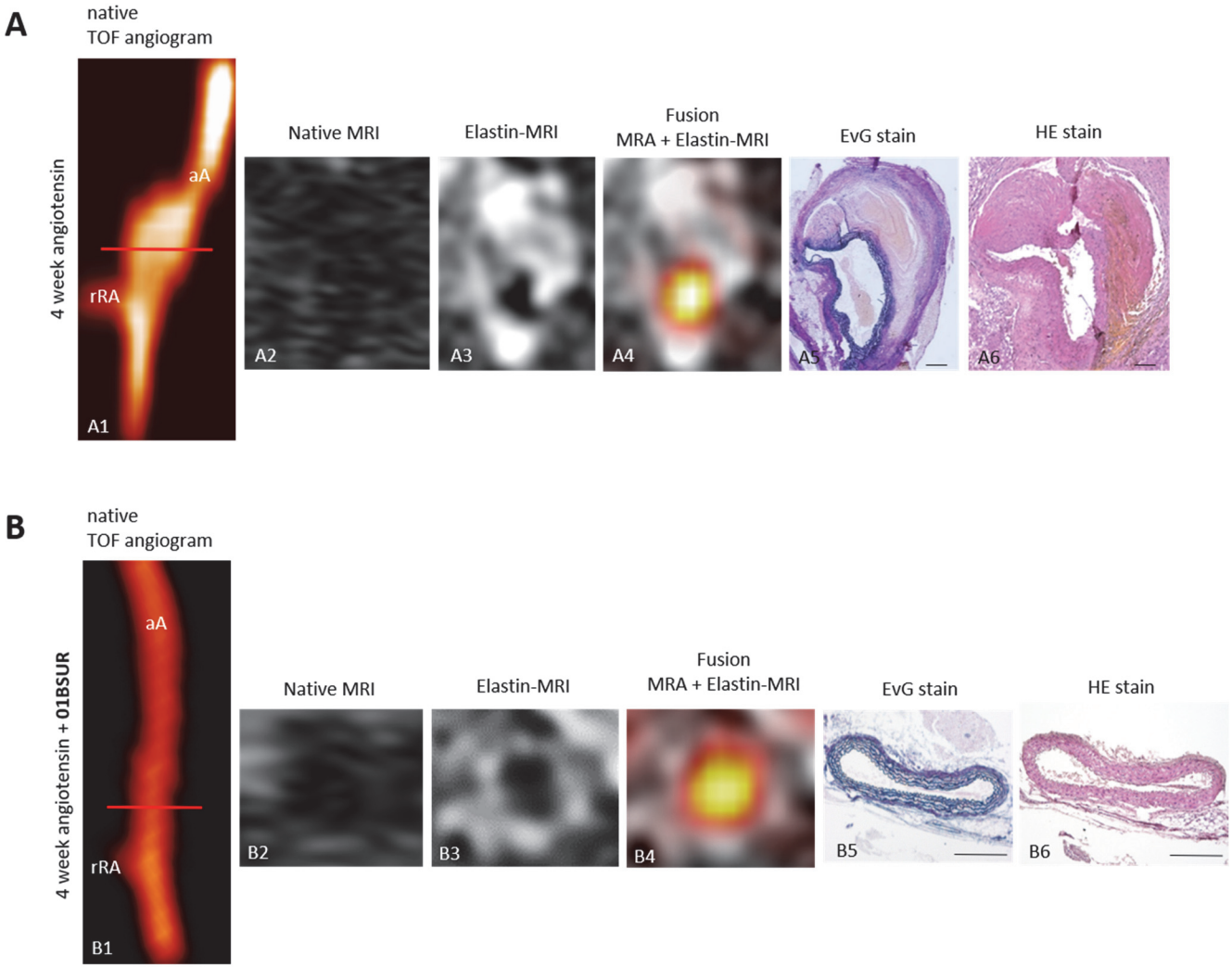

Figure 3: In vivo molecular MRI of extracellular-matrix of the aortic wall

Time-of-flight angiograms showing a suprarenal abdominal aorta including the right renal-artery of a male ApoE-/- mouse after 4 weeks of Ang-II infusion (A1). An extensive aortic aneurysm was developed after 4 weeks of Ang-II infusion including a strong remodeling of the extracellular matrix by an expression of elastic-fibers in the area of former elastin dissection which was observed in vivo by MRI after the administration of the elastin-specific-probe (A3, A4) and ex vivo by histological analysis (A5, A6). The abdominal aorta of a male ApoE-/- mouse treated with 01BSUR show no pathological changes of the aortic wall in vivo on the time-of-flight angiogram (B1), native MRI (B2) and T1-weighted-sequences using the elastin-specific-probe (B3, B4) or on corresponding ex vivo histology (B5, B6). Scale bars represent 200 µm. TOF: Time-of-flight, EvG: Elastica van Gieson staining, Elastic fibers are stained blue-black; HE: Hematoxylin-Eosin-staining; MRA: magnetic-resonance-angiography; aA: suprarenal abdominal-aorta; rRA: right renal-artery.

Fig. 4

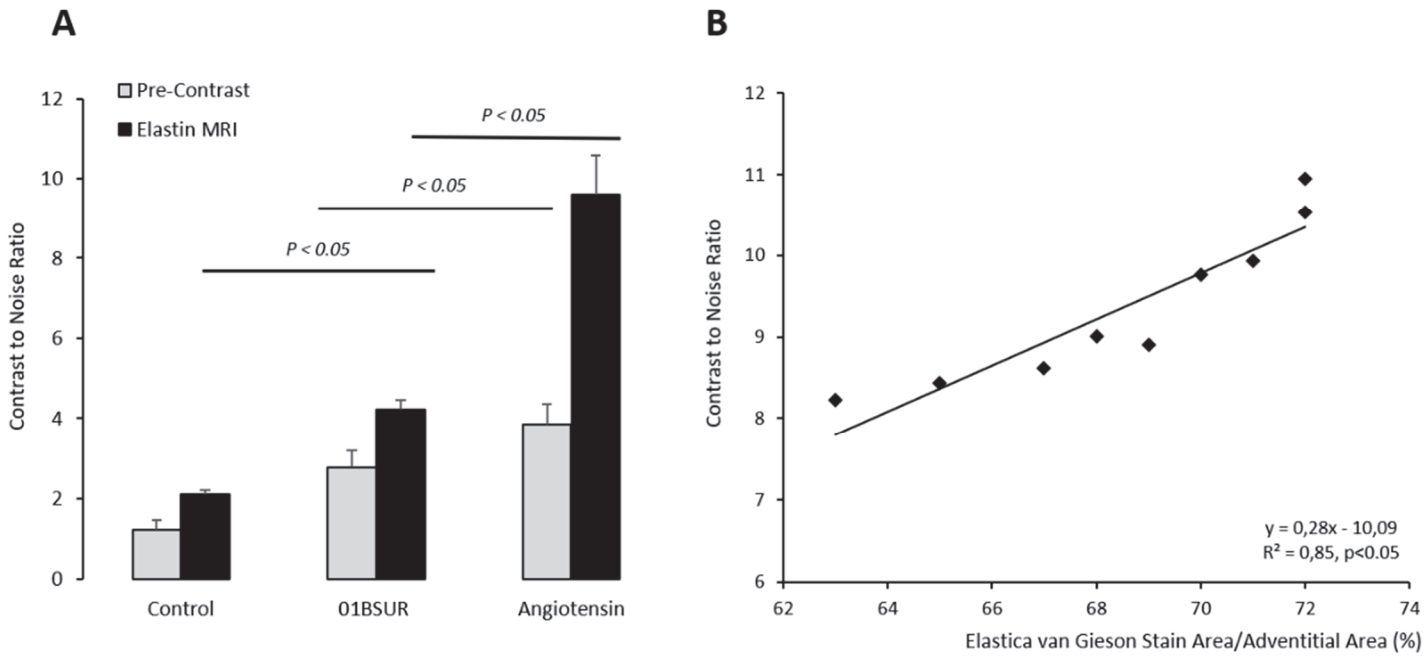

Figure 4: In vivo MRI signal measurements and ex vivo quantification of the gadolinium-based elastin specific probe

Contrast-to-noise-ratio (CNR) values before and following the administration of the gadolinium-based elastin-specific MR probe showed a significant increase in CNR in the aortic wall in mice of the Ang-II + 01BSUR group, Ang-II group and control group. The strongest signal enhancement was shown by the mice of the Ang-II group due to a strong remodeling and expression of elastic fibers in the aneurysmal wall. In vivo CNR measurements showed a strong correlation with ex vivo Elastica van Gieson (EvG) staining on corresponding histological sections (B).

Fig. 5

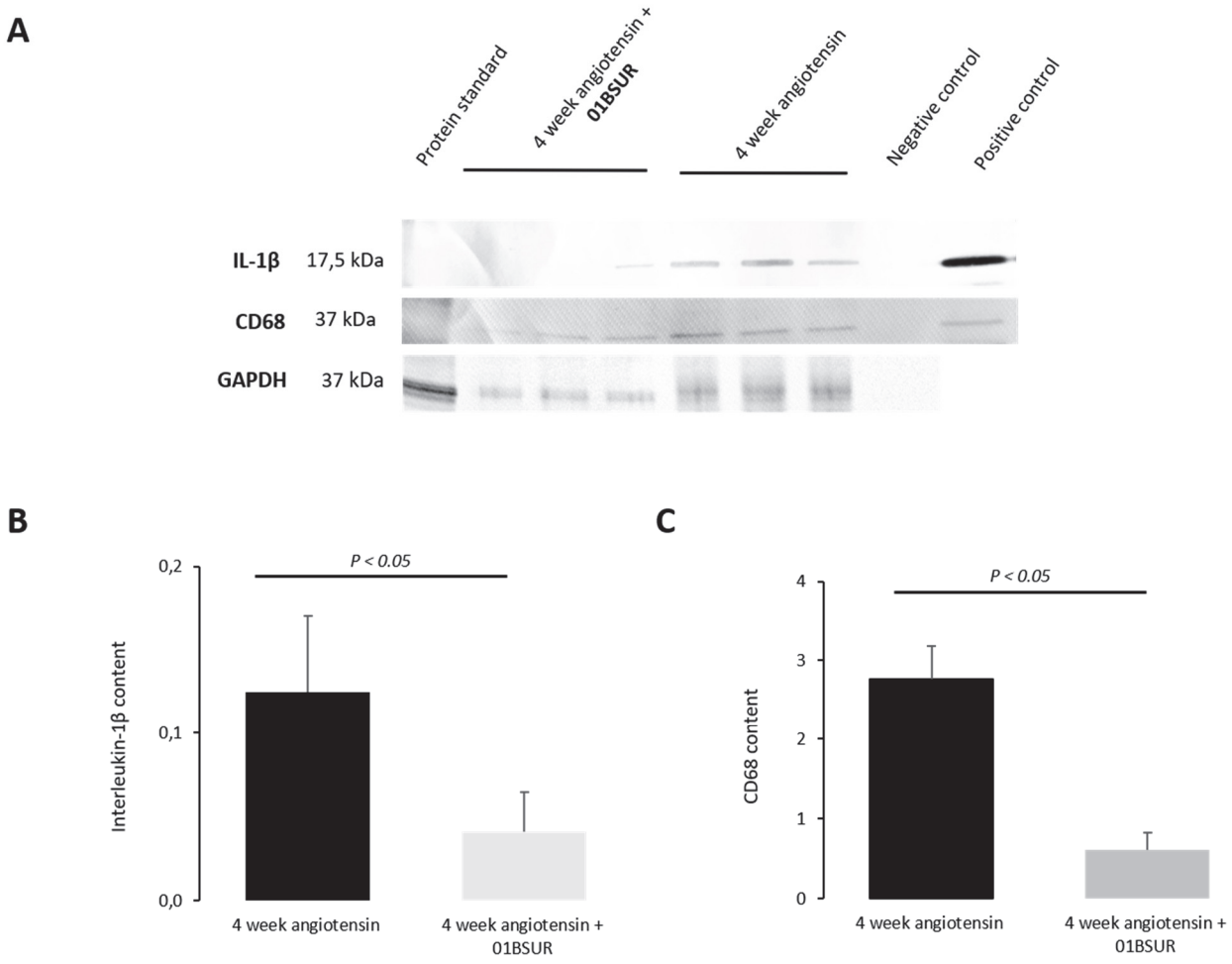

Figure 5: Western Blot analysis

Western Blot analysis (A) and quantification of protein bands (B, C) of suprarenal aortic tissue of ApoE-/- mice after 4 weeks of angiotensin II infusion (n=3) and ApoE-/- mice after 4 weeks of angiotensin II infusion treated with 01BSUR (n=3) using an interleukin-1β (17,5 kDa) antibody and CD68 (37 kDa) antibody. GAPDH (37 kDa) was used as loading control. A cropped Blot is displayed to improve conciseness.

Fig.6

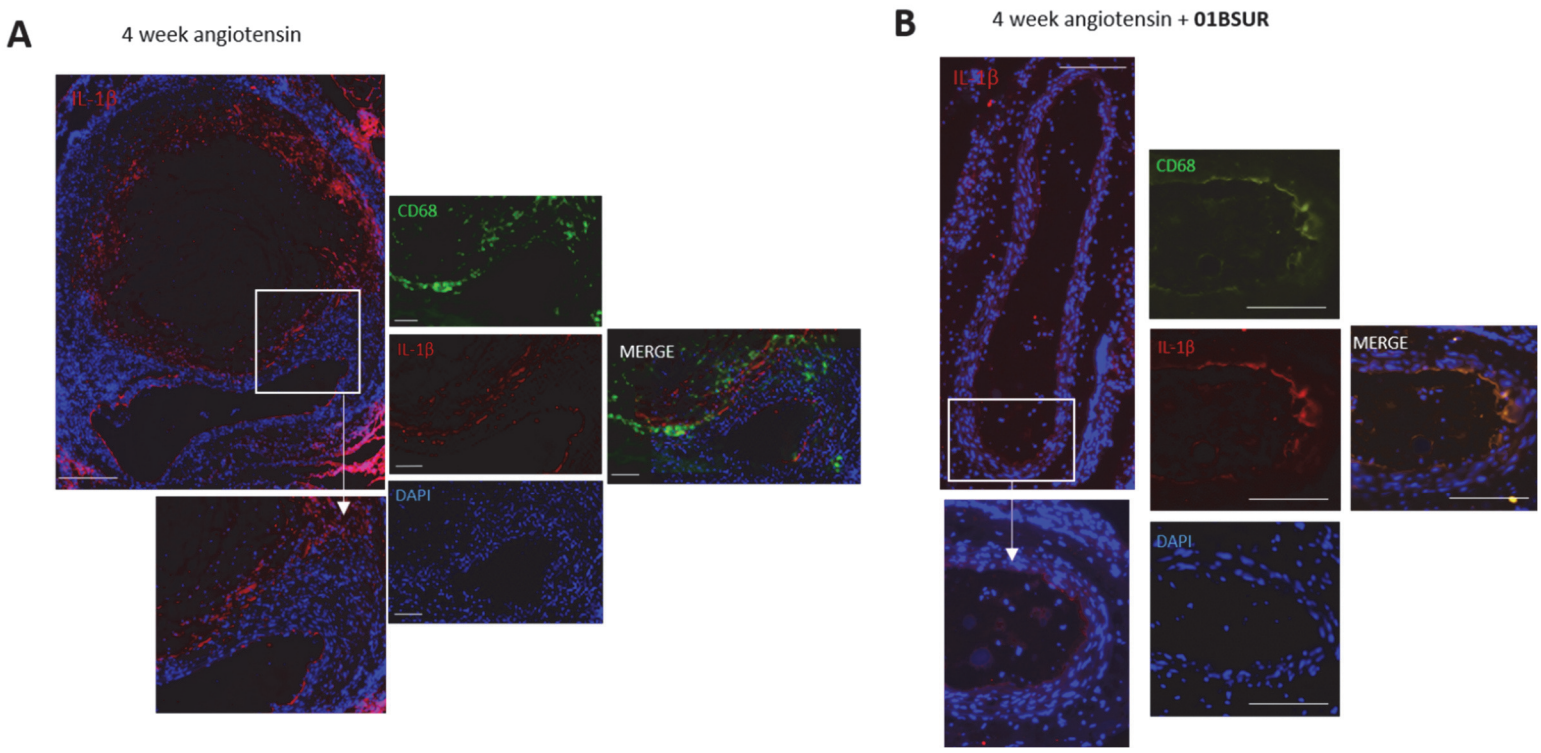

Figure 6: Ex vivo immunofluorescence measurements

Immunofluorescence staining with CD68 antibody was performed on histological slices of mice of the Ang-II group (A) and Ang-II + 01BSUR group (B). **A:** Mice of the AngII-group showed an increased expression of IL-1β in the aortic wall (on the left hand; scale bar represent 200 µm). On the right hand: Macrophages (CD68) are shown in green, Interleukin-1β in red and cell nuclei (DAPI) in blue. The stacked image demonstrates a clear co-localization of IL-1β with macrophages. Scale bars represent 100 µm. **B**: Mice of the Ang-II + 01BSUR group showed a significant lower IL-1β expression (on the left hand) as well as a trivial macrophage staining (on the right hand). Scale bars represent 200 µm. Different magnifications were used due to the relatively large size of the aneurysm.

Fig. 7

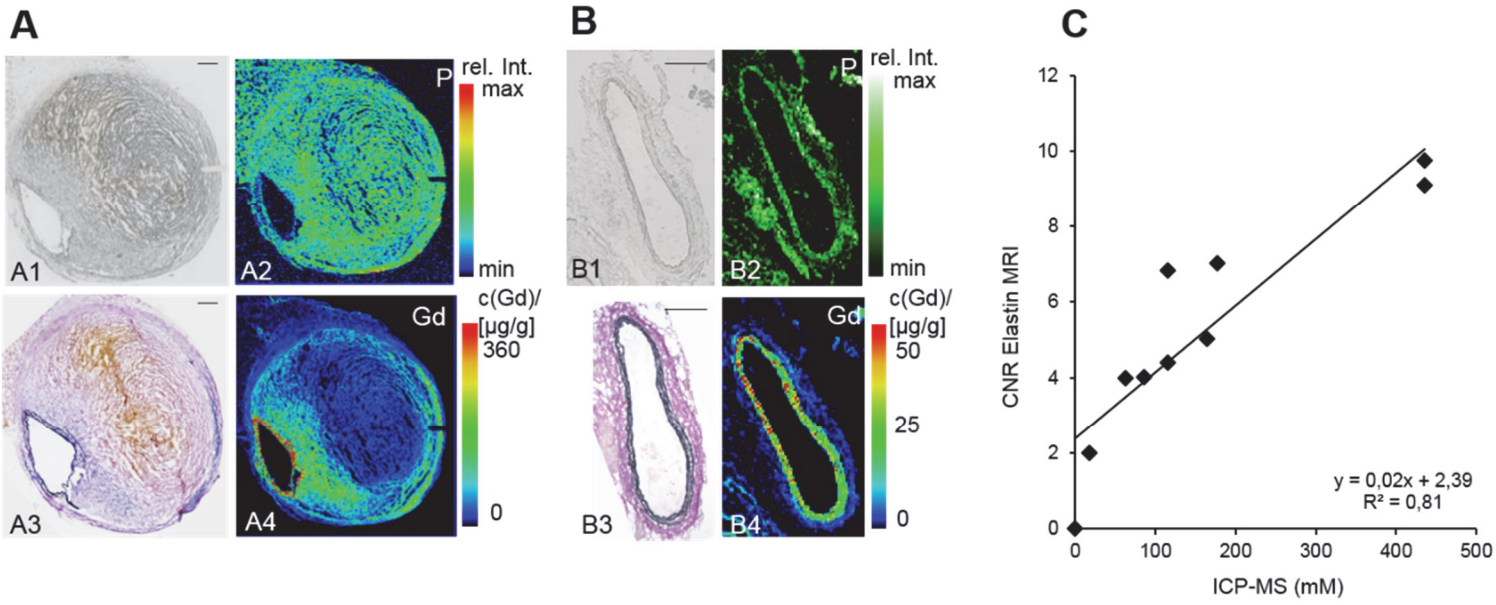

Figure 7: **Spatial localization of the elastin-specific gadolinium-based probe in the aortic wall using laser coupled mass spectrometry (LA-ICP-MS) and correlation of *in vivo* MRI signal measurements with ICP-MS**

The phosphorus distribution was measured using LA-ICP-MS to get an anatomical overview of the histological sections (A2, B2). LA-ICP-MS visualized the elastin-specific gadolinium-based probe within the aneurysmal wall (A4, B4) by the Gd signal. A clear co-localization of gadolinium accumulation with the elastic fibers in the Elastica van Gieson stain was shown (A3, B3). Scale bars represent 200 µm. C: A strong correlation of ICP-MS measurements for gadolinium with *in vivo* CNR measurements following the administration of the elastin-specific probe was demonstrated. CNR: Contrast to noise ratio; ICP-MS: Inductively coupled mass spectroscopy.

5 Discussion

5.1 Molecular MR imaging for diagnosis and characterization of aortic aneurysms

Molecular imaging represents a promising novel approach by using molecular probes that bind specifically to a molecular target for the visualization of pathological processes at a molecular and cellular level. In the context of abdominal aortic aneurysms, molecular imaging could improve the diagnosis as well as characterization of the changes within the aortic wall. Therefore, we have tested the feasibility of molecular MRI using an elastin-specific probe in combination with iron-oxide particles for the evaluation of AAA development and progression in a mouse model.

As the most abundant ECM protein in the tunica media, elastin is highly responsible for the integrity of the aortic wall, constituting over 30% of the dry weight of the aorta (112). The increased degradation of elastic fibers by enzymes, including MMPs secreted by macrophages and neutrophils, leads to a reduced ability of the aortic wall to withstand the intravascular pressure and pulsation, resulting in a progressive dilatation of the aorta (101). Since elastin fragmentation was shown to be one of the initiating events of aneurysm development (14), elastin degradation has become one of the promising *in vivo* biomarkers to improve AAA characterization. To visualize these changes in elastin structure and amount within the aortic wall, we have used a gadolinium-based elastin-specific probe which binds specifically elastic fibers. Over the course of 4 weeks, different stages of AAA development could be visualized *in vivo*, starting 1 week after Ang II infusion of male ApoE-/- mice. Already in this early-stage aneurysms, a disruption of elastic fibers could be observed *in vivo*, due to a significant MR signal enhancement in the aneurysmal wall after administration of the elastin-specific probe. Furthermore, the visualization of an intramural hematoma was feasible. In late-stage aneurysms, it was even possible to observe a potential stabilization or repair process of the aneurysmal wall by a strong expression of elastic fibers at the former rupture site and throughout the thrombus. This process is thought to be a compensatory response to resist the intravascular pressure (103). In addition, elastin-specific MRI allowed not only the visualization, but also the quantification of changes in elastin composition. This could yield important information especially for the prediction of aneurysm progression and rupture.

Besides the ECM degradation, inflammation was shown to be a key process in AAA formation. Especially monocytes and macrophages which migrate into the aortic wall to express various cytokines and proteases are of high interest as a new *in vivo* biomarker. To evaluate the inflammatory activity during AAA formation and progression, an ultra-small superparamagnetic iron oxide particle (ferumoxytol) was used in the first study. These USPIOs were taken up by

circulating macrophages that subsequently accumulate in the aneurysmal wall within 12-24h post injection. Causing a local shortening of the T2/T2* relaxation time, the accumulated macrophages could be visualized and quantified due to a corresponding signal void in the MR images. An increasing inflammatory response over the 4 weeks of AAA development was observed including an increasing accumulation of macrophages, particularly at the edges of the dissected elastin laminae, but also in regions of elastin degradation. These findings suggest that these macrophages release proteases, such as MMPs, which may directly degrade elastic fibers and other ECM proteins leading to a further aortic wall weakening and dilatation. The visualization of a high inflammatory status of the aneurysmal wall may, therefore, indicate a further AAA progression until potential fatal rupture.

Several preclinical and clinical studies confirmed these findings using either elastin-specific contrast agents or iron-oxide particles (102, 106, 108, 111, 113). To our knowledge, we were the first to test the feasibility of concurrent imaging of inflammatory activity and extracellular-matrix degradation by using two different molecular probes in one MR imaging session. Therefore, two crucial processes of AAA development could be visualized and quantified at the same time. Both probes could be distinguished easily during MR imaging because of their different effect on relaxation times. While the gadolinium-based elastin-specific probe causes a bright signal on T1-weighted sequences, the iron-oxide particle appears as signal void on T2/T2*-weighted sequences. Furthermore, we proved that there was no influence of the iron-based probe on the visualization and quantification of the gadolinium-based probe and vice versa. This fact is particularly important in the context of a potential future clinical application of concurrent imaging with two different MR probes. Further advantages regarding clinical translation include the approval of the used iron oxide particle ferumoxytol by the U.S Food and Drug Administration (FDA) for the treatment of iron deficiency anemia. Therefore, it can be used off-label as an MRI agent in clinical practice (114). The elastin-specific probe is comparable to MRI contrast agents already used in clinical practice regarding molecular size and composition, as well as clearance from the blood (115). In addition, both probes were administered at a clinical dose. By performing both studies using a clinical 3 Tesla MR scanner, several configurations such as relaxation, rotational correlation, and signal properties can furthermore be directly translated to human application.

5.2 Molecular MR imaging for the prediction of aortic aneurysms

Besides the diagnosis and visualization of AAAs, the prediction of further aneurysm development or even rupture represents one of the most important and difficult challenges regarding molecular imaging in the cardiovascular context. The potential of inflammation as a

biomarker of AAA prediction as well as ECM protein degradation as another possible biomarker has already been investigated independently in different preclinical and clinical studies (100, 111).

To our knowledge, our study was the first to investigate the feasibility of concurrent molecular MRI with two different imaging probes for the prediction of AAA rupture. Regarding the inflammatory processes, animals that showed already one week after AAA induction a high uptake of iron oxide particle in the aortic wall resulting in a high MR signal void suffered from subsequent AAA rupture compared to those animals that showed a significant lower iron oxide particle uptake. Consequently, a high inflammatory status including an extensive accumulation of macrophages within the aneurysmal wall may serve as a possible predictive biomarker for AAA rupture. Furthermore, the concurrent *in vivo* imaging of the extracellular matrix revealed that animals with subsequent deadly aneurysm rupture showed a significantly stronger breakdown of elastic fibers after one week of Ang II infusion compared to surviving animals. These results suggest that the degradation of elastic fibers could be another imaging biomarker for the prediction of aneurysm rupture. Even though iron oxide particle MRI, as well as MRI using the elastin-specific probe, enabled the prediction of AAA rupture with high sensitivity and specificity each, the highest accuracy was demonstrated by the combined assessment of both imaging probes. Therefore, both biomarkers have their independent values and advantages, but a combined MR based assessment of both pathological processes improves the risk of rupture prediction of AAAs.

5.3 Interleukin 1 beta – a new therapeutic target for AAA treatment

In our second study, we assessed the potential of a novel promising therapeutic approach including the disruption of the inflammatory pathways during AAA formation. One of the key mediators of inflammation represents the cytokine interleukin-1β. IL-1β is mainly expressed by macrophages whereas endothelial cells and smooth muscle cells are also capable of IL-1β synthesis when stimulated by IL-1β. This positive feedback loop system further enhances inflammatory processes. The wide-ranging effects of IL-1β on vascular cells include the regulation of smooth muscle cells and endothelial cells. As a result, smooth muscle cells secrete high amounts of IL-6 which stimulates primarily lymphocyte proliferation. Furthermore, IL-1β stimulates the induction of expression of endothelial cell adhesion molecules which further enhance the inflammatory response by recruiting additional inflammatory cells (116). It was shown that IL-1β contributes crucially to the formation and progression of AAAs especially by the activation of macrophages that produce various MMPs, including MMP-9, a protease with high elastolytic activity (117, 118). Therefore, IL-1β does not only promote the

inflammatory processes during AAA formation but also the destruction of ECM proteins like elastin. Since preclinical studies revealed the critical role of IL-1β in experimental AAA formation as well as a significant elevation of IL-1β was found in AAA patients, IL-1β has gained in interest as a potential target for AAA therapy (28, 116, 117).

The disruption of the IL-1β pathway *via* direct antibodies to IL-1β or IL-1 receptor (IL-1R) has been investigated previously in various studies. The IL-1R antagonist Anakinra which is already commercially available for the treatment of rheumatoid arthritis showed a significant protection against AAA formation and progression in a mouse model of AAA although administered in a 100-fold dose compared to the clinical dosage (119). The monoclonal IL-1β antibody 01BSUR used in our second study has also been evaluated already in different preclinical studies using mouse models of Kawasaki Disease, renal inflammation and abdominal aneurysms (120-122). These studies confirmed our findings that the repeated administration of 01BSUR results in a significant reduction of inflammation and ECM degradation within the aortic wall and therefore in a significant decrease in AAA formation. Moreover, in our study, we have used an already clinically approved dose of the anti-IL-1β antibody as used within a large phase 3 trial investigating the anti-IL-1β antibody canakinumab for the prevention of recurrent myocardial infarction (123). Further studies are now needed to evaluate the potential of this novel approach of AAA therapy to enable a future translation into clinical practice.

5.4 Molecular MR imaging for evaluation of AAA therapy

The evaluation of anti-inflammatory therapies of abdominal aneurysms using molecular MR imaging has gained clinical importance in the last several years. The aim of our second study was to prove the feasibility of molecular MRI for the evaluation and quantification of AAAs in response to anti-inflammatory treatment. The use of the elastin-specific probe allowed the visualization and quantification of changes in the ECM composition within the aortic wall. The anti-inflammatory treatment of Ang II-infused mice seemed to prevent the destruction of elastic fibers within the aortic wall and therefore the development of abdominal aortic aneurysms which could be clearly visualized on MR images. Molecular MR imaging may therefore be a useful tool for the monitoring of AAA patients receiving an anti-inflammatory therapy. Especially, an early identification of responders and non-responders to therapy could be feasible for identifying the most suitable therapy option for an AAA patient or adjusting the dosage of the administered medication. In the context of atherosclerosis, molecular MRI for the assessment of therapeutic responses to anti-inflammatory interventions was already successfully tested in a clinical setting. USPIO enhanced MRI demonstrated quantifiable changes in carotid plaque inflammation within the first 3 months of therapy in patients with

atherosclerotic lesions (124). This confirms our findings that molecular MRI represents a promising new approach not only for the *in vivo* characterization of aneurysms but also for the evaluation of the response to therapy.

5.5 Limitations

One main difference between human AAAs and those formed in the mouse model used in our studies is the anatomic location. In ApoE-/- mice, AAAs develop in the suprarenal region, whereas in humans AAAs develop preferentially in the infrarenal region (125-127). One possible explanation is the regional differences in collagen and elastin composition in the aortic wall, which lead to altered mechanical properties (128). Furthermore, there are differences in the embryologic lineage of vascular smooth muscle cells of the thoracic and abdominal aortas, determining their response to various cytokines and extracellular matrix proteins. (125, 129).

The molecular probes that were used in both studies are currently not approved for clinical use. Even though the used iron oxide particle ferumoxytol is already approved for the treatment of iron deficiency anemia, it has to be used off-label for MR imaging with care because of the potential risk of complement activation. In addition, the safety profile of the elastin-specific probe as well as the safety profile of both agents in combination has to be investigated before translation into a patient setting.

6 Summary

Development and evaluation of novel molecular probes for the characterization of abdominal aortic aneurysms using magnetic resonance imaging (MRI)

Abdominal aortic aneurysms represent a cardiovascular disease with potentially life-threatening consequences. Although ruptured AAAs being the third most common cause of sudden death after myocardial infarction and stroke, the exact causes, as well as pathological processes of AAA formation and progression, still remain unknown. Since the number of patients showing this irreversible dilatation of the infrarenal aorta has constantly increased in the last several years, novel approaches for AAA diagnosis and management are required.

Currently, there are different imaging techniques available in clinical practice for the diagnosis of abdominal aneurysms by measuring the aortic diameter, including ultrasound, computed tomography and magnetic resonance imaging. Since the aortic diameter was shown to be highly limited as a diagnostic and especially as a prognostic parameter for AAA rupture, molecular imaging which enables the assessment of changes within the aortic wall at a molecular level, has gained in attention. The aim of the present studies was therefore to investigate the feasibility of molecular MR imaging for the visualization and characterization of AAAs in a mouse model using different molecular probes. On the one hand, by using a gadolinium-based probe binding specifically elastic fibers, the pathological changes in the extracellular matrix of the aortic wall were clearly visualized and moreover also quantified. On the other hand, due to the concurrent administration of iron-oxide particles, the inflammatory processes during AAA development could be evaluated in the same MR imaging session. Furthermore, the future rupture of the aneurysmal wall could be reliably predicted based on the combined information from both molecular probes.

Molecular MR imaging has the potential not only to improve AAA diagnosis and risk stratification but also the assessment of responses to therapy. Consequently, we have aimed in our second study to investigate molecular MRI for the assessment of the therapeutic effects of an anti-interleukin-1β antibody on AAA formation. Using the elastin-specific probe, the anti-inflammatory effects of the IL-1β antibody within the aortic wall could be already early visualized and quantified. The neutralization of the pro-inflammatory cytokine IL-1β seemed to prevent AAA formation in the mouse model and offers therefore a new pathway for AAA treatment. Since the current management of abdominal aneurysm is limited to frequent monitoring until surgical intervention of large AAAs, an anti-inflammatory pharmacological treatment of AAAs would be a substantial improvement for patients.

The studies demonstrate that molecular MRI represents a novel imaging technique with potential to improve the diagnosis, characterization, risk assessment and visualization in response to therapy of abdominal aortic aneurysms. By combining two imaging probes, the two key processes of AAA development, inflammation and ECM protein degradation could be reliably evaluated. This new imaging parameters may complement already established morphological parameters, such as the aortic diameter, and may therefore improve especially the prediction of risk of aortic rupture. Nevertheless, various barriers have to be overcome to realize a future translation into clinical practice, including high regulatory hurdles and costs as well as the evaluation of safety profiles of novel imaging probes.

7 Zusammenfassung

Entwicklung und Evaluierung neuer niedrig-molekularer Sonden für die Charakterisierung von abdominalen Aortenaneurysmen mittels der Magnetresonanztomographie (MRT)

Abdominale Aortenaneurysmen (AAA) zählen zu den kardiovaskulären Erkrankungen mit potentiell lebensgefährlichen Folgen. Obwohl die Ruptur von AAAs die dritthäufigste Ursache für ein plötzliches Versterben darstellt, hinter Herzinfarkten und Schlaganfällen, sind sowohl die genauen Ursachen als auch die pathologischen Mechanismen der Entwicklung von Aneurysmen noch weitetestgehend ungeklärt. Da die Zahl an Patienten mit dieser irreversiblen Erweiterung der infrarenalen Aorta in den letzten Jahren konstant zugenommen hat, werden neue Ansätze in der Diagnostik und Behandlung von AAAs dringend benötigt.

Derzeit stehen in der klinischen Praxis verschiedene bildgebende Verfahren zur Diagnose von abdominalen Aortenaneurysmen zur Verfügung, darunter Ultraschall, Computertomographie und Magnetresonanztomographie. Bisher erfolgt die Diagnosestellung durch das Vermessen des Aortendurchmessers. Seit mehrere Studien gezeigt haben, dass sich der Durchmesser der Aorta diagnostisch und vor allem prognostisch für die weitere Entwicklung des Aneurysmas als sehr begrenzt erweist, hat die molekulare Bildgebung - die es ermöglicht, Veränderungen innerhalb der Aortenwand auf molekularer Ebene zu beurteilen - an Bedeutung gewonnen. Das Ziel unserer Studien war es daher, die Anwendbarkeit der molekularen MRT Bildgebung für die Visualisierung und Charakterisierung von AAAs in einem Mausmodell mit verschiedenen molekularen Sonden zu untersuchen. Einerseits konnten durch den Einsatz einer Gadolinium-basierten Sonde, welche spezifisch an elastische Fasern bindet, die pathologischen Veränderungen der extrazellulären Matrix dargestellt und darüber hinaus quantifiziert werden. Andererseits konnten durch die gleichzeitige Verabreichung von Eisenoxidpartikeln, die Entzündungsprozesse während der AAA-Entwicklung zeitgleich in derselben MRT Untersuchung evaluiert werden. Darüber hinaus konnte eine zukünftige Ruptur der Gefäßwand anhand der kombinierten Informationen beider molekularer Sonden zuverlässig vorhergesagt werden.

Die molekulare MRT Bildgebung hat das Potenzial, nicht nur die Diagnostik und Risikostratifizierung von AAAs zu verbessern, sondern auch die Beurteilung des Ansprechens auf Therapien. Daher war das Ziel unserer zweiten Studie, die molekulare MRT Bildgebung zur Beurteilung der therapeutischen Wirkung eines Interleukin-1β (IL-1β) Antikörpers auf die Bildung von AAAs zu untersuchen. Durch den Einsatz der Elastin-spezifischen Sonde, konnten die entzündungshemmenden Effekte des IL-1β Antikörpers innerhalb der Aortenwand bereits

frühzeitig visualisiert und quantifiziert werden. Die Hemmung des proinflammatorischen Zytokins IL-1β schien die Bildung der AAA im Mausmodell zu verhindern und bietet daher möglicherweise einen neuen therapeutischen Ansatz in der Behandlung von Aortenaneurysmen. Da das derzeitige Management von abdominalen Aortenaneurysmen lediglich eine regelmäßige Überwachung bzw. eine operative Behandlung großer AAAs beinhaltet, würde eine entzündungshemmende pharmakologische Behandlung von AAAs eine wesentliche Verbesserung für die Patienten darstellen.

Die Studien zeigen, dass molekulares MRT eine neuartige Bildgebungstechnik mit großem Potenzial zur Verbesserung der Diagnose, Charakterisierung, Risikobewertung und die Beurteilung des Ansprechens auf Therapien von abdominalen Aortenaneurysmen darstellt. Durch die Kombination zweier bildgebender Sonden konnten die beiden Schlüsselprozesse der AAA-Entwicklung, Entzündung und Abbau extrazellulärer Matrixproteine, zuverlässig bewertet werden. Diese neuen bildgebenden Parameter können die bereits etablierten morphologischen Parameter, wie den Aortendurchmesser, ergänzen und somit insbesondere die Vorhersage des Rupturrisikos der Gefäßwand verbessern. Dennoch müssen verschiedene Hindernisse überwunden werden, wie hohe regulatorische Hürden und Kosten sowie die Bewertung der Sicherheitsprofile dieser neuartigen Sonden, um eine zukünftige Umsetzung in die klinische Praxis zu realisieren.

8 References

1. Weiss N, Rodionov RN, Mahlmann A. Medical management of abdominal aortic aneurysms. Vasa. 2014;43(6):415-21.

2. Sakalihasan N, Limet R, Defawe OD. Abdominal aortic aneurysm. Lancet. 2005;365(9470):1577-89.

3. Upchurch GR, Jr., Schaub TA. Abdominal aortic aneurysm. Am Fam Physician. 2006;73(7):1198-204.

4. Howard DPJ, Banerjee A, Fairhead JF, Handa A, Silver LE, Rothwell PM, et al. Age-specific incidence, risk factors and outcome of acute abdominal aortic aneurysms in a defined population. BJS. 2015;102(8):907-15

5. Nevitt MP, Ballard DJ, Hallett JW, Jr. Prognosis of abdominal aortic aneurysms. A population-based study. N Engl J Metumd. 1989;321(15):1009-14.

6. Kent KC. Clinical practice. Abdominal aortic aneurysms. N Engl J Med. 2014;371(22):2101-8.

7. Wilmink TB, Quick CR, Hubbard CS, Day NE. The influence of screening on the incidence of ruptured abdominal aortic aneurysms. J Vasc Surg. 1999;30(2):203-8.

8. Thompson RW, Geraghty PJ, Lee JK. Abdominal aortic aneurysms: basic mechanisms and clinical implications. Curr Probl Surg. 2002;39(2):110-230.

9. Matsumura K, Hirano T, Takeda K, Matsuda A, Nakagawa T, Yamaguchi N, et al. Incidence of Aneurysms in Takayasu's Arteritis. Angiology. 1991;42(4):308-15.

10. Towbin JA, Casey B, Belmont J. The molecular basis of vascular disorders. Am J Hum Genet. 1999;64(3):678-84.

11. Johansen K, Koepsell T. Familial tendency for abdominal aortic aneurysms. JAMA. 1986;256(14):1934-6.

12. Hellenthal FA, Buurman WA, Wodzig WK, Schurink GW. Biomarkers of AAA progression. Part 1: extracellular matrix degeneration. Nat Rev Cardiol. 2009;6(7):464-74.

13. Burton AC. Relation of structure to function of the tissues of the wall of blood vessels. Physiological reviews. 1954;34(4):619-42.

14. Daugherty A, Cassis LA. Mechanisms of abdominal aortic aneurysm formation. Curr Atheroscler Rep. 2002;4(3):222-7.

15. Sakalihasan N, Heyeres A, Nusgens BV, Limet R, Lapiere CM. Modifications of the extracellular matrix of aneurysmal abdominal aortas as a function of their size. European journal of vascular surgery. 1993;7(6):633-7.

16. Dobrin PB, Mrkvicka R. Failure of elastin or collagen as possible critical connective tissue alterations underlying aneurysmal dilatation. Cardiovascular surgery. 1994;2(4):484-8.

17. Sakalihasan N, Delvenne P, Nusgens BV, Limet R, Lapiere CM. Activated forms of MMP2 and MMP9 in abdominal aortic aneurysms. Journal of vascular surgery. 1996;24(1):127-33.

18. Reilly JM. Plasminogen activators in abdominal aortic aneurysmal disease. Annals of the New York Academy of Sciences. 1996;800:151-6.

19. Thompson RW, Parks WC. Role of matrix metalloproteinases in abdominal aortic aneurysms. Annals of the New York Academy of Sciences. 1996;800:157-74.

20. Knox JB, Sukhova GK, Whittemore AD, Libby P. Evidence for altered balance between matrix metalloproteinases and their inhibitors in human aortic diseases. Circulation. 1997;95(1):205-12.

21. Anidjar S, Salzmann JL, Gentric D, Lagneau P, Camilleri JP, Michel JB. Elastase-induced experimental aneurysms in rats. Circulation. 1990;82(3):973-81.

22. Daugherty A, Cassis LA. Mouse models of abdominal aortic aneurysms. Arteriosclerosis, thrombosis, and vascular biology. 2004;24(3):429-34.

23. Menashi S, Campa JS, Greenhalgh RM, Powell JT. Collagen in abdominal aortic aneurysm: typing, content, and degradation. Journal of vascular surgery. 1987;6(6):578-82.

24. Shimizu K, Mitchell RN, Libby P. Inflammation and cellular immune responses in abdominal aortic aneurysms. Arteriosclerosis, thrombosis, and vascular biology. 2006;26(5):987-94.

25. Busuttil RW, Abou-Zamzam AM, Machleder HI. Collagenase activity of the human aorta. A comparison of patients with and without abdominal aortic aneurysms. Archives of surgery. 1980;115(11):1373-8.

26. Anidjar S, Dobrin PB, Eichorst M, Graham GP, Chejfec G. Correlation of inflammatory infiltrate with the enlargement of experimental aortic aneurysms. Journal of vascular surgery. 1992;16(2):139-47.

27. Koch AE, Kunkel SL, Pearce WH, Shah MR, Parikh D, Evanoff HL, et al. Enhanced production of the chemotactic cytokines interleukin-8 and monocyte chemoattractant protein-

1 in human abdominal aortic aneurysms. The American journal of pathology. 1993;142(5):1423-31.

28. Juvonen J, Surcel HM, Satta J, Teppo AM, Bloigu A, Syrjala H, et al. Elevated circulating levels of inflammatory cytokines in patients with abdominal aortic aneurysm. Arterioscler Thromb Vasc Biol. 1997;17(11):2843-7.

29. Hellenthal FA, Buurman WA, Wodzig WK, Schurink GW. Biomarkers of abdominal aortic aneurysm progression. Part 2: inflammation. Nature reviews Cardiology. 2009;6(8):543-52.

30. Lopez-Candales A, Holmes DR, Liao S, Scott MJ, Wickline SA, Thompson RW. Decreased vascular smooth muscle cell density in medial degeneration of human abdominal aortic aneurysms. The American journal of pathology. 1997;150(3):993-1007.

31. Henderson EL, Geng YJ, Sukhova GK, Whittemore AD, Knox J, Libby P. Death of smooth muscle cells and expression of mediators of apoptosis by T lymphocytes in human abdominal aortic aneurysms. Circulation. 1999;99(1):96-104.

32. Vorp DA, Lee PC, Wang DH, Makaroun MS, Nemoto EM, Ogawa S, et al. Association of intraluminal thrombus in abdominal aortic aneurysm with local hypoxia and wall weakening. Journal of vascular surgery. 2001;34(2):291-9.

33. Holmes DR, Liao S, Parks WC, Thompson RW. Medial neovascularization in abdominal aortic aneurysms: a histopathologic marker of aneurysmal degeneration with pathophysiologic implications. Journal of vascular surgery. 1995;21(5):761-71; discussion 71-2.

34. Wolinsky H, Glagov S. Nature of species differences in the medial distribution of aortic vasa vasorum in mammals. Circulation research. 1967;20(4):409-21.

35. Moxon JV, Parr A, Emeto TI, Walker P, Norman PE, Golledge J. Diagnosis and monitoring of abdominal aortic aneurysm: current status and future prospects. Curr Probl Cardiol. 2010;35(10):512-48.

36. Aggarwal S, Qamar A, Sharma V, Sharma A. Abdominal aortic aneurysm: A comprehensive review. Exp Clin Cardiol. 2011;16(1):11-5.

37. Fink HA, Lederle FA, Roth CS, Bowles CA, Nelson DB, Haas MA. The Accuracy of Physical Examination to Detect Abdominal Aortic Aneurysm. JAMA Internal Medicine. 2000;160(6):833-6.

38. LaRoy LL, Cormier PJ, Matalon TA, Patel SK, Turner DA, Silver B. Imaging of abdominal aortic aneurysms. AJR Am J Roentgenol. 1989;152(4):785-92.

39. Sparks AR, Johnson PL, Meyer MC. Imaging of abdominal aortic aneurysms. Am Fam Physician. 2002;65(8):1565-70.

40. Durham JR, Hackworth CA, Tober JC, Bova JG, Bennett WF, Schmalbrock P, et al. Magnetic resonance angiography in the preoperative evaluation of abdominal aortic aneurysms. The American Journal of Surgery. 1993;166(2):173-8.

41. Hollier LH, Taylor LM, Ochsner J. Recommended indications for operative treatment of abdominal aortic aneurysms. Report of a subcommittee of the Joint Council of the Society for Vascular Surgery and the North American Chapter of the International Society for Cardiovascular Surgery. J Vasc Surg. 1992;15(6):1046-56.

42. Lederle FA, Wilson SE, Johnson GR, Reinke DB, Littooy FN, Acher CW, et al. Immediate Repair Compared with Surveillance of Small Abdominal Aortic Aneurysms. New England Journal of Medicine. 2002;346(19):1437-44.

43. Mortality results for randomised controlled trial of early elective surgery or ultrasonographic surveillance for small abdominal aortic aneurysms. The Lancet. 1998;352(9141):1649-55.

44. Cao P, De Rango P, Verzini F, Parlani G, Romano L, Cieri E. Comparison of Surveillance Versus Aortic Endografting for Small Aneurysm Repair (CAESAR): Results from a Randomised Trial. European Journal of Vascular and Endovascular Surgery. 2011;41(1):13-25.

45. Ouriel K, Clair DG, Kent KC, Zarins CK. Endovascular repair compared with surveillance for patients with small abdominal aortic aneurysms. Journal of Vascular Surgery. 2010;51(5):1081-7.

46. Isselbacher EM. Thoracic and Abdominal Aortic Aneurysms. Circulation. 2005;111(6):816-28.

47. Lederle FA, Freischlag JA, Kyriakides TC, Matsumura JS, Padberg FT, Jr., Kohler TR, et al. Long-term comparison of endovascular and open repair of abdominal aortic aneurysm. N Engl J Med. 2012;367(21):1988-97.

48. De Bruin JL, Baas AF, Buth J, Prinssen M, Verhoeven ELG, Cuypers PWM, et al. Long-Term Outcome of Open or Endovascular Repair of Abdominal Aortic Aneurysm. New England Journal of Medicine. 2010;362(20):1881-9.

49. United Kingdom ETI, Greenhalgh RM, Brown LC, Powell JT, Thompson SG, Epstein D, et al. Endovascular versus open repair of abdominal aortic aneurysm. N Engl J Med. 2010;362(20):1863-71.

50. Baxter BT, Terrin MC, Dalman RL. Medical management of small abdominal aortic aneurysms. Circulation. 2008;117(14):1883-9.

51. Golledge J, Norman PE. Current status of medical management for abdominal aortic aneurysm. Atherosclerosis. 2011;217(1):57-63.

52. Dodd BR, Spence RA. Doxycycline inhibition of abdominal aortic aneurysm growth: a systematic review of the literature. Curr Vasc Pharmacol. 2011;9(4):471-8.

53. Lederle FA. Abdominal Aortic Aneurysm: Still No Pill. Annals of Internal Medicine. 2013;159(12):852-3.

54. Meijer CA, Stijnen T, Wasser MNJM, Hamming JF, van Bockel JH, Lindeman JHN, et al. Doxycycline for Stabilization of Abdominal Aortic Aneurysms: A Randomized Trial. Annals of Internal Medicine. 2013;159(12):815-23.

55. Mosorin M, Juvonen J, Biancari F, Satta J, Surcel H-M, Leinonen M, et al. Use of doxycycline to decrease the growth rate of abdominal aortic aneurysms: A randomized, double-blind, placebo-controlled pilot study. Journal of Vascular Surgery. 2001;34(4):606-10.

56. Baxter BT, Matsumura J, Curci J, McBride R, Blackwelder WC, Liu X, et al. Non-invasive Treatment of Abdominal Aortic Aneurysm Clinical Trial (N-TA(3)CT): Design of a Phase IIb, placebo-controlled, double-blind, randomized clinical trial of doxycycline for the reduction of growth of small abdominal aortic aneurysm. Contemp Clin Trials. 2016;48:91-8.

57. Høgh A, Vammen S, Ostergaard L, Joensen JB, Henneberg EW, Lindholt JS. Intermittent Roxithromycin for Preventing Progression of Small Abdominal Aortic Aneurysms: Long-Term Results of a Small Clinical Trial. Vascular and Endovascular Surgery. 2009;43(5):452-6.

58. Vammen S, Lindholt JS, Østergaard L, Fasting H, Henneberg EW. Randomized double-blind controlled trial of roxithromycin for prevention of abdominal aortic aneurysm expansion. BJS. 2001;88(8):1066-72.

59. Lindholt JS, Ashton HA, Scott RAP. Indicators of infection with Chlamydia pneumoniae are associated with expansion of abdominal aortic aneurysms. Journal of Vascular Surgery. 2001;34(2):212-5.

60. Bellosta S, Via D, Canavesi M, Pfister P, Fumagalli R, Paoletti R, et al. HMG-CoA reductase inhibitors reduce MMP-9 secretion by macrophages. Arterioscler Thromb Vasc Biol. 1998;18(11):1671-8.

61. Schweitzer M, Mitmaker B, Obrand D, Sheiner N, Abraham C, Dostanic S, et al. Atorvastatin modulates matrix metalloproteinase expression, activity, and signaling in abdominal aortic aneurysms. Vasc Endovascular Surg. 2010;44(2):116-22.

62. Takagi H, Yamamoto H, Iwata K, Goto S, Umemoto T. Effects of Statin Therapy on Abdominal Aortic Aneurysm Growth: A Meta-analysis and Meta-regression of Observational Comparative Studies. European Journal of Vascular and Endovascular Surgery. 2012;44(3):287-92.

63. Ferguson CD, Clancy P, Bourke B, Walker PJ, Dear A, Buckenham T, et al. Association of statin prescription with small abdominal aortic aneurysm progression. American Heart Journal. 2010;159(2):307-13.

64. Paraskevas KI, Mikhailidis DP, Giannoukas AD. Statins: A sine qua non of the management of patients with abdominal aortic aneurysms. International Journal of Cardiology. 2013;168(4):4528.

65. Sweeting MJ, Thompson SG, Brown LC, Powell JT, collaborators R. Meta-analysis of individual patient data to examine factors affecting growth and rupture of small abdominal aortic aneurysms. Br J Surg. 2012;99(5):655-65.

66. Thompson SG, Brown LC, Sweeting MJ, Bown MJ, Kim LG, Glover MJ, et al. Systematic review and meta-analysis of the growth and rupture rates of small abdominal aortic aneurysms: implications for surveillance intervals and their cost-effectiveness. Health Technol Assess. 2013;17(41):1-118.

67. da Cunha V, Tham DM, Martin-McNulty B, Deng G, Ho JJ, Wilson DW, et al. Enalapril attenuates angiotensin II-induced atherosclerosis and vascular inflammation. Atherosclerosis. 2005;178(1):9-17.

68. Iida Y, Xu B, Schultz GM, Chow V, White JJ, Sulaimon S, et al. Efficacy and mechanism of angiotensin II receptor blocker treatment in experimental abdominal aortic aneurysms. PLoS One. 2012;7(12):e49642.

69. Kaschina E, Schrader F, Sommerfeld M, Kemnitz UR, Grzesiak A, Krikov M, et al. Telmisartan prevents aneurysm progression in the rat by inhibiting proteolysis, apoptosis and inflammation. J Hypertens. 2008;26(12):2361-73.

70. Lange C, Sommerfeld M, Namsolleck P, Kintscher U, Unger T, Kaschina E. AT2R (Angiotensin AT2 Receptor) Agonist, Compound 21, Prevents Abdominal Aortic Aneurysm Progression in the Rat. Hypertension. 2018;72(3):e20-e9.

71. Yoshimura K, Morikage N, Nishino-Fujimoto S, Furutani A, Shirasawa B, Hamano K. Current Status and Perspectives on Pharmacologic Therapy for Abdominal Aortic Aneurysm. Curr Drug Targets. 2018;19(11):1265-75.

72. Daugherty A, Cassis LA. Mouse Models of Abdominal Aortic Aneurysms. Arteriosclerosis, Thrombosis, and Vascular Biology. 2004;24(3):429-34.

73. Anidjar S, Salzmann JL, Gentric D, Lagneau P, Camilleri JP, Michel JB. Elastase-induced experimental aneurysms in rats. Circulation. 1990;82(3):973-81.

74. Pyo R, Lee JK, Shipley JM, Curci JA, Mao D, Ziporin SJ, et al. Targeted gene disruption of matrix metalloproteinase-9 (gelatinase B) suppresses development of experimental abdominal aortic aneurysms. The Journal of Clinical Investigation. 2000;105(11):1641-9.

75. Bhamidipati CM, Mehta GS, Lu G, Moehle CW, Barbery C, DiMusto PD, et al. Development of a novel murine model of aortic aneurysms using peri-adventitial elastase. Surgery. 2012;152(2):238-46.

76. Bi Y, Chen H, Li Y, Yu Z, Han X, Ren J. Rabbit aortic aneurysm model with enlarging diameter capable of better mimicking human aortic aneurysm disease. PloS one. 2018;13(6):e0198818-e.

77. Moláček J, Třeška V, Kobr J, Čertík B, Skalický T, Kuntscher V, et al. Optimization of the Model of Abdominal Aortic Aneurysm – Experiment in an Animal Model. Journal of Vascular Research. 2009;46(1):1-5.

78. Chiou AC, Chiu B, Pearce WH. Murine Aortic Aneurysm Produced by Periarterial Application of Calcium Chloride. Journal of Surgical Research. 2001;99(2):371-6.

79. Longo GM, Xiong W, Greiner TC, Zhao Y, Fiotti N, Baxter BT. Matrix metalloproteinases 2 and 9 work in concert to produce aortic aneurysms. The Journal of Clinical Investigation. 2002;110(5):625-32.

80. Gertz SD, Kurgan A, Eisenberg D. Aneurysm of the rabbit common carotid artery induced by periarterial application of calcium chloride in vivo. The Journal of Clinical Investigation. 1988;81(3):649-56.

81. Tanaka A, Hasegawa T, Chen Z, Okita Y, Okada K. A novel rat model of abdominal aortic aneurysm using a combination of intraluminal elastase infusion and extraluminal calcium chloride exposure. Journal of Vascular Surgery. 2009;50(6):1423-32.

82. Czerski A, Bujok J, Gnus J, Hauzer W, Ratajczak K, Nowak M, et al. Experimental methods of abdominal aortic aneurysm creation in swine as a large animal model. J Physiol Pharmacol. 2013;64(2):185-92.

83. Daugherty A, Manning MW, Cassis LA. Angiotensin II promotes atherosclerotic lesions and aneurysms in apolipoprotein E-deficient mice. The Journal of clinical investigation. 2000;105(11):1605-12.

84. Manning MW, Cassi LA, Huang J, Szilvassy SJ, Daugherty A. Abdominal aortic aneurysms: fresh insights from a novel animal model of the disease. Vasc Med. 2002;7(1):45-54.

85. Saraff K, Babamusta F, Cassis LA, Daugherty A. Aortic Dissection Precedes Formation of Aneurysms and Atherosclerosis in Angiotensin II-Infused, Apolipoprotein E-Deficient Mice. Arteriosclerosis, Thrombosis, and Vascular Biology. 2003;23(9):1621-6.

86. Zhang SH, Reddick RL, Piedrahita JA, Maeda N. Spontaneous hypercholesterolemia and arterial lesions in mice lacking apolipoprotein E. Science. 1992;258(5081):468-71.

87. Ishibashi S, Goldstein JL, Brown MS, Herz J, Burns DK. Massive xanthomatosis and atherosclerosis in cholesterol-fed low density lipoprotein receptor-negative mice. J Clin Invest. 1994;93(5):1885-93.

88. Grover VPB, Tognarelli JM, Crossey MME, Cox IJ, Taylor-Robinson SD, McPhail MJW. Magnetic Resonance Imaging: Principles and Techniques: Lessons for Clinicians. J Clin Exp Hepatol. 2015;5(3):246-55.

89. van Geuns R-JM, Wielopolski PA, de Bruin HG, Rensing BJ, van Ooijen PMA, Hulshoff M, et al. Basic principles of magnetic resonance imaging. Progress in Cardiovascular Diseases. 1999;42(2):149-56.

90. McGowan JC. Basic Principles of Magnetic Resonance Imaging. Neuroimaging Clinics of North America. 2008;18(4):623-36.

91. Chavhan GB, Babyn PS, Thomas B, Shroff MM, Haacke EM. Principles, techniques, and applications of T2*-based MR imaging and its special applications. Radiographics. 2009;29(5):1433-49.

92. Hong H, Yang Y, Liu B, Cai W. Imaging of Abdominal Aortic Aneurysm: the present and the future. Current vascular pharmacology. 2010;8(6):808-19.

93. Kiruluta AJM, Gonzalez RG. Magnetic resonance angiography: physical principles and applications. Handb Clin Neurol. 2016;135:137-49.

94. Hartung MP, Grist TM, François CJ. Magnetic resonance angiography: current status and future directions. J Cardiovasc Magn Reson. 2011;13(1):19-.

95. Klessen C, Hein PA, Huppertz A, Voth M, Wagner M, Elgeti T, et al. First-pass whole-body magnetic resonance angiography (MRA) using the blood-pool contrast medium gadofosveset trisodium: comparison to gadopentetate dimeglumine. Invest Radiol. 2007;42(9):659-64.

96. Massoud TF, Gambhir SS. Molecular imaging in living subjects: seeing fundamental biological processes in a new light. Genes Dev. 2003;17(5):545-80.

97. Golledge J, Tsao PS, Dalman RL, Norman PE. Circulating markers of abdominal aortic aneurysm presence and progression. Circulation. 2008;118(23):2382-92.

98. Chen K, Chen X. Design and development of molecular imaging probes. Curr Top Med Chem. 2010;10(12):1227-36.

99. Nolting DD, Nickels ML, Guo N, Pham W. Molecular imaging probe development: a chemistry perspective. Am J Nucl Med Mol Imaging. 2012;2(3):273-306.

100. Klink A, Heynens J, Herranz B, Lobatto ME, Arias T, Sanders HMHF, et al. In vivo characterization of a new abdominal aortic aneurysm mouse model with conventional and molecular magnetic resonance imaging. Journal of the American College of Cardiology. 2011;58(24):2522-30.

101. Brangsch J, Reimann C, Collettini F, Buchert R, Botnar RM, Makowski MR. Molecular Imaging of Abdominal Aortic Aneurysms. Trends in Molecular Medicine. 2017;23(2):150-64.

102. Okamura H, Pisani LJ, Dalal AR, Emrich F, Dake BA, Arakawa M, et al. Assessment of Elastin Deficit in a Marfan Mouse Aneurysm Model Using an Elastin-Specific Magnetic Resonance Imaging Contrast Agent. Circulation: Cardiovascular Imaging. 2014;7(4):690-6.

103. Botnar RM, Wiethoff AJ, Ebersberger U, Lacerda S, Blume U, Warley A, et al. In Vivo Assessment of Aortic Aneurysm Wall Integrity Using Elastin-Specific Molecular Magnetic Resonance Imaging. Circulation: Cardiovascular Imaging. 2014;7(4):679-89.

104. Bary Cv, Makowski M, Preissel A, Keithahn A, Warley A, Spuentrup E, et al. MRI of Coronary Wall Remodeling in a Swine Model of Coronary Injury Using an Elastin-Binding Contrast Agent. Circulation: Cardiovascular Imaging. 2011;4(2):147-55.

105. Turner GH, Olzinski AR, Bernard RE, Aravindhan K, Boyle RJ, Newman MJ, et al. Assessment of macrophage infiltration in a Murine model of abdominal aortic aneurysm. Journal of Magnetic Resonance Imaging. 2009;30(2):455-60.

106. Yao Y, Wang Y, Zhang Y, Li Y, Sheng Z, Wen S, et al. In vivo imaging of macrophages during the early-stages of abdominal aortic aneurysm using high resolution MRI in ApoE mice. PloS one. 2012;7(3):e33523-e.

107. Bazeli R, Coutard M, Duport BD, Lancelot E, Corot C, Laissy JP, et al. In vivo evaluation of a new magnetic resonance imaging contrast agent (P947) to target matrix metalloproteinases in expanding experimental abdominal aortic aneurysms. Invest Radiol. 2010;45(10):662-8.

108. Richards JMJ, Semple SI, MacGillivray TJ, Gray C, Langrish JP, Williams M, et al. Abdominal Aortic Aneurysm Growth Predicted by Uptake of Ultrasmall Superparamagnetic Particles of Iron Oxide. Circulation: Cardiovascular Imaging. 2011;4(3):274-81.

109. Sadat U, Taviani V, Patterson AJ, Young VE, Graves MJ, Teng Z, et al. Ultrasmall Superparamagnetic Iron Oxide-enhanced Magnetic Resonance Imaging of Abdominal Aortic Aneurysms–A Feasibility Study. European Journal of Vascular and Endovascular Surgery. 2011;41(2):167-74.

110. Nchimi A, Defawe O, Brisbois D, Broussaud TKY, Defraigne J-O, Magotteaux P, et al. MR Imaging of Iron Phagocytosis in Intraluminal Thrombi of Abdominal Aortic Aneurysms in Humans. Radiology. 2010;254(3):973-81.

111. Investigators MRS. Aortic Wall Inflammation Predicts Abdominal Aortic Aneurysm Expansion, Rupture, and Need for Surgical Repair. Circulation. 2017;136(9):787-97.

112. Krettek A, Sukhova GK, Libby P. Elastogenesis in Human Arterial Disease. Arteriosclerosis, Thrombosis, and Vascular Biology. 2003;23(4):582-7.

113. Botnar RM, Brangsch J, Reimann C, Janssen CHP, Razavi R, Hamm B, et al. In Vivo Molecular Characterization of Abdominal Aortic Aneurysms Using Fibrin-Specific Magnetic Resonance Imaging. J Am Heart Assoc. 2018;7(11).

114. Hood MN, Blankholm AD, Stolpen A. The Rise of Off-Label Iron-Based Agents in Magnetic Resonance Imaging. Journal of Radiology Nursing. 2019;38(1):38-41.

115. Makowski MR, Wiethoff AJ, Blume U, Cuello F, Warley A, Jansen CHP, et al. Assessment of atherosclerotic plaque burden with an elastin-specific magnetic resonance contrast agent. Nature Medicine. 2011;17(3):383-8.

116. Pearce WH, Sweis I, Yao JST, McCarthy WJ, Koch AE. Interleukin-1β and tumor necrosis factor-α release in normal and diseased human infrarenal aortas. Journal of Vascular Surgery. 1992;16(5):784-9.

117. Newman KM, Jean-Claude J, Li H, Ramey WG, Tilson MD. Cytokines that activate proteolysis are increased in abdominal aortic aneurysms. Circulation. 1994;90(5 Pt 2):II224-7.

118. Pyo R, Lee JK, Shipley JM, Curci JA, Mao D, Ziporin SJ, et al. Targeted gene disruption of matrix metalloproteinase-9 (gelatinase B) suppresses development of experimental abdominal aortic aneurysms. J Clin Invest. 2000;105(11):1641-9.

119. Johnston WF, Salmon M, Pope NH, Meher A, Su G, Stone ML, et al. Inhibition of interleukin-1β decreases aneurysm formation and progression in a novel model of thoracic aortic aneurysms. Circulation. 2014;130(11 Suppl 1):S51-S9.

120. Isoda K, Akita K, Kitamura K, Sato-Okabayashi Y, Kadoguchi T, Isobe S, et al. Inhibition of interleukin-1 suppresses angiotensin II-induced aortic inflammation and aneurysm formation. Int J Cardiol. 2018;270:221-7.

121. Hashimoto Y, Fukazawa R, Nagi-Miura N, Ohno N, Suzuki N, Katsube Y, et al. Interleukin-1beta Inhibition Attenuates Vasculitis in a Mouse Model of Kawasaki Disease. J Nippon Med Sch. 2019;86(2):108-16.

122. Kitamura K, Isoda K, Akita K, Okabayashi Y, Kadoguchi T, Shimada K, et al. Abstract 11695: An Anti-Interleukin-1β Antibody Suppresses Both Angiotensin II-induced Renal Inflammation and Hypertension. Circulation. 2017;136(suppl_1):A11695-A.

123. Ridker PM, Everett BM, Thuren T, MacFadyen JG, Chang WH, Ballantyne C, et al. Antiinflammatory Therapy with Canakinumab for Atherosclerotic Disease. N Engl J Med. 2017;377(12):1119-31.

124. Tang TY, Howarth SPS, Miller SR, Graves MJ, Patterson AJ, U-King-Im J-M, et al. The ATHEROMA (Atorvastatin Therapy: Effects on Reduction of Macrophage Activity) Study: Evaluation Using Ultrasmall Superparamagnetic Iron Oxide-Enhanced Magnetic Resonance Imaging in Carotid Disease. Journal of the American College of Cardiology. 2009;53(22):2039-50.

125. Saraff K, Babamusta F, Cassis LA, Daugherty A. Aortic dissection precedes formation of aneurysms and atherosclerosis in angiotensin II-infused, apolipoprotein E-deficient mice. Arterioscler Thromb Vasc Biol. 2003;23(9):1621-6.

126. Daugherty A, Manning MW, Cassis LA. Angiotensin II promotes atherosclerotic lesions and aneurysms in apolipoprotein E-deficient mice. J Clin Invest. 2000;105(11):1605-12.

127. Wang YX, Martin-McNulty B, Freay AD, Sukovich DA, Halks-Miller M, Li WW, et al. Angiotensin II increases urokinase-type plasminogen activator expression and induces aneurysm in the abdominal aorta of apolipoprotein E-deficient mice. Am J Pathol. 2001;159(4):1455-64.

128. Halloran BG, Davis VA, McManus BM, Lynch TG, Baxter BT. Localization of aortic disease is associated with intrinsic differences in aortic structure. J Surg Res. 1995;59(1):17-22.

129. Thieszen SL, Dalton M, Gadson PF, Patterson E, Rosenquist TH. Embryonic lineage of vascular smooth muscle cells determines responses to collagen matrices and integrin receptor expression. Exp Cell Res. 1996;227(1):135-45.

9 Publications

Kaufmann JO, **Brangsch J**, Kader A, Saatz J, Schwaar T, Wilke M, Adams L, Mangarova D, Möckel J, Botnar RM, Taupitz M, Traub H, Hamm B, Weller MG, Makowski MR. Identification and development of an ADAMTS4-specific in vivo MR probe. Nature Biotechnology Jan 2021 *in submission*

Collettini F*, Reimann C*, **Brangsch J**, Chapiro J, Savic LJ, Onthank DC, Robinson SP, Karst U, Buchholz R, Keller S, Hamm B, Goldberg SN, Makowski MR. Elastin-specific MRI of extracellular matrix-remodelling following hepatic radiofrequency-ablation in a VX2 Liver Tumor Model. Sci Rep. Jan 2021 *under Revision*
**shared first authorship*

Collettini F*, **Brangsch J***, Reimann C, Chapiro J, Savic LJ, Karst U, Buchholz R, Keller S, Hamm B, Goldberg SN, Makowski MR. Hepatic radiofrequency ablation: Longitudinal evaluation of ablation-induced inflammatory cell recruitment in the periablational rim using USPIO-enhanced macrophage MR imaging. Investigative Radiology Jan 2021 *accepted for publication*
**shared first authorship*

Kader A, **Brangsch J**, Kaufmann JO, Zhao J, Mangarova DB, Moeckel J, Adams LC, Sack I, Taupitz M, Hamm B, Makowski MR. Molecular MR Imaging of Prostate Cancer. Biomedicines. 2020 Dec 22;9(1):1

Keller S, Borde T, **Brangsch J**, Kader A, Reimann C, Gebert P, Hamm B, Makowski M. Native T1 Mapping Magnetic Resonance Imaging as a Quantitative Biomarker for the Characterization of the Extracellular Matrix in a Rabbit Hepatic Cancer Model. Biomedicine 2020, 8(10), 412

Keller S, Chapiro J, **Brangsch J**, Reimann C, Collettini F, Sack I, Savic LJ, Hamm B, Goldberg SN, Makowski M. Assessment of the Hepatic Tumor Extracellular Matrix using Elastin-specific Molecular Magnetic Resonance Imaging in an Experimental Rabbit Cancer Model. Sci Rep. 2020 Nov 27;10(1):20785

Zhao J, Mangarova DB, **Brangsch J**, Kader A, Hamm B, Brenner W, Makowski MR. Correlation between Intraprostatic PSMA Uptake and MRI PI-RADS of [68Ga]Ga-PSMA-11 PET/MRI in Patients with Prostate Cancer: Comparison of PI-RADS Version 2.0 and PI-RADS Version 2.1. Cancers (Basel). 2020 Nov 26;12(12):3523

Brangsch J, Reimann C, Kaufmann JO, Adams LC, Onthank DC, Thone-Reineke C, Robinson SP, Wilke M, Weller M, Buchholz R, Karst U, Botnar RM, Hamm B, Makowski MR. Molecular MR-imaging for the noninvasive quantification of the anti-inflammatory effects of targeting interleukin-1β in a mouse model of aortic aneurysm. Mol Imaging. 2020 Jan-Dec;19:1536012120961875

Adams LC, Reimann C, **Brangsch J**, Kaufmann JO, Buchholz R, Karst U, Botnar RM, Hamm B, Makowski MR. Simultaneous molecular MRI of extracellular matrix collagen and inflammatory activity to predict abdominal aortic aneurysm rupture. Sci Rep.10, 15206 (2020)

Mangarova DM, **Brangsch J**, Mohtashamdolatshahi A, Kosch O, Paysen H, Wiekhorst F, Klopfleisch R, Buchholz R, Karst U, Taupitz M, Schnorr J, Hamm B, Makowski MR. Ex vivo magnetic particle imaging of vascular inflammation in abdominal aortic aneurysm in a murine model. Sci Rep. 2020;10(1):12410

Mangarova DM, **Brangsch J,** Moeckel J, Kader A, Ludwig A, Hamm B, Makowski MR. Current trend in moleculat magnetic resonance imaging of the extracellular matrix in atherosclersis. J Transl Sci May 2020 DOI: 10.15761/JTS.1000393

Adams LC, **Brangsch J**, Reimann C, Kaufmann JO, Nowak K, Buchholz R, Karst U, Botnar RM, Hamm B, Makowski MR. Noninvasive imaging of vascular permeability to predict the risk of rupture in abdominal aortic aneurysms using an albumin-binding probe. Sci Rep. 2020;10(1):3231

Keller S, Chapiro J, **Brangsch J**, Reimann C, Collettini F, Sack I, Savic LJ, Hamm B, Goldberg SN, Makowski M. Quantitative Magnetic Resonance Imaging for Assessment of Treatment Outcomes in a Rabbit VX2 Hepatic Tumor Model. J Magn Reson Imaging. 2019

Reimann C, **Brangsch J**, Kaufmann JO, Adams LC, Onthank DC, Thöne-Reineke C, Robinson SP, Hamm B, Botnar RM, Makowski MR. Dual-probe molecular MRI for the in vivo characterization of atherosclerosis in a mouse model: Simultaneous assessment of plaque inflammation and extracellular-matrix remodeling. Sci Rep. 2019;9(1):13827

Reimann C, **Brangsch J**, Adams LC, Thone-Reineke C, Hamm B, Makowski MR. MR Angiography of the Head/Neck Vascular System in Mice on a Clinical MRI System. Contrast Media Mol Imaging. 2019;2019:5461809

Brangsch J, Reimann C, Kaufmann JO, Adams LC, Onthank DC, Thone-Reineke C, Robinson SP, Buchholz R, Karst U, Botnar RM, Hamm B, Makowski MR. Concurrent Molecular Magnetic Resonance Imaging of Inflammatory Activity and Extracellular Matrix Degradation for the Prediction of Aneurysm Rupture. Circ Cardiovasc Imaging. 2019;12(3):e008707

Reimann C, **Brangsch J**, Kaufmann JO, Adams LC, Onthank DC, Robinson SP, Botnar RM, Collettini F, Makowski MR. Contrast-Enhanced Magnetic Resonance Angiography Using a Novel Elastin-Specific Molecular Probe in an Experimental Animal Model. Contrast Media Mol Imaging. 2018;2018:9217456

Botnar RM, **Brangsch J**, Reimann C, Janssen CHP, Razavi R, Hamm B, Makowski MR. In Vivo Molecular Characterization of Abdominal Aortic Aneurysms Using Fibrin-Specific Magnetic Resonance Imaging. J Am Heart Assoc. 2018;7(11)

Brangsch J, Reimann C, Collettini F, Buchert R, Botnar RM, Makowski MR. Molecular Imaging of Abdominal Aortic Aneurysms. Trends in Molecular Medicine. 2017;23(2):150-64

Jansen CHP, **Brangsch J**, Reimann C, Adams L, Hamm B, Botnar RM, Makowski MR. In Vivo High-Frequency Ultrasound for the Characterization of Thrombi Associated with Aortic Aneurysms in an Experimental Mouse Model. Ultrasound Med Biol. 2017;43(12):2882-90

Jansen CHP, Reimann C, **Brangsch J**, Botnar RM, Makowski MR. In vivo MR-angiography for the assessment of aortic aneurysms in an experimental mouse model on a clinical MRI scanner: Comparison with high-frequency ultrasound and histology. PLoS One. 2017;12(6):e0178682

Reimann C, **Brangsch J**, Colletini F, Walter T, Hamm B, Botnar RM, Makowski MR. Molecular imaging of the extracellular matrix in the context of atherosclerosis. Adv Drug Deliv Rev. 2017;113:49-60

10 Danksagung

Ich möchte mich an dieser Stelle bei allen bedanken, die mich während der letzten Jahre begleitet und unterstützt haben. Besonderer Dank gilt Frau Prof. Dr. Christa Thöne-Reineke für die stetige wohlwollende Unterstützung und Beratung während der gesamten Bearbeitung meiner Dissertation.

Zudem danke ich Herrn Prof. Dr. Marcus Makowski, der mir sein Vertrauen als Gründungsmitglied seiner Arbeitsgruppe geschenkt hat und mich über die Jahre stets tatkräftig und geduldig unterstützt hat.

Weiterer Dank gilt meinen lieben Kollegen an der Charité Universitätsmedizin Berlin, insbesondere meinen Kollegen der AG Makowski, die mir jederzeit fachlich zur Seite standen und stets für gute Laune im Büro sorgten. Zusätzlich möchte ich mich bei allen externen Kooperationspartnern der Bundesanstalt für Materialforschung und -prüfung, Universität Münster und King’s College London für die hervorragende und produktive Zusammenarbeit bedanken.

Nicht zuletzt möchte ich mich bei meiner Familie und meinen Freunden für ihre Zeit und Mühe beim Korrekturlesen sowie ihre motivierenden Worte bedanken.

11 Selbstständigkeitserklärung

Hiermit bestätige ich, dass ich die vorliegende Arbeit selbständig angefertigt habe. Ich versichere, dass ich ausschließlich die angegebenen Quellen und Hilfen Anspruch genommen habe.

Berlin, den 10.02.2021 Julia Brangsch

Druck: Mensch und Buch Verlag Berlin